UNIVERSIDADE DE LISBOA
FACULDADE DE CIÊNCIAS
DEPARTAMENTO DE BIOLOGIA ANIMAL

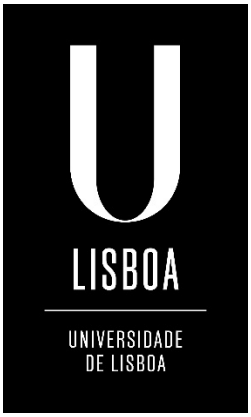

The metabolism of central nervous system metastasis: Cerebrospinal fluid metabolome

Joana Ribeiro Noronha Vasques Sousa

Mestrado em Biologia Humana e Ambiente

Dissertação

2014

UNIVERSIDADE DE LISBOA
FACULDADE DE CIÊNCIAS
DEPARTAMENTO DE BIOLOGIA ANIMAL

The metabolism of central nervous system metastasis: Cerebrospinal fluid metabolome

Joana Ribeiro Noronha Vasques Sousa

Mestrado em Biologia Humana e Ambiente

Dissertação orientada por:

Doutor Luís Gafeira Gonçalves (orientação externa)
Cell Physiology and NMR group
Instituto de Tecnologia Química e Biológica da Universidade Nova de Lisboa

Professora Doutora Deodália Dias (orientação interna)
Departamento de Biologia Animal
Faculdade de Ciências da Universidade de Lisboa

2014

Acknowledgments

First of all, I would like to thank everyone who, directly or indirectly, made the realization of this Master's thesis possible. A long term project such as a thesis is always the reflection of the support of all the people who took the time and effort to help in any way they could. For that, I am truly thankful.

I would like to begin by thanking my external supervisor Doctor Luís Gafeira Gonçalves, for welcoming me and giving the opportunity to perform my studies at ITQB. I would like to express my gratitude for all the patience, guidance, support and helpful discussions which always stimulated my scientific criticism and helped me grow scientifically.

I am very thankful to Professor Deodália Dias, for the availability and for accepting being my internal supervisor.

I also want to thank Professor Helena Santos, group leader at ITQB, who proportionate insightful and dynamic discussions about this work. She also gave me strength and encouraged me to go further as an aspiring scientist.

I would like to thank Gonçalo Graça for always taking the time to answer all my questions and for sharing with me his knowledge. Thanks also for the time dedicated to this work and above all his friendship, support, patience, encouragement and confidence.

I want to thank Professor Jacinta Serpa who gave me the opportunity to work in a different research line. Her critical spirit really served as inspiration and as a guide for the elaboration of this work. Her availability and patience helped me get here.

I want to express my gratitude and friendship to my lab coworkers Cristiana, Andreia, Inês, Sara and Dário who guided me, gave me advices and were always ready to help me. They also made lunches and coffee breaks much more entertaining. I will never forget the jokes and all the good time spent inside and outside the lab.

I am also grateful for the help, support and patience of Filipa and Carolina. They were both very kind and always ready to help me find whatever I needed in the lab.

I want to acknowledge the IMM team involved in the project.

I will always remember my friends for all the good times shared, for their unconditional patience, for the advices and for always having comforting words when I most needed. I am particularly thankful to Nídia and Andreia for all the laughs and crazy moments shared and for always being there when I needed.

And last but definitely not the least, I would like to thank my family for all the support and encouragement to always keep moving forward. I thank my brother for being a sweetheart and an annoying midge at the same time, and for always being there with the right words to make me smile. I would like to thank my grandparents, who in their eighties, still dedicated a great amount of their time and patience to share with me their wisdom. Thank you both for giving me a brilliant education during 22 years of my life. I would also like to thank my mother who shows me every day that every obstacle is just another one and with strength and perseverance it can be overcome, and in the end it was nothing but a mere obstacle, one of many along the way. I am grateful for her helpful advices, huge patience, continuous support and unconditional love.

This work was performed at ITQB and supervised by Dr. Luís Gafeira Gonçalves, in the framework of the project *Cerebrospinal fluid metabolome: an instructive niche for CNS metastasis* supported by Fundação para a Ciência e a Tecnologia (PTDC/BIM-ONC/1242/2012).

The NMR spectrometer used is part of The National NMR Facility, supported by Fundação para a Ciência e a Tecnologia (RECI/BBB-BQB/0230/2012).

The present work also had the assistance of *Instituto Português de Oncologia de Lisboa Francisco Gentil E. P. E.* and *Instituto de Medicina Molecular*.

Sumário

O cancro é considerado como um dos maiores problemas de saúde pública em todo o mundo (Siegel *et al.*, 2012).De acordo com a Organização Mundial de Saúde (OMS), é definido como um crescimento rápido de células anormais que são capazes de invadir qualquer parte do corpo e alastrar-se para outros órgãos, iniciando o processo de metastização.

As metástases são um dos timbres do cancro e são a principal causa de morbilidade e mortalidade em doentes com cancro, pelo que o seu estudo é de grande importância (Seyfried & Shelton, 2010).

O sistema nervoso é importante no funcionamento de grande parte dos órgãos do corpo humano. O sistema nervoso central (CNS), uma das subdivisões do sistema nervoso, é constituído pelo cérebro e pela medula espinal. Ambos encontram-se protegidos por três camadas de tecido, as meninges: dura máter, aracnóide e pia máter. Entre a segunda e a terceira camada existe um espaço chamado de subaracnoide, que é preenchido por vasos sanguíneos e pelo líquido cefalorraquidiano (LCR) (Seeley *et al.*, 2003).

O LCR é produzido pelas células ependimárias, num sistema de cavidades do cérebro chamados de ventrículos. O conjunto destas células formam a barreira hemato-encefálica (BHE), responsável pela entrada de metabolites necessários ao normal funcionamento neuronal (Seeley *et al.*, 2003).

O fluído cerebrospinal banha o cérebro e a medula espinal, protegendo o CNS. Para além disso, o CSF é responsável pela distribuição de nutrientes e químicos filtrados pelo sangue, contribuindo para um balanço iónico estável. Como a sua composição depende directamente do metabolismo do cérebro e da funcionalidade e integridade da BHE, a análise do CSF pode contribuir para o estudo e a compreensão de desordens que afectem o SNC (Seeley *et al.*, 2003; Wishart *et al.*, 2008).

As metástases do SNC, uma das desordens do SNC, são definidas como a entrada de células tumorais do tumor primário para o SNC. Estima-se que cerca de 10 a 30% dos pacientes com tumores primários e mais tarde diagnosticados com metástases no SNC. São ainda uma das principais causas de morbilidade e mortalidade (Aragon-Ching & Zujewski, 2007; Barnholtz-Sloan *et al.*, 2004; Buckner *et al.*, 2007).

Actualmente, as técnicas de diagnóstico que existem são citologia, examinação neurológica e neuroimagem, técnicas que apresentam um baixo nível de sensibilidade (Weston *et al.*, 2011). As principais abordagens de tratamento são excisão cirúrgica, radiocirurgia, sensibilizadores de radiação, quimioterapia citotóxica, terapias direccionadas e drogas capazes de atravessar o BHE (Aragon-Ching & Zujewski, 2007).

O porquê destas células terem uma predilecção aumentada para o CNS ainda não é totalmente conhecido. A detecção e caracterização de células malignas no LCR poderá proporcionar uma melhor compreensão da biologia das metástases através da identificação e caracterização das populações de células de cancro capazes de se infiltrarem no CSF (Aragon-Ching & Zujewski, 2007).

O perfil metabólico do CSF usando a técnica de RMN já tem sido estudado no sentido de encontrar biomarcadores de desordens do SNC (An *et al.*, 2014; Blasco *et al.*, 2010; Dunn *et al.*, 2011; Lutz *et al.* 2007; Meissner *et al.*, 2014; Sinclair *et al.*, 2010; Smolinska *et al.*, 2012). A combinação da metabonómica com a técnica de RMN potencia a descoberta de novos biomarcadores e a descoberta e compreensão dos mecanismos que são responsáveis por essas doenças (Smolinska *et al.*, 2012), incluindo as metástases do SNC.

Com esta tese pretende-se estudar o LCR de pacientes com e sem metástases no SNC, usando a técnica de RMN para definir uma "assinatura metabólica" do grau de comprometimento e/ou invasão do SNC por células tumorais. Pretende-se ainda estudar a progressão tumoral e a importância do microambiente tumoral num modelo murino de leucemia exposto a diferentes dietas (normal e rica em colesterol) usando diferentes abordagens, incluindo a metabolómica, o estudo dos níveis de expressão génicos e proteicos e ainda a análise do ciclo celular e da morte celular.

Quanto ao primeiro estudo, foram analisadas por RMN 186 amostras, sendo que 10 correspondiam a pacientes com metástases no SNC. Foi possível identificar 48 metabolitos diferentes (incluindo álcoois, aminoácidos, ácidos orgânicos e açúcares), 40 dos quais encontrados em todas as amostras analisadas.

A análise multivariada do LCR dos pacientes sem metástases no SNC sugere que crianças e adultos apresentam perfis metabólicos distintos, confirmando resultados previamente obtidos noutros estudos, mas a influencia deste parâmetro parece ser limitada. Tendo em conta estas diferenças, foram também analisados os parâmetros género e localização do tumor primário. Nesta análise verificou-se que não existem diferenças a nível metabólico entre homens/mulheres e entre os diferentes tipos de tumor primário.

Numa segunda análise multivariada foram analisadas as amostras de paciente com e sem metástases no SNC. Os resultados aqui obtidos sugerem que o perfil metabólico dos pacientes sem metástases é ligeiramente diferente do perfil dos pacientes com metástases no SNC. É possível que outros factores possam estar a influenciar este resultado, incluindo o número baixo de amostras incluído no estudo.

No segundo estudo foram analisadas linhas celulares de leucemia linfoblástica aguda (linha celular 697-GFP) injectadas em modelo murino exposto a duas dietas diferentes, uma normal e outra rica em colesterol, estabelecidas pelos nossos colaboradores no Instituto de Medicina Molecular.

A análise luminescente dos modelos murinos revelou que aqueles que tinham sido expostos previamente a uma dieta rica em colesterol tinha uma maior carga de doença que aqueles que tinham passado por uma dieta normal. Estes resultados sugerem que o colesterol tem um papel importante na progressão e desenvolvimento tumoral.

A análise metabolómica por RMN dos extractos aquosos destas células suportam os resultados anteriormente obtidos, uma vez que a análise multivariada demonstrou que células de murinos expostos a diferentes dietas têm perfis metabólicos diferentes. Formato, glucose, creatina, glutamina, lactato, isoleucina, leucina e valina foram os

metabolitos que se encontram aumentados nas células de murinos expostos a dieta rica em colesterol.

No sentido de estudar o papel da dieta rica em colesterol no crescimento de células leucémica foram também avaliados os níveis de expressão de algumas enzimas-chave que pudessem explicar as diferenças encontradas a nível metabólico. Verificou-se que a expressão de SGLT1 (transportador de glucose) estava aumentada na linha celular de murinos expostos à dieta rica em colesterol, sugerindo que esta enzima poderá esta a contribuir significativamente para a entrada de glucose nestas células. A expressão de GLUT1, outro transportador de glucose, encontrava-se aumentada nas linhas celulares que tinham passado pelos murinos, sugerindo que este gene não está relacionado com a presença de glucose nas células de murinos expostos a dieta rica em colesterol, mas poderá estar relacionado com a selecção *in vivo* de células tumorais.

Sendo que o lactato é considerada uma fonte alternativa de energia nas células cancerígenas, a análise da expressão de enzimas envolvidas no metabolismo e transporte de lactato foram também estudadas. Os níveis de expressão de LDHA encontravam-se aumentados em ambas as linhas celulares que passaram pelos murinos, resultados estes que estavam em concordância com os obtidos em GLUT1, visto que uma elevada taxa de captação de glucose permite um aumento da taxa de glicólise e, consequentemente, leva à produção de lactato catalisada por LDHA. No caso dos transportadores de lactato MCT1 e MTC4 não foram verificados resultados significativos.

Sendo que a análise por RMN detectou a presença de glucose nas linhas celulares de murinos sujeitos a dieta rica em colesterol, foram avaliados também os níveis de expressão de enzimas que fazem parte da gluconeogénese. Aqui verificou-se que PFKFB1 estava inibida nestas células, o que sugere que a gluconeogénese poderá ser uma das vias envolvidas na acumulação de glucose dentro das células de murinos expostos a uma dieta rica em colesterol. Em resumo, estes resultados sugerem que colesterol poderá ter um papel importante na progressão e no desenvolvimento tumoral.

Adicionalmente, a análise da proliferação celular e da apoptose nestas células não revelou diferenças entre as diferentes linhas celulares em estudo.

Em conclusão, estes estudos podem contribuir na compreensão da patofisiologia desta doença, incluindo as propriedades das células tumorais e o microambiente do SNC.

Palavras-chave: líquido cefalorraquidiano (LCR), ressonância magnética nuclear (RMN), tumor primário, metástase, metabolómica.

Abstract

Central nervous system (CNS) metastasis is a devastating complication of cancer and is associated with high morbidity and poor prognosis. However, the mechanisms that underlie CNS invasion by tumor cells are still poorly understood.

Hence, in this thesis it was studied the CSF of cancer patients with and without metastasis in the CNS using NMR approach to define a "metabolic signature" of the degree of impairment and/or invasion of the CNS by tumor cells. Metabolomic analysis suggests that adults and children have different metabolic profiles. Additionally, it was seen that CSF composition is not affected by gender and primary tumor origin. The analysis of all CSF samples indicates that CSF without cell invasion has a somewhat different metabolic profile from CSF with cell invasion.

In addition, it was also studied tumor progression and the importance of tumor's microenvironment in a leukemia murine model exposed to different diets (normal and fat diet) using different approaches including metabolomics, gene and protein expression and analysis of cell cycle and cell death. The metabolic analysis of cell extracts of these cell lineages from murine revealed that the type of diet affects more the cell metabolism than the localization of the tumor. The gene and protein expression analysis indicated that GLUT1 and LDHA may play a role in the *in vivo* selection of tumor cells. Moreover, SGLT1 expression was increased in the cells from mice exposed to fat diet. Additionally, gluconeogenesis may be one of the pathways involved in the tumor progression in mice exposed to a diet rich in cholesterol. These results support that cholesterol may contribute to cancer progression and development.

Overall, these studies may help in understanding the pathophysiology of this disease, including the site-specific properties of tumor cells and the CNS microenvironment.

Keywords: cerebrospinal fluid, nuclear magnetic resonance, primary tumor, metastasis, metabolomics.

Contents

Acknowledgments i

Sumário iv

Abstract ix

Contents x

Index of figures xii

Index of tables xvi

List of abreviations xvii

1. Introduction 1

1.1. Overview of Cancer 1

1.2. Central Nervous System (CNS) metastasis: biology, incidence, metabolism and current approaches 2

1.3. Metabolic profiling of CSF and metastatic cells using nuclear magnetic resonance (NMR) spectroscopy 8

2. Aims 12

3. Materials and Methods 13

3.1. Study of CSF from patients with and without CNS metastasis by ^{1}H NMR spectroscopy 13

3.1.1. Biological Material 13

3.1.2. Metabolic profiling by NMR spectroscopy 15

3.2. *In vitro* study of CNS metastasis in human acute lymphoblastic leukemia (697-GFP) cell line 19

3.2.1. Biological Material 19

3.2.2. Metabolic profiling by NMR spectroscopy 21

3.2.3. Gene expression 22

3.2.4. Protein levels 25
3.2.5. Cell cycle analysis by FACS 29
3.2.6. Cell death (apoptosis and necrosis) analysis by FACS 30
3.2.7. Statistical analysis 31

4. Results and discussion 32

4.1. Study of CSF from patients with and without CNS metastasis by ^{1}H NMR spectroscopy 32
4.1.1. ^{1}H-NMR profiling 32
4.1.2. Multivariate analysis of control samples 35
4.1.3. Multivariate analysis of control and cell invasion samples 42

4.2. *In vitro* study of CNS metastasis in human acute lymphoblastic leukemia (697-GFP) cell line 46
4.2.1. Luminescence analysis 46
4.2.2. Metabolic profiling by NMR spectroscopy 48
4.2.3. Gene and protein expression levels 54
4.2.4. Cell cycle analysis by FACS 66
4.2.5. Cell death (apoptosis and necrosis) analysis by FACS 68

5. Concluding Remarks 70

6. Future Perspectives 72

7. References 73

Appendix A 85

Index of figures

Figure 1 - Representation of the meningeal sheaths surrounding the brain. Adapted from (Seeley *et al.* 2003). 3

Figure 2 - Representation of the meningeal sheaths in the spinal cord. Adapted from (Seeley *et al.* 2003). 4

Figure 3 -Venn diagram showing the overlap of CSF metabolites detected by global NMR, GC–MS and LC–FTMS methods compared to the detectable CSF metabolome (Wishart *et al.*, 2008). 11

Figure 4 - Schematic representation of the steps involved in metabolic detection by NMR spectroscopy. 15

Figure 5 – PCA score plot of the two first PCs using ^{1}H-NMR data of control samples (n=176) and colored according to age (77 adults and 99 children). PC1 = 46.3 % and PC2 = 6.93 %. 35

Figure 6 – PCA loading plot of PC2 using ^{1}H-NMR data of adults samples of control samples with the metabolites that are found increased (positive part of PC2) and decreased (negative part of PC2) in the children and that are increased (negative part of PC2) and decreased (positive part of PC2) in the adults. 36

Figure 7 – OPLS-DA score plot of the first and the orthogonal components using ^{1}H-NMR data of control samples (n=176), colored according to the age of the patients (77 adults and 99 children). R2Y (cum) = 0.726 and Q^2 (cum) = 0.511. 37

Figure 8 – OPLS-DA loading plot of PC1 using ^{1}H-NMR data of control samples (n=176), with the metabolites that are found increased (positive part of PC1) and decreased (negative part of PC1) in the children and that are increased (negative part of PC1) and decreased (positive part of PC1) in the adults. 38

Figure 9 – PCA score plot of the two first PCs using ^{1}H-NMR data of children samples (n=99) and colored according to gender (58 males and 41 females). PC1 = 43.8 % and PC2 = 6.19 %. 39

Figure 10 – PCA score plot of the two first PCs using ^{1}H-NMR data of adults samples (n=77) and colored according to gender (39 males and 38 females). PC1 = 52.7 % and PC2 = 6.19 %. 40

Figure 11 – PCA score plot of the two first PCs using ^{1}H-NMR data of children samples (n=99) and colored according to the type of primary tumor (13 lymphoma, 83 leukemia, 2 rhabdomyosarcoma, 1 germ cell tumor). PC1 = 43.8 % and PC2 = 6.19 %. 41

Figure 12 – PCA score plot of the two first PCs using ^{1}H-NMR data of adults samples (n=77) and colored according to the type of primary tumor (46 lymphoma, 21 leukemia, 5 breast carcinoma, 1 non-melanoma skin cancer, 1 multiple myeloma and 1 colorectal cancer). PC1 = 52.7 % and PC2 = 6.19 %. 42

Figure 13 – PCA score plot of the two first PCs using ^{1}H-NMR data of all samples (n=99) and colored according to the presence or absence of cell invasion in the CNS. PC1 = 44.8 % and PC2 = 11.3 %. 43

Figure 14 – OPLS-DA score plot of the first and the orthogonal components using ^{1}H-NMR data of controls and cell invasion samples from the sub-group of adults (n=77). R2Y (cum) = 0.626 and Q^2 (cum) = 0.327. 44

Figure 15 – OPLS-DA loading plot of PC1 using 1H-NMR data of control and cell invasion samples (n=77), with the metabolites that are increased (positive part of PC1) and decreased (negative part of PC1) in the cell invasion samples and that are increased (negative part of PC1) and decreased (positive part of PC1) in the control samples. 45

Figure 16 – Luminescence analysis of tumor cells from 697-GFP lineage in mice exposed to a normal diet (on the left) and in mice exposed to fat diet (on the right). The scale shows the grade of disease burden. This analysis was performed by our collaborators in the *Instituto de Medicina Molecular*. 47

Figure 17 – Representative ^{1}H NMR spectra of (A) culture medium (B) aqueous extract and (C) organic extract, with some of the metabolites identified. 49

Figure 18 – PCA score plot of the two first PCs using ^{1}H-NMR data of supernatants (n=9) and colored according to the localization of tumor metastasis on the mice (1 parental lineage, 3 brain metastases, 4 skin metastasis and 1 bone marrow metastasis). PC1 = 43.5 % and PC2 = 22.6 %. 50

Figure 19– PCA score plot of the two first PCs using ^{1}H-NMR data of supernatants (n=9) and colored according to the type of mice diet (1 parental lineage, 3 normal diet and 5 fat diet). PC1 = 43.5 % and PC2 = 22.6 %. 50

Figure 20 – PCA score plot of the two first PCs using ^{1}H-NMR data of organic extracts (n=9) and colored according to the localization of tumor metastasis on the mice (1

parental lineage, 3 brain metastases, 4 skin metastasis and 1 bone marrow metastasis). PC1 = 57.4 % and PC2 = 29.6 %. 51

Figure 21– PCA score plot of the two first PCs using ^{1}H-NMR data of organic extracts (n=9) and colored according to the type of mice diet (1 parental lineage, 3 normal diet and 5 fat diet). PC1 = 57.4 % and PC2 = 29.6 %. 52

Figure 22 – PCA score plot of the two first PCs using ^{1}H-NMR data of aqueous extracts (n=9) and colored according to the localization of tumor metastasis on the mice (1 parental lineage, 3 brain metastases, 4 skin metastasis and 1 bone marrow metastasis). PC1 = 41.9 % and PC2 = 20.8 %. 52

Figure 23 – PCA score plot of the two first PCs using ^{1}H-NMR data of aqueous extracts (n=9) and colored according to the type of mice diet (1 parental lineage, 3 normal diet and 5 fat diet). PC1 = 41.9 % and PC2 = 20.8 %. 53

Figure 24 – PCA loading plot of PC2 using ^{1}H-NMR data of aqueous extracts with the identification of the metabolites that are increased (positive part of PC2) and decreased (negative part of PC2) in the cells from mice exposed to fat diet and that are increased (negative part of PC2) and decreased (positive part of PC2) in the cells from mice exposed to normal diet and from parental lineage. 54

Figure 25 – Relative gene expression of SGLT1 and GLUT1. 18S gene was the endogenous control. Expression levels were normalized to parental lineage. Data are mean ± error bars of triplicates. * $p \leq 0.05$; ** $p \leq 0.01$ 55

Figure 26 – Relative gene expression of IDH1 and IDH2. 18S gene was the endogenous control. Expression levels were normalized to parental lineage. Data are mean ± error bars of triplicates.* $p \leq 0.05$. 56

Figure 27– Relative gene expression of enzymes involved in lactate metabolism LDHA, LDHB and LDHC. 18S gene was the endogenous control. Expression levels were normalized to parental lineage. Data are mean ± error bars of triplicates. * $p \leq 0.05$; ** $p \leq 0.01$. 58

Figure 28– LDHB protein levels assessed by western blot. Protein levels were normalized to β-actin and are relative to those obtained in the parental lineage. 58

Figure 29 – Relative gene expression of lactate transporters MCT1 and MCT4. 18S rRNA gene was the endogenous control. Expression levels were normalized to parental lineage. Data are mean ± error bars of triplicates. *** $p \leq 0.001$. 60

Figure 30 – MCT1 and MCT4 protein levels assessed by western blot. Protein levels were normalized to β-actin and are relative to those obtained in the parental lineage... 60

Figure 31 – Immunofluorescence for MCT1 and MCT4 (green) in parental lineage, skin fat diet lineage, skin normal diet lineage, brain fat diet lineage, brain normal diet lineage and bone marrow normal diet lineage. Nuclei were labelled with dapi (blue). Fluorescence microscopy (magnification: 200x and 400x). 61

Figure 32– Relative gene expression of gluconeogenic enzymes ALT, PCK1, PCK2, FBP1 and PFKFB1. 18S rRNA gene was the endogenous control. Expression levels were normalized to parental lineage. Data are mean ± error bars of triplicates. 63

Figure 33 – PCK1 and PFKFB1 protein levels assessed by western blot. Protein levels were normalized to β-actin and are relative to those obtained in the parental lineage... 63

Figure 34 – Cell cycle analysis by FACS (PI staining) in all cell lineages, at time point 0, 2, 4, 8, 26, 32 and 50 h. Data are means of triplicates. In brain fat diet lineage it is included the results of the two cultures and in skin fat diet is included the results of the three cultures. 67

Figure 35 – Apoptosis (annexin V positive cells) and necrosis (PI positive cells) analysis by FACS, at time points 0 and 24 h. Data are means of triplicates ± error bars of triplicates. In brain fat diet lineage it is included the results of the two cultures and in skin fat diet is included the results of the three cultures. 69

Index of tables

Table 1 – Groups of CSF samples subdivided in age and gender. 14

Table 2 – Groups of CSF samples subdivided in type of tumor and then in age. 14

Table 3 – Acquisition and processing parameters of the experiments performed for all samples. 17

Table 4 - Diet and localization of tumor metastases in mice inoculated with 697-GFP cell line. 20

Table 5 – Program utilized for cDNA synthesis. 23

Table 6 – Program utilized for RQ-PCR. 25

Table 7 – Full list of the metabolites identified in CSF samples and respective signals. 34

List of abreviations

1D	One-dimensional
2D	Two-dimensional
AA	Antibiotic-antimycotic
ALL	Acute lymphoblastic leukemia
ALT	Alanine transaminase
Anova	Analysis of variance
BBB	Blood brain barrier
BM	Bone marrow
BMRB	Biological Magnetic Resonance Bank
BSA	Bovine serum albumin
cDNA	DNA copy
CNS	Central nervous system
CSF	Cerebrospinal fluid
DAPI	4'-6-diamidino-2-phenylindole
ddH2O	Double-destilled water
DNA	Deoxyribonucleic acid
dNTPs	Deoxynucleotides
D_2O	Deuterium water
DS	Dummy scans
DTT	Dithiothreitol
F1	Frequency domain 1
F1,6BP	Fructose-1,6-biphosphate
F2	Frequency domain 2
F2,6BP	Fructose-2,6-biphosphatase
F6P	Fructose-6-phosphate
FACS	Fluorescence-activated cell sorting
FBP1	Fructose-1,6-bisphosphatase
FBS	Fetal bovine serum
For	Forward
gLS1	Glutaminase isoform 1
GLS2	Glutaminase isoform 2
GLUT1	Glucose transporter 1
h	Hours
HMDB	Human Metabolome database
HRP	Horse raddish peroxidase
HSQC	Heteronuclear single quantum correlation
Hz	Hertz
IDH1	Isocitrate dehydrogenase 1
IDH2	Isocitrate dehydrogenase 2
***J*-res**	*J*-resolved spectroscopy
LB	Line broadening
LDHA	Lactate dehydrogenase subunit A

LDHB	Lactate dehydrogenase subunit B
LDHC	Lactate dehydrogenase subunit C
MCT	Monocarboxylate anion transporter
MCT1	Monocarboxylate transporter 1
MCT4	Monocarboxylate transporter 4
MHz	Megahertz
min	Minutes
mRNA	Messenger ribonucleic acid
MVA	Multivariate analysis
NADH	Nicotinamide adenine dinucleotide reduced
NMR	Nuclear magnetic ressonance
NS	Number of scans
OPLS -DA	Orthogonal partial least squares - discriminant analysis
PCA	Principal component analysis
PCK1	Phosphoenolpyruvate carboxykinase cytosolic
PCK2	Phosphoenolpyruvate carboxykinase mitochondrial
PCR	Polymerase chain reaction
PFKFB1	Fructose-2,6-bisphosphatase
PC	Principal component
PI	Propidium iodide
PS	Phosphatidyl serine
Q^2	Goodness of prediction or predictive power of a OPLS-DA model
R2Y	Cumulative explained variance
RD	Relaxation Delay
Rev	Reverse
RIPA	Radio-immunoprecipitation assay
RNA	Ribonucleic acid
RQ-PCR	Real time quantitative polymerase chain reaction
RT-PCR	Reverse transcription polymerase chain reaction
rRNA	Ribossomic RNA
SDS-PAGE	Sodium dodecyl sulphate-polyacrylamide gel electrophoresis
SGTL1	Sodium-glucose transporter 1
SI	Size of real spectrum
SIMCA	Soft independent modeling of class analogy
SW	Spectral width
TBS	Tris Buffered Saline
TCA	Tricarboxylic acid
TD	Time domain
TGS	Tris-Glycine-SDS
Tm	Mixing time
TOCSY	Total correlation spectroscopy
V	Volume
W	Weight
WHO	World health organization

1. Introduction

1.1. Overview of Cancer

Cancer is considered a worldwide public health problem (Siegel *et al.*, 2012). According to World Health Organization (WHO), cancer is described as a rapid growth of abnormal cells that can invade any part of the body and spread to the surrounding tissues and distant organs, initiating the metastatic process. Metastasis are the principal cause of morbidity and mortality in cancer patients (Seyfried & Shelton, 2010).

In 2012, WHO estimates 14.1 million new cancer cases worldwide, 8.2 million cancer deaths and 32.6 million people living with cancer (within 5 years of diagnosis). Statistics also say that most cases occurred in developing regions as 57% (8 million) of new cancer cases, 65% (5.3 million) of the cancer deaths and 48% (15.6 million) of the 5-year prevalent cancer are reported from these areas. The most deathly cancers are lung (1.59 million deaths), liver (745 000 deaths), stomach (723 000 deaths), colorectal (694 000 deaths), breast (521 000 deaths) and oesophageal cancer (400 000 deaths) (Ferlay *et al.*, 2013).

An important research line in cancer is understanding the biological process underlying the passage of normal cells to malignant cancer cells, and what are the changes in its cell physiology (Seyfried & Shelton, 2010).

Hanahan and Weinberg suggested that six main alterations in cell physiology can underlie malignant cell growth of nearly all type of cancers (Hanahan and Weinberg, 2000). These six alterations, also called “hallmarks” are: self-sufficiency in growth signals, insensitivity to growth under inhibitory signals, resistance to cell death (apoptosis), replicative immortality, angiogenesis and tissue invasion and metastasis (Hanahan & Weinberg, 2000; Seyfried & Shelton, 2010). In a recent review, two hallmarks were added to this list: reprogramming of energy metabolism and evasion of immune system (Hanahan & Weinberg, 2011). Additionally, tumors exhibit another dimension of complexity: they can recruit normal cells that contribute to the acquisition

of hallmark traits by creating the "tumor microenvironment". In resume, malignant transformation is conditioned by tumor microenvironment (Hanahan & Weinberg, 2011).

Metastasis, one of the hallmarks of cancer, is the main causes of death in cancer and consequently its study is of great importance. This process involves a complex series of sequential and interrelated steps. In order to complete the metastatic cascade, cancer cells must detach from the primary tumor, intravasate into the circulation and lymphatic system, evade immune attack, extravasate at a distant capillary bed, and invade and proliferate in distant organs (Bacac & Stamenkovic, 2008; Chambers*et al.*, 2002; Duffy *et al.*, 2008; Fidler, 2003; Steeg, 2006). Metastatic cells are also capable of establishing a microenvironment that facilitates development and proliferation and lead to the formation of macroscopic malignant secondary tumors. Although these major steps of metastasis are well studied, the knowledge process that underlies the capacity of metastatic cells arise from populations of non-metastatic cells of the primary tumor is still very low (Pawelek, 2008; Steeg, 2006, Steeg, 2008).

1.2. Central Nervous System (CNS) metastasis: biology, incidence, metabolism and current approaches

The nervous system (NS) is involved in most of the organic functions of human body. This system is subdivided in two parts: the central nervous system and the peripheral nervous system (Seeley *et al.*, 2003).

The central nervous system (CNS) is constituted by the brain and the spinal cord. The brain is located inside the cranium and the spinal cord is housed within the spinal canal, formed by the vertebrae. The brain and spinal cord are in continuity with each other through the foramen magnum. The spinal cord extends from the foramen magnum down to the level of the second lumbar vertebra region where this narrows into a cone, forming the *conus medullaris* (Seeley *et al.*, 2003).

Three layers of tissue, called meninges, surround and protect the brain (Figure 1) and the spinal cord (Figure 2). The most superficial layer, dura mater, is thick and

surrounds the brain, spinal cord and spinal nerves, being separated from the vertebral canal by the epidural space, a space that contains blood vessels, connective tissue and fat. The second meningeal layer is called the arachnoid and is very thin and slender. The space between arachoid and the dura mater is the subdural space. This layer contains only a small amount of serous fluid. The third meningeal layer is called the pia mater. It binds very tightly to the surface of the brain and spinal cord. The space formed between the arachnoid layer and the layer pia mater is called subarachnoid space and it is filled by blood vessels and the cerebrospinal fluid (CSF) (Seeley *et al.*, 2003).

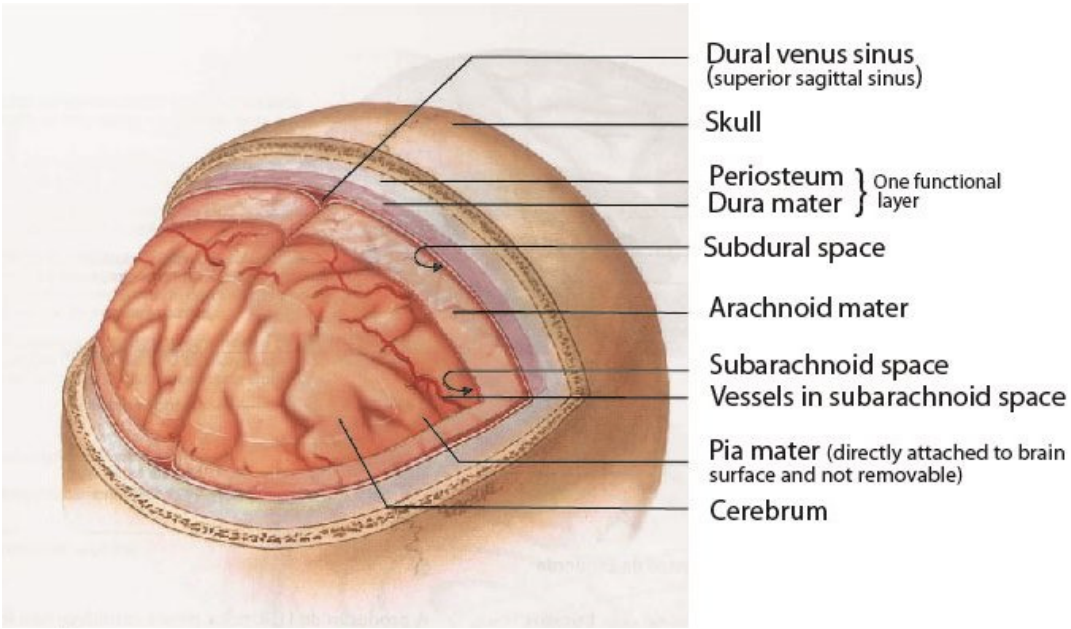

Figure 1 - Representation of the meningeal sheaths surrounding the brain (Seeley *et al.*, 2003).

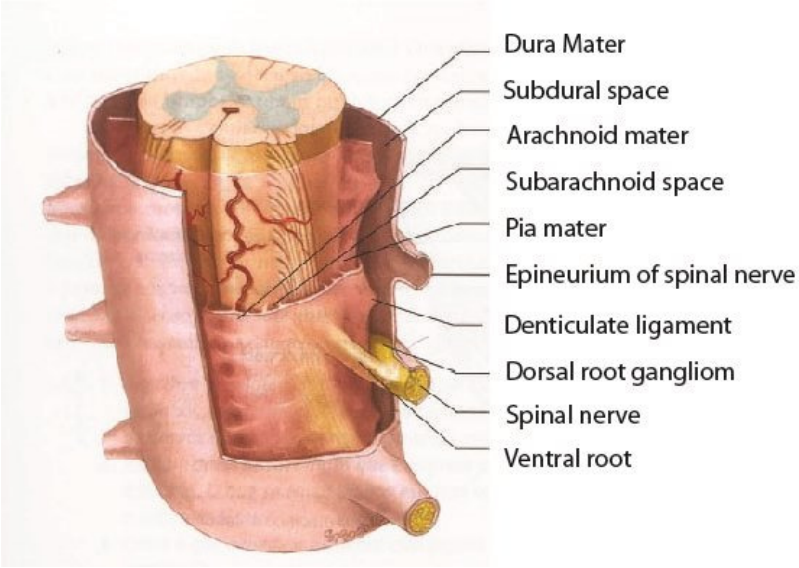

Figure 2 - Representation of the meningeal sheaths in the spinal cord (Seeley *et al.*, 2003).

Within the brain there is a system of void cavities called ventricles. The network of linked cavities in the brain (cerebral ventricles) is continuous with the central canal of the spinal cord. The ventricles are filled with cerebrospinal fluid which is produced by specialized epithelium (ependymal cells) located within the ventricles. The ependymal cells and the associated support tissues and blood vessels form the choroid plexus. The endothelial cells of the choroid plexus, which are connected by tight junctions, form the blood-brain barrier (BBB) or blood-CSF barrier. This barrier allows the passage of water, some gases and lipid soluble molecules by passive diffusion, and the passage of glucose, amino acids and other metabolites essential for normal neural function (Seeley *et al.*, 2003).

CSF composition is similar to that of blood serum, cleared of most of its protein content. It bathes the brain and the spinal cord, constituting a protective cushion around the CNS. Besides its protective role, CSF has an important role the distribution of the nutrients and chemicals filtered by the blood, contributing to a stable ionic balance. Since its composition depends directly of the brain metabolism and the BBB function and integrity, metabolomic analysis of CSF can offer a deeper understanding of the disorders affecting the CNS (Seeley *et al.*, 2003; Wishart *et al.*, 2008).

CNS metastasis are defined as the spread of cancer cells from the original (primary) tumor to the CNS. At macroscopically level, metastatic lesions are usually sharply demarcated, spherical masses that often do not infiltrate the surrounding brain parenchyma, but cause edema due to mass effect (Pekmezci & Perry, 2013).

Metastases of the CNS are a frequent complication and cause of death of solid tumors. Despite of the use of surgery or radiation therapy for the initial control of the primary solid tumor, the development of CNS metastases can still lead to a high mortality rate and affects the survival, neurocognition, speech, coordination behavior and life quality (Barnholtz-Sloan *et al.*, 2004; Buckner *et al.*, 2007).

It is estimated that 10 to 30% of patients with solid tumors are later diagnosed with CNS metastases. CNS metastasis risks changed with the type of primary cancer, being the most prone, in solid tumor: lung, breast, melanoma, kidney and colorectal (Aragon-Ching & Zujewski, 2007; Barnholtz-Sloan *et al.*, 2004).

The incidence of brain metastases has been increasing mainly due to the life span expansion and an increase in the number of elderly people which stimulated the urge to development the detection of subclinical disease with better imaging and better control of systemic disease (Aragon-Ching & Zujewski, 2007).

The current approaches to detect the spread of cancer into the CSF are cytology, neurologic examination and neuroimaging. Even though the combination of these methods can increase the accuracy of the diagnosis, the level of sensitivity of these methods remains low, delaying treatment (Weston, Glantz, & Connor, 2011).

The major treatment approaches for CNS metastases are surgical excision, radiosurgery, radiation sensitizers, cytotoxic chemotherapy, targeted therapies and drugs capable of crossing the BBB (Aragon-Ching & Zujewski, 2007).

Why tumor cells have an increased predilection for the nervous system is not yet fully understood, but the incidence of brain metastases from different cancers appears to be increasing and the mechanisms involved are unknown, although it is considered that

there are different factors playing an important role in the process (Aragon-Ching & Zujewski, 2007).

The mechanisms of dissemination of cancer cells through the CSF are poorly studied. Detection and characterization of malignant cells in the CSF may proportionate a better understanding of the metastatic spread biology through identification and characterization of the cancer cell populations capable of infiltrating the CSF (Weston *et al.*, 2011).

Tumor cells may reach the CSF through hematogenous spread, direct extension from the tumor itself or by migration along perineural [1] or perivascular [2] spaces (Weston *et al.*, 2011). However, in rare cases, neoplasms can reach to the CNS by spread via cranial nerves, especially in squamous cell carcinomas (SCC) of the head and neck region and malignant salivary gland neoplasms (Nussbaum *et al.*, 1996; Spencer *et al.*, 2005). The majorly of tumor cells reach the brain via the pulmonary arterial circulation, either as a primary lung cancer or a metastasis to the lung from other systemic primaries. The majority of the brain metastases are parenchymal, but metastases to leptomeninges/subarachnoid space, dura and skull are not uncommon. Additionally, approximately 80% of brain metastases are located in the cerebral hemispheres, 15% in the cerebellum, and 5% in the brain stem (Patchell, 2003). Other rare sites include choroid plexus, pineal gland, pituitary, and optic nerve. There are also case reports of metastases to primary CNS tumors (Takei & Powell, 2009).

Several studies about acute lymphoblastic leukemia (ALL) have been done. ALL is an acute form of leukemia characterized by the overproduction of cancerous immature white blood cells (the lymphoblasts) in the bone marrow (BM) and peripheral blood (PB) and has been a target of several studies with the intuit to better understand the mechanisms of dissemination of cancerous cells through the CSF (Barnholtz-Sloan *et al.* 2004; DeVita, *et al.*, 2008). The survival rates of pediatric ALL are above 80%, and extramedullary relapses have become extremely rare. The CNS, an important source of extramedullary relapse, is a sanctuary site in ALL, due to the role of the BBB in protecting

[1] Cancer spreading to the space surrounding a nerve.
[2] Cancer spreading to the space surrounding a blood vessel.

the CNS from exposure to xenobiotic toxins. To improve relapse-free survival sites in ALL, strategies to penetrate the BBB were needed. This led to the use of prophylactic cranial irradiation, which was effective in preventing CNS relapse, but it was accompanied by major discomfort and potentially severe side effects (Aragon-Ching & Zujewski, 2007; DeVita *et al.*, 2008; Pui & Evans, 2006; Pui, 2006; Weston *et al.*, 2011).

CNS study is difficult and study its disorders using human subjects are somewhat limited, because of evident ethical and practical reasons. To overcome this limitation, researchers have developed model systems to study the brain metastasis and to gain mechanistic insights into the brain metastasis pathogenesis. The use of model animals gave an enormous impact in how brain tumor perfusion, angiogenesis, metabolism and response to therapy can be approached (Gillies *et al.*, 2000). Neverthless, Palmieri and co-workers (2007) describe that although rodent systems were developed for brain metastasis in melanoma, lung carcinoma and breast carcinoma, they are not sufficient to represent the heterogeneity of CNS metastasis observed in the clinic. In addition, almost no comparison has been made between the molecular characteristics of model systems and the clinical CNS metastasis (Aragon-Ching & Zujewski, 2007; Palmieri *et al.*, 2007). Initially, cancer cells that constitutes tumors have been portrayed as reasonably homogeneous cell populations until relatively late in the course of tumor progression, when hyperproliferation combined with increased genetic instability results in a distinct clonal subpopulations (Hanahan and Weinberg, 2011). Additionally, Wu and co-workers (2012) verified that, in human meduloblastoma (a histological type of brain tumor), metastasis of an individual are extremely similar but a significant level of heterogeneity is observed from this cells to the ones found in the primary tumor. The bi-compartimental nature of metastatic medulloblastoma is an obstacle to the development of effective targeted therapies (Clifford, 2012; Wu *et al.*, 2012) and more studies are needed to further understand the pathophysiology of CNS metastasis regarding site-specific properties of the tumor cell and its microenvironment. The goal is to develop new and improve directed therapies to effectively eliminate these toxic and deathly cells (Aragon-Ching & Zujewski, 2007).

1.3. Metabolic profiling of CSF and metastatic cells using nuclear magnetic resonance (NMR) spectroscopy

Metabolic profiling is the measurement in biological systems of the complement of low-molecular-weight metabolites and their intermediates that reflects the dynamic response to genetic modification and physiological, pathophysiological, and/or developmental stimuli (Beckonert *et al.*, 2007).

Metabonomics and metabolomics appeared at the end of the 90's and early 2000's, respectively (Nicholson *et al.*, 1999; Oliver, Winson, Kell, & Baganz, 1998). Metabonomics is defined as the "quantitative measurement of the dynamic multiparametric metabolic response of living systems to pathophysiological stimuli or genetic modification" (Nicholson *et al.*, 1999). For Metabolomics it is used a very similar definition: "study of the quantitative complement of metabolites in a biological system and changes in metabolite concentrations or fluxes related to genetic or environmental perturbations" (Dunn *et al.*, 2011). In the literature, both terms are very often used interchangeably. The concept of metabonomics may be viewed, in part, as a successor of the term metabolomics (Ellis, Dunn, Griffin, Allwood, & Goodacre, 2007; Fiehn, 2002; Nicholson *et al.*, 1999).

There are two possible approaches that can be used in metabolic profiling, a targeted or a global non-targeted analysis of metabolites (endogenous[3] or exogenous) for the discovery of disease diagnosis biomarkers or drug effects (Lindon *et al.*, 2004; Nicholson & Lindon, 2008). According to the official National Institutes of Health, biomarker is defined as 'characteristic that is objectively measured and evaluated as an indicator of normal biologic processes, pathogenic processes, or pharmacologic responses to a therapeutic intervention' (Atkinson *et al.*, 2001). This includes both metabolites and metabolic profiles. Biomarkers have emerged as an attractive and valuable tool for

[3] Intracellular metabolites, including aminoacids, amines, sugars, steroids, nucleic acid bases and other substances that function as intermediates of cell metabolism.

accurate diagnose of diseases. In the case of metabolic profiles, they can be particularly useful for comparison between healthy and dysfunctional systems in the early stage of disease and therefore provide new possibilities for preventing therapies (Smolinska *et al.*, 2012).

Metabolic profiling is a developing field since the number of target studies have been increasing. This type of approach has been fundamental to the development of many areas of biomedical research, like toxicology studies, nutritional effects, metabolic consequences of genetic modifications, inborn errors of metabolism, diabetes, cancer diagnostics and diagnostic of neurological diseases (Beckonert *et al.*, 2007; Beger, Schnackenberg, Holland, Li, & Dragan, 2006; Blasco *et al.*, 2010; Bogdanov *et al.*, 2008; Coen, Holmes, Lindon, & Nicholson, 2008; Constantinou *et al.*, 2005; Ellis *et al.*, 2007; Gowda *et al.*, 2008; Hori *et al.*, 2011).

Metabolic profiling studies were been performed in diverse biomatrices: plasma, urine, seminal fluid, saliva, CSF, lung aspirates, gastrointestinal fluids, bile, tears, fluids obtained from cysts and blisters, amniotic fluid, synovial fluid, dialysis fluid, tissue specimens and tissue extracts (Beckonert *et al.*, 2007; Lindon *et al.*, 2007).

The identification of biochemical biomarkers in biofluids for CNS disorders, such as amyotrophic lateral sclerosis, multiple sclerosis, alzheimer, parkinson and cancer, has been a target of metabolomics studies (An *et al.*, 2014; Blasco *et al.*, 2010; Bogdanov *et al.*, 2008; Kork *et al.*, 2009; Kumar *et al.*, 2010; Lutz & Cozzone, 2011; Meissner *et al.*, 2014; Sinclair *et al.*, 2010; Wishart *et al.*, 2008).

Nowadays, the diagnostic of most of the neurological diseases is based on the list of symptoms, but most times it is difficult to rapidly obtain an accurate diagnosis. Since the complexity of this type of diseases probably arise from molecular and microenvironment alterations, it is possible that changes in the metabolic profiles can be found (Quinones & Kaddurah-Daouk, 2009; Smolinska *et al.*, 2012).

Metabolomic study is suited for brain research since small molecules play fundamental roles (Holmes *et al.* , 2006). Since the CSF composition depends directly on

the rate of production of metabolites in the brain, metabolomic analysis of CSF can offer perspectives in biochemical CNS disorders (Seeley *et al.*, 2003; Wishart *et al.*, 2008).

For biomarker discovery, it is important discriminate the meaningful data from metabolic profiles of biofluids. Chemometrics can be useful to identify relevant metabolites. There are several different mutltivariate techniques that allow exploration, visualization, classification and prediction of the data. Nowadays, there are different analytical platforms that are commonly used for metabolic profiling. This includes nuclear magnetic resonance (NMR) spectroscopy and mass spectrometry (MS) based techniques, such as gas chromatography-mass spectrometry (GC-MS) and liquid chromatography-mass spectrometry (LC-MS). All these techniques have their advantages and disadvantages (Smolinska *et al.*, 2012).

Nuclear magnetic resonance (NMR) spectroscopy is a physical phenomenon in which nuclei in a magnetic field absorb and re-emit electromagnetic radiation. NMR spectroscopy possesses many attributes of an ideal platform for metabolic profiling. This includes minimal sample pre-treatment and is untargeted, quantitative, high reproducibility, not-destructive and unbiased. Although NMR spectroscopy is less sensitive than MS-based techniques, the availability of cryogenic NMR probes and spectrometers with higher magnetic fields has improved the sensitivity. NMR is also capable of detect compounds that are too volatile for GC-MS (Dumas *et al.*, 2006; Keun *et al.*, 2002; Smolinska *et al.*, 2012). In a study, Wishart and co-workers (2008) verified that NMR was the technique that can detect more metabolites (53 metabolites, 21 unique of this technique), as demonstrated in figure 3, although it is more advantageous the combination of different techniques to be possible the identification of more metabolites. The authors conclude that NMR appears to be the best method for performing global or non-targeted metabolic profiling of CSF (Wishart *et al.*, 2008).

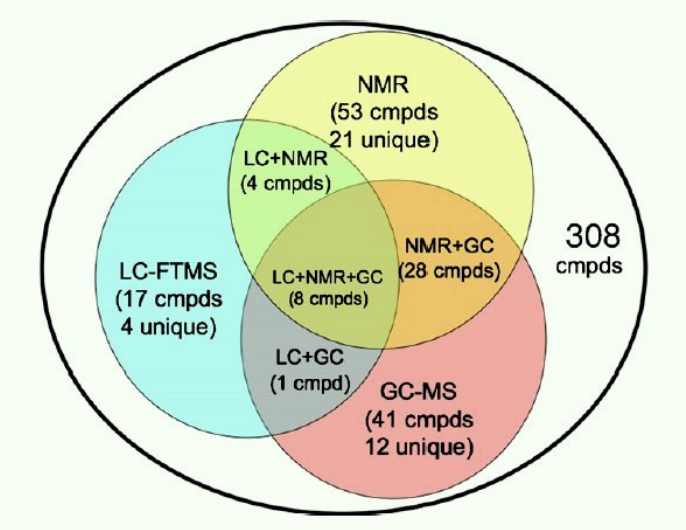

Figure 3 -Venn diagram showing the overlap of CSF metabolites detected by global NMR, GC–MS and LC–FTMS methods compared to the detectable CSF metabolome (Wishart *et al.*, 2008).

Metabolic profiling of CSF using NMR has been performed to find diagnostic biomarkers for CNS disorders (An *et al.*, 2014; Blasco *et al.*, 2010; Dunn *et al.*, 2011; Lutz *et al.*, 2007; Meissner *et al.*, 2014; Sinclair *et al.*, 2010; Smolinska *et al.*, 2012). This potentiates biomarker discovery and also contribute to uncover disease mechanism that underlie this complex neurological diseases (Smolinska *et al.*, 2012), including CNS metastases.

The use of metabonomics based on NMR also allows the characterization of cell metabolome in intact cells or cells extracts and interpret them in terms of metabolic changes in a wide range of situations, in order to begin to explain the more complex metabolic pathways occur in the body (Duarte *et al.*, 2009). Moreover, much research work has focused on metabolic differentiation between tumor and healthy tissue in order to find biomarkers for the presence and / or different levels of development of various cancers, such as breast, brain, prostate, cervical, colorectal, liver, kidney and gastric cancer (Duarte *et al.*, 2010).

2. Aims

The first main objective of this master thesis is to study the cerebrospinal fluid (CSF) metabolome of cancer patients with and without metastasis in the central nervous system (CNS), resorting to nuclear magnetic resonance (NMR), to define a "metabolic signature" of the degree of impairment and/or invasion of the CNS by tumor cells.

The second main objective is to study tumor progression and the importance of tumor's microenvironment in a leukemia murine model exposed to different diets (normal and fat diet) using different approaches including metabolomics, gene and protein expression and analysis of cell cycle and cell death (apoptosis and necrosis).

3. Materials and Methods

This chapter describes the biological material used for this study and all experimental procedures and analysis methods applied in each study.

3.1. Study of CSF from patients with and without CNS metastasis by ^{1}H NMR spectroscopy

3.1.1. Biological Material

The cerebrospinal fluid (CSF) samples were collected after the informed consent, according the guidelines of *Instituto Português de Oncologia Francisco Gentil EPE*.

The CSF samples were obtained from cancer patients with several types of primary tumor (leukemia, lymphoma, breast carcinoma, multiple myeloma, rhabdomyosarcoma, germ cell tumor, lung cancer, non-melanoma and melanoma) and result from the lumbar punction performed for CNS metastasis diagnosis.

A total of 186 CSF samples were collected and analyzed between September 2013 and July 2014. For each CSF sample, information about age, gender, types of primary tumor and presence or absence of tumor metastasis in CNS of the donor were obtained from patients clinical records. The control group was composed by samples from patients without the presence cells on the CNS. Cell invasion group was composed by the samples from patients with metastatic cell invasion of the CNS. The data concerning the population study is in Table 1 and Table 2.

Table 1 - Groups of CSF samples subdivided in age and gender.

Groups of patients	Number of patients	Age		Gender	
		children	adults	female	male
Controls	176	99	77	79	97
Cells invasion [4]	10	1	9	5	3

Table 2 -Groups of CSF samples subdivided in type of tumor and then in age.

Groups of patients	Type of primary tumor	
	children	adult
Controls	93 leukemia 13 lymphoma 2 rhabdomyosarcoma 1 germ cell tumor	21 leukemia 46 lymphoma 5 breast carcinoma 1 non-melanoma 3 multiple myeloma 1 colorectal cancer
Cells invasion [5]	1 leukemia	2 lymphoma 1 leukemia 1 breast carcinoma 1 lung cancer 1 melanoma 1 lymphoma

An arbitrary code was attributed to each sample to ensure the confidentiality of the patients after its collection and during the analysis process.

After collection, the CSF was immediately centrifuged at 1200 rpm at 4°C for 5 min. The cells and the supernatant were stored at 4°C for two days, after which they are placed at -80°C until further analysis.

[4] No information known about the gender of two patients of this group.

[5] No information known about the type of primary tumor of two patients of this group.

CSF samples colored due to blood contamination (xantochromic or erythrochromic) were discarded.

3.1.2. Metabolic profiling by NMR spectroscopy

The schematic representation of the steps involved in this procedure is shown in Figure 4.

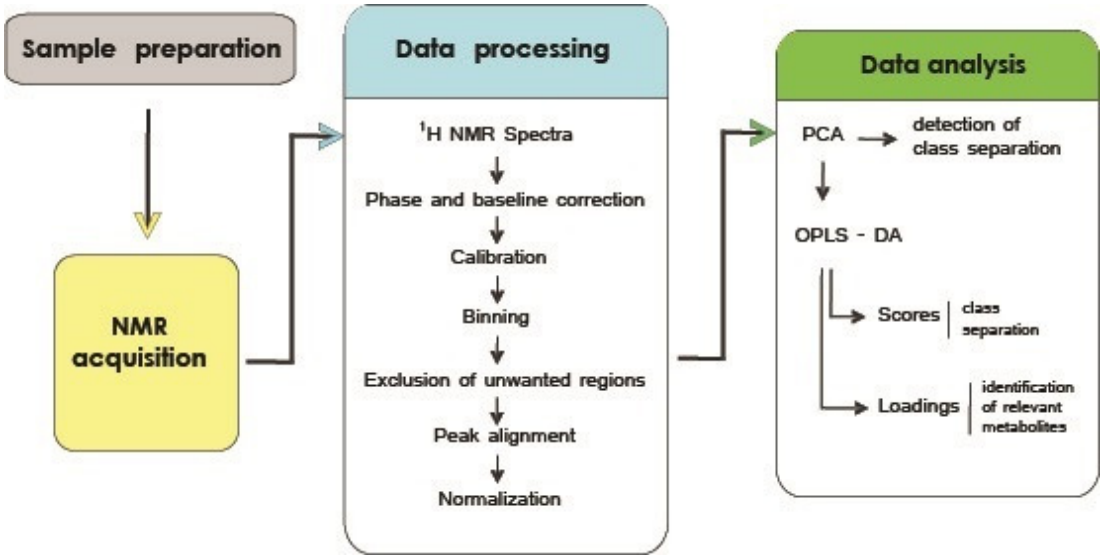

Figure 4 - Schematic representation of the steps involved in metabolic detection by NMR spectroscopy.

3.1.2.1. Samples preparation

CSF samples were thawed at room temperature. Each CSF sample (300 µL) was diluted with 300 µL of phosphate buffer solution 0.75 M with 2 mM sodium azide (NaN_3) and 100% of D_2O, to minimize inter-sample pH differences and provide a field lock. A volume of 550 µL of each prepared sample was then transferred to a 5 mm borosilicate NMR tube (*NewEra*), prior to NMR acquisition.

3.1.2.2. Equipment

The spectral acquisition was performed at CERMAX facility at *Instituto de Tecnologia Química e Biológica* (ITQB-UNL) in *Bruker Avance II+* 800 MHz spectrometer with 5mm TXI probe, at 298 K. All 1D and 2D experiments were acquired and analyzed using Topspin 2.1 software (*Bruker*).

3.1.2.3. Experiments

^{1}H noesy1d and j-resolved experiments were acquired in all samples. The utilization of the noesygppr1d pulse program allowed efficient water suppression, necessary for increase the intensities of the other signals on the samples. To in order to resolve signal overlapping in the spectra, it was used *J*-resolved experiment (jresqfpr pulse program). Acquisition and processing parameters used during this work were the same for all samples, allowing the comparison between samples (Table 3).

To assist metabolite identification other experiments were performed, such as 1D Carr-Purcell-Meiboom-Gill (CPMG), homonuclear 2D (^{1}H correlation spectroscopy (COSY) and ^{1}H Total Correlation Spectroscopy (TOCSY)) and heteronuclear 2D ^{1}H-^{13}C Heteronuclear Single Quantum Correlation (HSQC)) experiments.

Table 3 – Acquisition and processing parameters of the experiments performed for all samples.

^{1}H Noesy (noesygppr1d)	***J*-resolved (jresqfpr)**
Acquisition parameters	
NS = 128 DS = 4 RD = 5 s SW = 16025,64 Hz TD = 128K points Tm = 100 ms	NS = 1 DS = 16 RD = 2 s TD[F1] = 40 TD[F2] = 8192 SW[F1] = 78,125 Hz SW[F2] = 13368,984 Hz
Processing parameters	
SI = 128K points LB = 0.3 Hz WDW = exponential	SI [F1] = 40 SI [F2] = 8192 WDW = qsine

3.1.2.4. Data processing

Data processing is an intermediate step between spectra acquisition and data analysis necessary for the preparation of the metabolic profiling data to multivariate analysis. This step includes phase and baseline correction, chemical shift calibration, data-point reduction or "binning", the removal of redundant spectral regions, peak alignment (if necessary) and normalization.

Phase correction, baseline correction and calibration were carried out manually in *Bruker* TopSpin 2.1 software. The reference used for calibration was the α-glucose 1-H resonance at 5.22 ppm.

Prior to multivariate analysis, data was organized into two-dimension data tables of spectral intensities, in which each line corresponds to a sample and the columns to the chemical shifts, using R software application (www.r-project.org/). The spectra organized into a matrix were binned, the peaks were aligned with respect to all the peaks across the data set, the redundant spectral regions (namely noise regions, the water and urea peaks) were removed and the spectra were normalized.

Spectral binning was used in order to reduce the data dimensionality. This involves the averaging the intensities over intervals of 8 points in order to reduce the contribution from the noise, thus resulting in the reduction the number of points from 131072 to 16384 (Savorani *et al.*, 2010; Smolinska *et al.*, 2012). Since there are small chemical shifts differences between in some of the peaks of different spectra, peak alignment was performed using Cluster-based Peak Alignment (CluPA) algorithm (Vu *et al.*, 2011). The water region (4.60 – 4.90 ppm) present in all samples and the urea resonance (5.60 - 6.00 ppm). At the end, normalization is performed to take into account variations of the total amount of material and dilution of the samples.

3.1.2.5. Spectral assignments

The metabolite identification was based on the assignments achieved through the 1D and 2D NMR experiments and by comparison with spectra of pure standards from the Human Metabolome Database (HMDB) (Wishart *et al.*, 2007) and BioMagResBank (BMRB) (Ulrich *et al.*, 2008) databases, and from the Chenomx NMR suite 7.4 software internal database.

3.1.2.6. Multivariate analysis

Multivariate analysis was performed using SIMCA 13.0.3 software (Umetrics, Umeå, Sweden).

Firstly, data sets were analyzed using the unsupervised method Principal Component Analysis (PCA), which is a method doesn't take into account any prior information of the data. PCA expresses most of the variance within a dataset using a smaller number of variables, the Principal Components (PC). The first principal component represents as much of the variability of the data as possible and each succeeding PC takes into account as much as possible of the remaining variability. The analysis of NMR data by PCA results in two plots: the scores and the loadings. The scores plot represents a summary of all spectra since each point represents one spectrum, showing how related they are to each other and allowing to find trends, groupings and outliers. The loadings plots shows which variable from the NMR spectra are responsible for the trend observed in the corresponding scores plot (Jolliffe, 2002)

The supervised multiple regression method used was the Orthogonal Partial Least Squares Discriminant Analysis (OPLS-DA). In this model it is possible to compare two independent groups of samples and model predictive power was evaluated by Q^2 (goodness of prediction), a parameter obtained from randomly cross-validation of samples to avoid overfitting, to obtain the Q^2 distributions for the randomly permuted samples and for the original class of that samples. After validation, the relevant metabolite signals were identified in the loadings plots (Eriksson *et al.*, 2001; Madsen, Lundstedt, & Trygg, 2010)

3.2. *In vitro* study of CNS metastasis in human acute lymphoblastic leukemia (697-GFP) cell line

3.2.1. Biological Material

In order to study the tumor progression and the importance of tumor's microenvironment, our collaborators in the *Instituto de Medicina Molecular*, established

a leukemia murine model. Mice were inoculated in the tail vein with cells from 697 cell line, a commercial lineage of an in vitro model of Human Pre-B cell leukemia (American Type Culture Collection (ATCC)). This cell line was transduced with a luciferase-green fluorescence protein (Luc-GFP) reporter gene allowing the *in vivo* and *in vitro* visualization of the cells in order to evaluate the disease progression in further studies by fluorescence microscopy, sorting by fluorescence-activated cell sorting (FACS) analysis or luminescence analysis.

Two groups of mice where maintained with two distinct types of diets: a normal and a fat diet (1.2% cholesterol), in order to study the influence of diet in tumor metastasis. Leukemia cells were isolated from the places where the cells appeared: skin, bone marrow (BM) and brain. The data regarding the diet and the localization of tumor metastasis is represented in Table 4.

Table 4 - Diet and localization of tumor cells in mice inoculated with 697-GFP cell line.

Tumor cells culture	Mouse diet	Localization of tumor metastasis
S	Normal	Skin
B	Normal	Brain
BM	Normal	Bone marrow
B2 and B3	Fat	Brain
S1, S2 and S3	Fat	Skin

The cell lines were cultured at 37°C in a humidified 5% CO_2 environment in RPMI 1640 medium without L-glutamine (BE12-167F, *Lonza*). Medium was supplemented with 10% fetal bovine serum (FBS) (S 0615, *Biochrom*), 1% Antibiotic-Antimycotic (AA) (15240062, Anti-Anti, *Invitrogen*) and 1% L-Glutamine (25030-024, *Gibco, Life Technologies*).

Cell lines were propagated until approximately $1x10^6$ cell/ml and splitted 1:2 for them to continue to grow. Cell number was determined by using a *Bürker* counting chamber (haemocytometer).

Parental lineages (not inoculated in mice) were grown in parallel and used as control.

3.2.2. Metabolic profiling by NMR spectroscopy

NMR assay was performed to determine the metabolic profile of parental cells and cells isolated from mice.

Cells ($1x10^7$) were submitted to starvation in order to synchronize cells in the same stage of cell division, being cultured in 40 mL of RPMI 1640 medium (BE12-167F, *Lonza*) supplemented with 1% AA (15240062, Anti-Anti, *Invitrogen*) and L-Glutamine 200 mM (25030-024, *Gibco, Life Technologies*), at 37°C and 5% CO_2 without FBS. After 8 h, culture medium was supplemented with 1% of FBS (S 0615, *Biochrom*) and 48 h later, cells were harvested by centrifugation at 1200 rpm for 3 min at room temperature. Afterwards, supernatants (cell media) were collected and stored at -80°C and cell pellets washed twice with phosphate buffered saline (PBS).

A methanol and chloroform extraction was performed in cell pellets, in order to extract the organic and the aqueous fractions. It was added 4 ml methanol for 1 g wet cell weight and 2 volumes of water. Mixed and incubated on ice for 5 min; 1 volume of chloroform was added and mixed, and 1 volume of water was added and incubated on ice for 10 min. Finally, samples were centrifuged at 4000 rpm for 15 min at 4°C, the organic (lower) and aqueous (upper) phases were collected separately and stored at -20°C until they were dried under speed vaccum in a Speed Vac Plus *Savant SC110A*.

The aqueous phases were dissolved in 540 µL of D_2O with 60 µl of phosphate buffer 0.35 M with 2 mM sodium azide (NaN_3) in 100% of D_2O. Samples were mixed in the vortex and transferred to a 5 mm NMR tube (*New Era*).

The organic phases were dissolved in 600 µL of deuterated chloroform ($CDCl_3$), mixed in the vortex and transferred to a 5 mm NMR tube (*New Era*).

To 300 µL supernatants, 240 µL of D_2O and 60 µL of phosphate buffer 0.35 M with 2 mM sodium azide (NaN_3) in 100% of D_2O. The sample was mixed in the vortex and transferred to a 5 mm NMR tube (*New Era*).

The equipment used was the same as in section **3.1.2.2**. The experiments performed for the analysis of supernatants and aqueous extracts were the same as in section **3.1.2.3.** For organic phases, *zg* pulse program was the standard 1D experiment used. The data processing, spectral assignments and multivariate analysis steps were similar to those used for CSF samples.

3.2.3. Gene expression

In order to understand the role of fat diet in leukemia growth and disease burden in mice models, the expression of key metabolic genes was evaluated to determine which pathways were responsible for the metabolic patterns found in 697-GFP parental cell lines and in cells isolated from mice maintained in normal and fat diet.

The evaluated genes are involved in gluconeogenesis (ALT, PCK1, PCK2, FBP1, PFKFB1); lactate metabolism and transport (MCT1, MCT4, LDHA, LDHB, LDHC); glucose transport (SGLT1, GLUT1) and the conversion of glutamate into α-ketoglutarate (IDH1, IDH2).

3.2.3.1. Reverse transcription polymerase chain reaction (RT-PCR)

Reverse transcription polymerase chain reaction (RT-PCR) is one of the variants in polymerase chain reaction (PCR), mostly utilized in molecular biology to quantify mRNA expression levels from biologic samples. This technique is used to synthesize single-stranded complementary DNA copy (cDNA) from a RNA template, using a

reverse transcriptase. The resulting cDNA is then amplified and quantified by PCR (Freeman *et al.*, 1999).

Total ribonucleic acid (RNA) was extracted from each cell lineage using TRI Reagent® (T9424, *SIGMA-ALDRICH®*), according to the manufacturer's protocol. Samples were stored at -80^{0}C. The quantification of RNA was determined in a *Nanodrop 2000* spectrophotometer (*Thermo Scientific*).

Total cDNA was synthesized from 1 µg of the RNA extracted and it was performed in a *T3000* thermocycler (*Biometra*), according to the program described in Table 5.

Table 5 – Program utilized for cDNA synthesis.

Stage	Cycles	Temperature (°C)	Time (min)
Denaturation	1	70	10
Cooling	1	4	5
cDNA synthesis	1	42	90
Inactivation	1	75	15
Cooling	-	4	∞

For each synthesis reaction it was prepared a mix of 8 µL containing 1 µg RNA in RNase free water up to 7.5 µL and 0.5 µL random primers (11034731001, *Roche*).

This mix was incubated at 70°C for 10 min, for the annealing between RNA and the random primers. Afterwards, the temperature was decreased to 4^{0}C in order to add a second mixture composed by: 4 µl first Strand Buffer 5X (Y02321, *Invitrogen*), 2 µL dithiothreitol 0.1 M (DTT) (Y00147, *Invitrogen*), 2 µL deoxynucleotides (dNTPs) mix (10 mM) (28-4065-22V, 28-4065-02V, 28-4065-12V and 28-4065-32V, *GE Healthcare*), 1 µL RNAse OUT™ Recombinant RNase Inhibitor 40 U/ µL (10777-019, *Invitrogen*), 1

µL Superscript II® 200 U/ µL (18064-022, *Invitrogen*) and double-destilled water (ddH2O) in order to have a total volume of 12 µL.

3.2.3.2. Real time quantitative polymerase chain reaction (RQ-PCR)

Real time quantitative polymerase chain reaction (RQ-PCR) allows the detection and measurement of products generated during each cycle of the polymerase chain reaction (PCR), process which are directly proportionate to the amount of template prior to the start of the PCR process (Ginzinger, 2002). Currently, this technique has various applications in many fields of biological research since it permits the analysis of gene expression with accuracy, sensitive and fast results, as for example in relative quantification of messenger ribonucleic acid (mRNA transcription) (Derveaux *et al.*, 2010).

In RQ-PCR, a reaction mixture was prepared for all the genes mentioned in section **3.2.3** for each cell sample, in triplicates. Each reaction mixture contained 1 µL of cDNA, 4 µL of Power SYBR® Green PCR master mix (4367659, Applied Biosystems by *Life Technologies*), 3 µL Power SYBR® Green PCR master H_2O (4367659, Applied Biosystems by *Life Technologies*), and 0.15 µL of both forward and reverse primers (5 µM), to a final volume of 7.3 µL per well.

All samples were run in triplicate (biological triplicates) and 18S rRNA was the housekeeping gene used to normalize the results. RQ-PCR was performed in LightCycler© 480 instrument (*Roche*), according to the program ABI389 from Applied Biosystems by *Life Technologies* described in table 6.

Table 6 – Program utilized for RQ-PCR.

Stage	Cycles	Temperature (°C)	Time
Incubation	1	50	2 min
Incubation	1	95	10 min
PCR			
Denaturation	45	95	15 seconds
Annealing		60	15 seconds
Elongation		72	20 seconds
Melting curves	1	95	15 seconds
		60	15 seconds
		95	continuous
Cooling	1	40	10 seconds

The results obtained in RQ-PCR were analyzed in LightCycler 480 software (*Roche*). Expression levels from each sample were normalized to 18S rRNA and relatively quantified to those obtained in the parental lineage. For each cell lineage, average and standard deviation of the relative gene expression values were calculated and statistical analysis was performed.

3.2.4. Protein levels

Since the metabolic effectors are proteins, the levels of gluconeogenic proteins (ALT, PCK1, PCK2, FBP1 and PFKFB1), lactate transporters (MCT1 and MCT4) and conversion of pyruvate into lactate (LDHA and LDHB) were evaluated by western blot for all the cell lineages specified in **3.2.1**.

3.2.4.1. Western Blotting

Western blotting is a powerful and widely used method for protein detection in complex biologic samples. This technique consists in the immunodetection of proteins that were previously separated by electrophoresis, transferred onto a membrane and detected with specific antibodies (Kurien & Scofield, 2006).

Cell pellets were collected, centrifuged and washed with Phosphate Buffered Saline (PBS).

To obtain the cytoplasmic proteins, the cell pellet was resuspended with Radio-Immunoprecipitation Assay (RIPA) buffer (Appendix A) and stored at -20^{0}C, where cell lysis occurred. For trans-membrane proteins, cell extracts were performed with a Mitochondria Isolation Kit (MITOISO2, *SIGMA*), according to the manufacturer's protocol.

The lysates were centrifuged at 14000 rpm for 5 min at 4°C. Part of the supernatants were used for the determination of protein concentration based on the Bradford method, using protein assay reagent (500-0006, *Bio-Rad*), through spectrophotometric quantification at 595 nm. After quantification, Loading Buffer 5X (Appendix A) and 10% β-mercaptoethanol (M3148, *Sigma-Aldrich*®) were added to the lysates, and protein was denatured by boiling at 95-100°C for 10 min. The samples were then centrifuged at 14000 rpm for 2 min at 4°C and placed on ice.

From each sample, the same amount of total protein was loaded into a 15% SDS-polyacrylamide gel (SDS-PAGE) (Appendix A). Electrophoresis was carried out in MINI-PROTEAN Tetra Electrophoresis System (Bio-Rad) at 135 V for 1h30 in TGS buffer (Tris-Glycine-SDS buffer 10X, 161-0772, *BioRad*). After electrophoresis the proteins were transferred to an Immun-Blot® PVDF membrane with a Mini Trans-Blot® Electrophoretic Transfer Cell (*BioRad*), using transfer buffer (Appendix A), overnight at 4^{0}C and 60 volts. To block non-specific bindings to the membrane 5% (w/v) non-fat milk (Molico, Nestlé) in PBS 0.1% (v/v) Tween 20 (Appendix A) was used, incubation occured for 2 h at room temperature, with slow shaking. For the detection of the proteins

of interest, the membranes were incubated with primary specific antibodies Anti-PCK1 (R04368, *Sigma-Aldrich*®), Anti-PFKFB1 (SAB1408617, *Sigma-Aldrich*®), monoclonal anti-rabbit MCT1 (AB3538P, *Milipore*), monoclonal anti-rabbit MCT4 (SC-50329, *Santa Cruz*), monoclonal anti-mouse LDHB (WH0003945M1, *Sigma-Aldrich*®) at concentration 1:250 in 5% (w/v) non-fat milk (Molico, Nestlé) in PBS 0.1% (v/v) Tween 20 (Appendix A), overnight at 4°C, with mild shaking.

To remove unbound primary antibody, the membranes were rinsed 3 times, for 5 min, with PBS 0.1% (v/v) Tween 20 (Appendix A). The membranes were then incubated with secondary antibody IgG-conjugated Horse raddish peroxidase (HRP) anti-rabbit (31460, Thermo Scientific) or anti-mouse (31430, Thermo Scientific) diluted 1:5000 in 5% (w/v) non-fat milk in PBS 0.1% (v/v) Tween 20 (Appendix A), for 2 h, at room temperature.

After incubation, the membranes were rinsed 3 times, for 5 min, with PBS 0.1% (v/v) Tween 20 (Appendix A). Immunoreactive bands were detected by using SuperSignal® West Pico Chemiluminescent Substrate (34080, *Thermo Scientific*) and converted to digital images in a ChemiDoc XRS System (*BioRad*) equipped with Image Lab software.

β-actin was used as endogenous control for protein quantification in the Western-blot membranes. For this purpose, after development of the bands of interest, the membranes were again rinsed 3 times, for 5 min, with PBS 0.1% (v/v) Tween 20 (Appendix A) and re-incubated overnight at 4°C with anti-β-actin (A5441, *Sigma-Aldrich*®) diluted 1:1000 in 5% (w/v) non-fat milk in PBS 0.1% (v/v) Tween 20 (Appendix A) with mild shaking. Later, the membranes were revealed as describe above and converted to digital images. Image J software (rsb.info.nih.gov/ij/) was used to analyze and quantify all bands obtained.

3.2.4.2. Immunofluorescence

Immunofluorescence is a technique that uses antibodies labeled with fluorochromes to detect specific target antigens within a cell, allowing their visualization in a fluorescence microscope (Odell & Cook, 2013).

Cells were collected and centrifuged at 1200 rpm for 2 min and ressuspended in 500 µL of PBS. Cell suspensions (100 µL) were transferred onto a glass slide by centrifugation in a *Citospin* at 1200 rpm for 5 min, where it formed

Cells were fixed with methanol, for 30 min. Each group of cells was delimitated with a hydrophobic pen (S2002, *Dako*) and then was added PBS 0.1% (w/v) BSA (Appendix A) for 30 min at room temperature, to block unspecific bindings. Each circle (except the negative controls, for secondary antibody specificity) was incubated with 50 µL of primary antibodies MCT1 (monoclonal anti-rabbit, AB3538P, *Milipore*) and MCT4 (monoclonal anti-rabbit, SC-50329, *Santa Cruz*) diluted 1:100 in PBS 0.1% (w/v) BSA (Appendix A), overnight at 4°C, in a humid chamber. In the negative controls it was added 50 µL PBS 0.1% (w/v) BSA (Appendix A).

Slides were rinsed with PBS 3 times for 5 min, and incubated with secondary antibody Alexa Fluor© 488 anti-rabbit (A-11034, *Invitrogen - Life Technologies Inc*) diluted 1:1000 in PBS 0.1% (w/v) BSA (Appendix A) for 2 h at room temperature, protected from light.

After incubation, slides were rinsed 3 times for 5 min with PBS and then mounted with *Vectashield* mounting medium with DAPI (4'-6-diamidino-2-phenylindole) (H-1200, *Vector Labs*) and sealed with a lamella and nail polish.

Slides were observed under a fluorescence microscope Axio Imager Z1 microscope (*Zeiss*). Images were acquired at x200 and x400 magnification with *AxioVision* software.

3.2.5. Cell cycle analysis by FACS

Loss of control over cell proliferation is regarded as one of the most important traits of cancer. Therefore, it is necessary to study cell proliferation and cell cycle activity in tumor cells. A significant improvement in these studies was achieved by the introduction of the technique of Fluorescence-activated cell sorting (FACS) analysis (Eidukevicius *et al.*, 2005).

FACS is a technique used for the analysis of multiple parameters of different types of cells within heterogeneous populations. This is based upon the passage of cells through a laser excitatory beam, capturing the fluorescence emitted by each labeled cell as it passes along the laser and analyses the quantity and intensity of the fluorescence, converting the information to histograms (Macey, 2007).

With this technique it is possible to quantify the DNA of the cells stained with propidium iodide (PI), a fluorescent DNA intercalating dye that binds to cells. This analysis allows to recognize four distinct phases of the cell cycle - G1, S, G2, M phases – in a proliferating cell population. However, G2 and M phases cannot be distinguished (Cecchini, Amiri, & Dick, 2012; Macey, 2007).

Cells ($1x10^7$) were synchronized by starvation, being cultured in 40 mL of RPMI 1640 medium (BE12-167F, *Lonza*) supplemented with 1% AA (15240062, Anti-Anti, *Invitrogen*) and L-Glutamine 200 mM (25030-024, *Gibco, Life Technologies*), at 37°C and 5% CO_2 without FBS. After about 8 h, cell pellets were collected (time point 0) and the medium was supplemented with 1% of FBS (S 0615, *Biochrom*). Afterwards, cells were collected at different time points: 2, 4, 8, 26, 32 and 50 h after FBS stimulation.

Each cell samples were harvested at each time point and washed twice with PBS cell and pellets were fixed and permeabilized in 500 µL of ethanol 70% (v/v). After that, 100 µL propidium iodide solution (50 µg/mL) (Appendix A) was added to each sample, followed by incubation at 37°C for 40 min. Samples were washed with PBS and centrifuged at 1200 rpm for 5 min at 4°C.

Finally supernatants were discarded and cells were ressuspended in 200 μL PBS 0.1% (w/v) BSA (Appendix A) and analyzed by FACS (*FACScalibur, Becton Dickinson*). All samples were made in triplicates.

FACS analysis was performed in *FlowJo* software. In this analysis, dead cells and aggregated cells were excluded.

3.2.6. Cell death (apoptosis and necrosis) analysis by FACS

Apoptosis is a carefully regulated process of cell death that plays an important role in tissue homeostasis. This physiological process, unlike necrosis or accidental cell death, is characterized by some specific morphological and biochemical changes that, such as nuclear chromatin condensation and fragmentation, cytoplasmic shrinkage and compaction, loss of plasma membrane asymmetry (Allen, Hunter, & Agrawal, 1997; Darzynkiewicz *et al.*, 1992; Duvall & Wyllie, 1986; Kroemer, Petit, Zamzami, Vayssière, & Mignotte, 1995; Lincz, 1998; van Engeland *et al.*, 1998).

Phosphatidylserine (PS) is an important phospholipid membrane component, located on the surface of the cell membrane of normal live cells. However, when a cell undergoesapoptosis, PS naturally flips from the intracellular side to the extracellular surface of the cell, resulting in the exposure of PS to external cellular environment (van Engeland *et al.*, 1998).

Annexin V was shown to interact strongly and specifically with PS which allows a quick and reliable detection method of apoptosis by targeting the loss of plasma membrane asymmetry.

Propridium iodide (PI), a nucleic acid binding dye which cannot penetrate live cells and apoptotic cells, can stain dead cells by binding tightly to the nucleic acids from the cell. The simultaneous use of Annexin V and PI allows the discrimination of intact cells (Annexin−/PI−) from early apoptotic cells (Annexin+/PI−), late apoptotic cells

(Annexin+/PI+) and necrotic cells (Annexin−/PI+) (van Engeland *et al.*, 1998; Vermes *et al.*, 1995).

Within the context of the present thesis, apoptosis assay was performed to identify potential differences in the cell death and apoptosis patterns of the tumor cell lines isolated from the mice exposed to different diets (normal and fat diet) and due to the occurrence of tumor in different organs (BM, CNS and skin).

Cells were plated in 48 plate tissue dishes at a $1x10^4$ cells/mL concentration, with 300 µL of RPMI 1640 medium (BE12-167F, *Lonza*) supplemented with 1% AA (15240062, Anti-Anti, *Invitrogen*) and L-Glutamine 200 mM (25030-024, *Gibco, Life Technologies*), at 37ºC and 5% CO_2 without FBS. After about 8 h, 1% of FBS was added (S 0615, *Biochrom*).

Cells were collected at 0 h and 24 h and centrifuged at 1200 rpm for 2 min and washed with 500 µL PBS 0.2% (w/v) BSA (Appendix A). Afterwards, samples were resuspended in 100 µL of annexin V binding buffer (Appendix A), stained with 1 µL FITC Annexin V (640906, *Bio Legend*) and 1 µl PI solution (50 µg/mL). Samples were incubated for 5 min at room temperature in the darkand then analyzed by FACS (*FACScalibur, Becton Dickinson*). All samples were performed in triplicates.

FACS data analysis was performed in *FlowJo* software.

3.2.7. Statistical analysis

Results were analyzed by 2-way ANOVA to evaluate its statistical significance, using GraphPad Prism 6 software. Results were considered significant when ‘p-value < 0.05’.

4. Results and discussion

4.1. Study of CSF from patients with and without CNS metastasis by ^{1}H NMR spectroscopy

The work presented on this chapter aims to study the CSF from cancer patients with and without cell invasion to the CNS based on a metabonomic approach using NMR technique. This includes the compositional analysis of these samples using both unsupervised and supervised multivariate analysis.

4.1.1. ^{1}H-NMR profiling

As mentioned in section **3.1.**, ^{1}H-NMR spectra were obtained from a total of 186 samples of CSF, in which 176 were from patients without cell invasion in the CNS (control samples) and the other 10 samples were from patients diagnosed with cell invasion in the CNS. Typical spectra of these two groups are shown in Figure 4, some of the metabolites identified are indicated. We were able of identify 48 metabolites in the CSF spectra, 40 of them present in all samples (the metabolites are listed in Table 7 with its corresponding chemical shifts).

Some of the metabolites, for example lactate and glucose, were immediately identifiable in the spectra. In the case of these two metabolites, it is clear differences in their content between the two groups, suggesting that the metabolic profiles of CSF samples with and without the presence of tumor cells are significantly different.

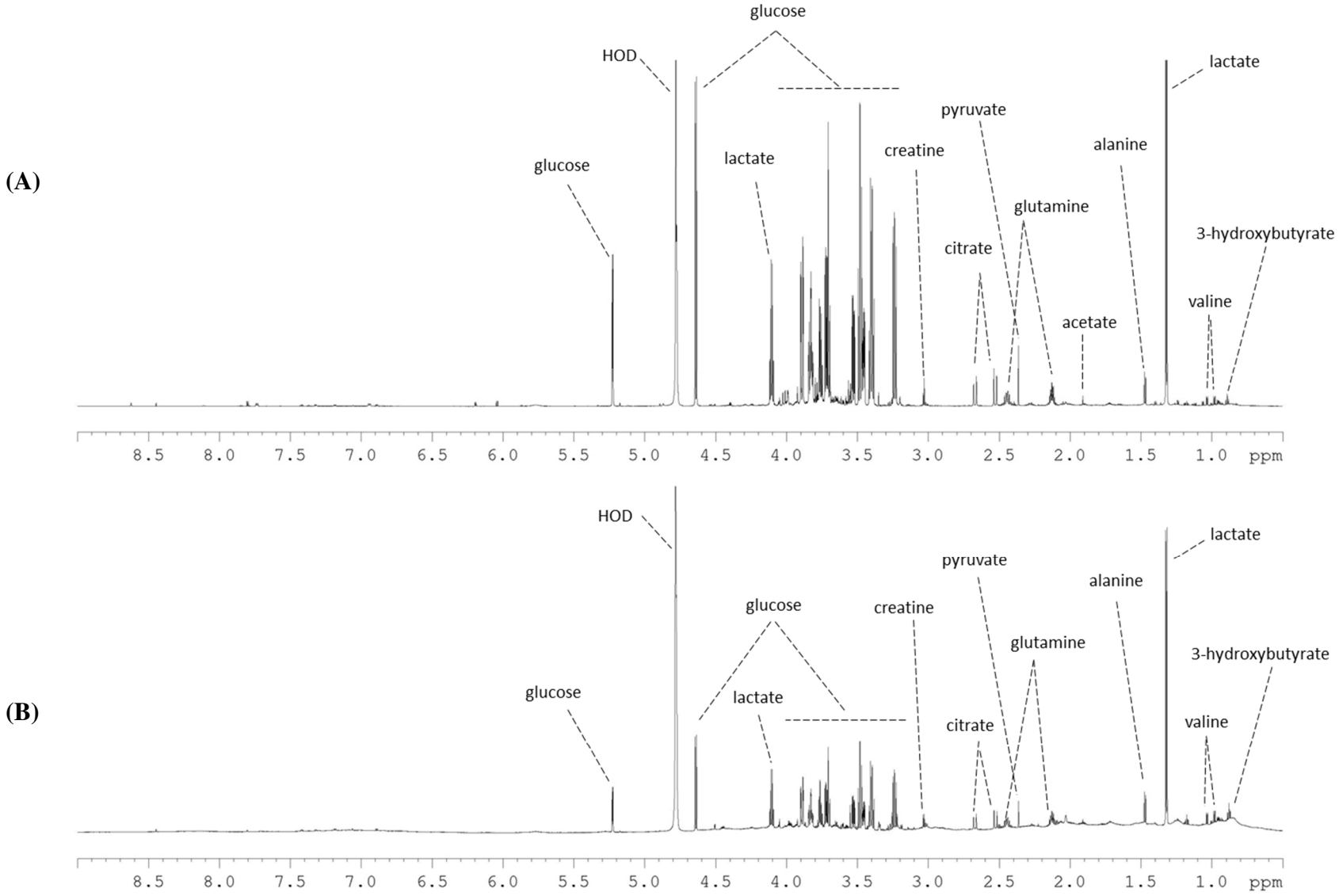

Figure 4 – Representative ^{1}H NMR spectra for (A) control samples and (B) cell invasion samples, with some of the most intense metabolites identified.

Table 7 – Full list of the metabolites identified in CSF samples and respective signals.

	Metabolites	δ ^{1}H (ppm)
Alcohols	ethanol	1.11 (t), 3.61 (q)
	glycerol	3.55 (m), 3.64 (m), 3.78 (tt)
	methanol	3.34 (s)
	propylene glycol *	1.13 (d), 3.43 (dd), 3.58 (dd), 3.87 (m)
Amino acids	alanine	1.46 (d), 3.76 (q)
	arginine *	1.68 (m), 1.90 (m), 3.23 (t), 3.76 (t)
	citrulline *	1.56 (m), 1.87 (m), 3.14 (q), 3.74 (dd)
	glutamine	2.04 (m), 2.12 (m), 2.34 (m), 3.75 (dd)
	glutamate	2.12 (m), 2.45 (m), 3.77 (t)
	glycine	3.54 (s)
	histidine	3.16 (dd), 3.23 (dd), 3.98 (dd), 7.09 (d), 7.90 (d)
	isoleucine	0.93 (t), 0.997 (d), 1.25 (m), 1.46 (m), 1.97 (m), 3.66 (d)
	leucine	0.95 (t), 1.70 (m), 3.72 (m)
	proline *	1.99 (m), 2.06 (m), 2.34 (m), 3.33 (dt), 3.41 (dt), 4.12 (dd)
	methionine *	2.16 (m), 2.63 (t), 3.85 (dd)
	lysine	1.46 (m), 1.71 (m), 1.89 (m), 3.02 (t), 3.74 (t)
	valine	0.97 (d), 1.03 (d), 2.26 (m), 3.60 (d)
	phenylalanine	3.19 (m), 3.98 (dd), 7.32 (d), 7.36 (m), 7.42 (m)
	threonine	1.31 (d), 3.58 (d), 4.24 (m)
	tryptophan	3.29 (dd), 3.47 (dd), 4.07 (dd), 7.19 (m), 7.27 (m), 7.31 (s), 7.53 (d), 7.72 (d)
	tyrosine	3.02 (dd), 3.17 (dd), 3.92 (dd), 6.88 (m), 7.17 (m)
Organic acids	2-hydroxyisovalerate	0.82 (d), 0.95 (d)
	2-hydroxybutyrate	0.89 (t), 1.64 (m), 1.73 (m), 3.99 (m)
	3-hydroxyisobutyrate	1.11 (d), 2.65 (m), 3.69 (m)
	3-hydroxyisovalerate	1.26 (s), 2.35 (s)
	3-hydroxybutyrate	1.20 (d), 2.31 (ABX), 2.41 (ABX), 4.18 (ABX)
	3-methyl-2-oxovalerate	0.90 (t), 1.10 (d), 1.46 (m), 1.70 (m), 2.93 (m)
	acetate	1.91 (s)
	acetoacetate	2.27 (s), 3.43 (s)
	ascorbate	3.33 (m), 4.01 (m), 4.50 (d)
	lactate	1.32 (d), 4.10 (q)
	citrate	2.53 (d), 2.65 (d)
	formate	8.44 (s)
	pyruvate	2.46 (s)
	succinate *	2.39 (s)
Sugars	glucose	alpha: 3.40 (t), 3.52 (dd), 3.70 (t), 3.75 (m), 3.82 (m), 3.83 (ddd), 5.22 (d)
		beta: 3.23 (dd), 3.39 (t), 3.45 (ddd), 3.48 (ddd), 3.71 (dd), 3.88 (dd), 4.63 (d)
	fructose	3.58 (m), 3.70 (m), 3.82 (m), 3.90 (dd), 4.01 (m), 4.03 (dd), 4.12 (m)
	mannose	3.37 (dd), 3.58 (t), 3.65 (m), 3.74 (m), 3.80 (m), 3.84 (m), 3.88 (dd), 3.92 (m), 5.17 (d)
	myo-inositol	3.26 (t), 3.52 (dd), 3.61 (t), 4.05 (t)
Others	acetaminophen *	1.97 (s), 6.66 (d), 7.32 (d), 9.11 (s), 9.63 (s)
	acetone	2.22 (s)
	choline	3.18 (s), 3.50 (dd), 4.05 (ddd)
	creatine	3.02 (s), 3.92 (s)
	creatinine	3.03 (s), 4.05 (s)
	dimethyl sulfone *	3.14 (s)
	urea	5.78 (s)
	xanthine	7.89 (s)

*, metabolites found only in some samples.
s, singlet; d, doublet; dd, doublet of doublets, ddd, doublet of doublet of doublets; t, triplet; m, multiplet; ABX, ABX pattern.

4.1.2. Multivariate analysis of control samples

After the spectra processing step mentioned in **3.1.2.4.**, explorative analysis was performed by multivariate analysis on the entire spectral dataset of control samples. For all samples some clinical information was supplied: the type of primary tumor, gender and age (children/adult), according to Table 1.

Both age and gender are being increasingly recognized as important factors influencing CNS structure and function. However, there are relatively few data on actual neurochemical differences between the sexes in human subjects or on their interaction with age (Zubieta, Dannals, & Frost, 1999).

Principal component analysis (PCA), an unsupervised analysis, is the most widely used multivariate analysis method in metabolic fingerprinting and chemometrics in general. The objective of PCA is to achieve a linear transformation that preserves as much of the variance in the original data as possible, in the lower dimensionality output data (Jolliffe, 2002).

PCA analysis was applied to the NMR data of 176 CSF samples (control samples). In the Figure 5 are represent the PCA score plots (PC1 vs PC2) of control samples dataset with each point (or spectrum) colored according the age of the patient, providing a map of how the points relate to each other.

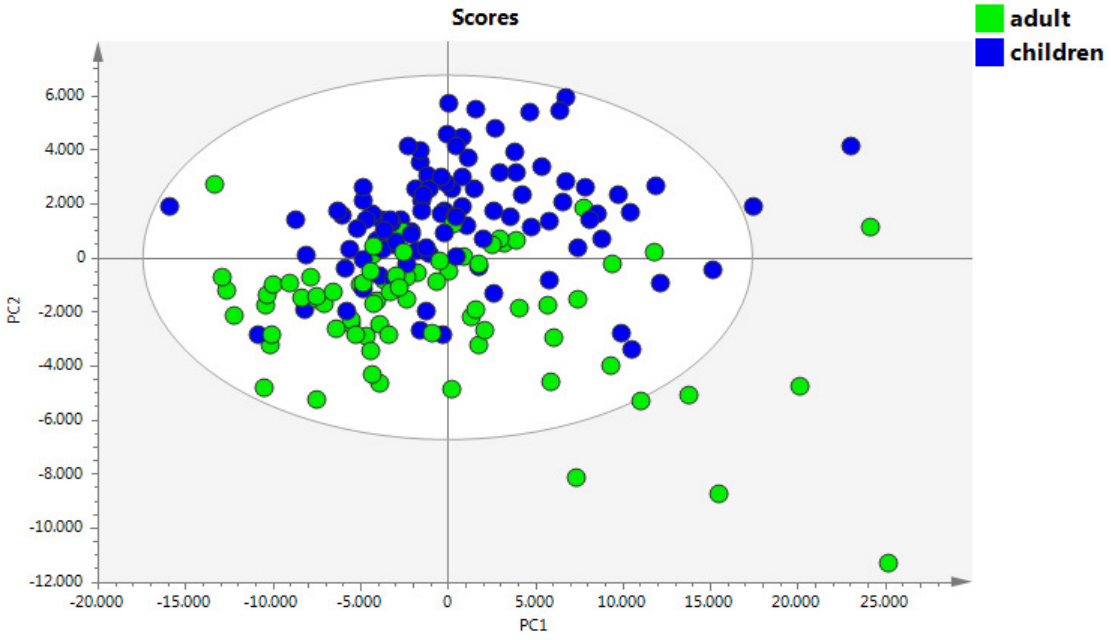

Figure 5 – PCA score plot of the two first PCs using ^{1}H-NMR data of control samples (n=176) and colored according to age (77 adults and 99 children). PC1 = 46.3 % and PC2 = 6.93 %.

The PCA analysis based on the age of the patients shows that the sub-group children have a tendency to be separated from the adults sub-group along the PC2. This indicates that children and adults have different metabolic profiles. The discrimination between the two groups is based in the content of some metabolites. Formate, tyrosine, ascorbate, *myo*-inositol, arginine, creatinine, glutamine, acetate, lactate, 3-hydroxybutyrate, ethanol, isoleucine, leucine and valine are increased in the children (and consequently decreased in the adults); while glucose, glycerol, citrate, alanine and others metabolite(s) unidentified are found decreased in the children and increased in the adults (Figure 6).

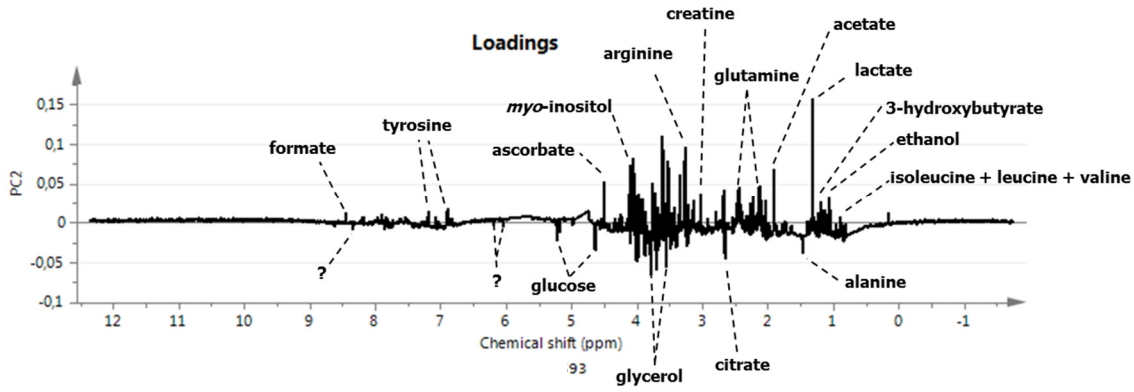

Figure 6 – PCA loading plot of PC2 using ^{1}H-NMR data of adults samples of control samples with the metabolites that are found increased (positive part of PC2) and decreased (negative part of PC2) in the children and that are increased (negative part of PC2) and decreased (positive part of PC2) in the adults.

To explore the discrimination of children samples from adults' samples, supervised methods were applied. This type of approach may facilitate the discovery of the largest discrimination between two groups, in contrast to unsupervised methods (PCA) that only allow identifying the main sources of variability within a data set.

The Orthogonal Partial Least Squares Discriminant Analysis (OPLS-DA) model using the class identity age as response variable (Y) was obtained, with one predictive and three orthogonal components. Cumulative explained variance (R2Y) of 0.726 and goodness of prediction (Q2) of 0.511 were obtained by the model, which is higher than the empirically inferred acceptable value of ≥ 0.4 for a biological model. This result is visually represented in the OPLS-DA score plot (Figure 7), where most of the samples are separated from each other by the value 0. These results suggest that the metabolite

composition of the CSF from children and adults is different, although the influence of this parameter appears be limited.

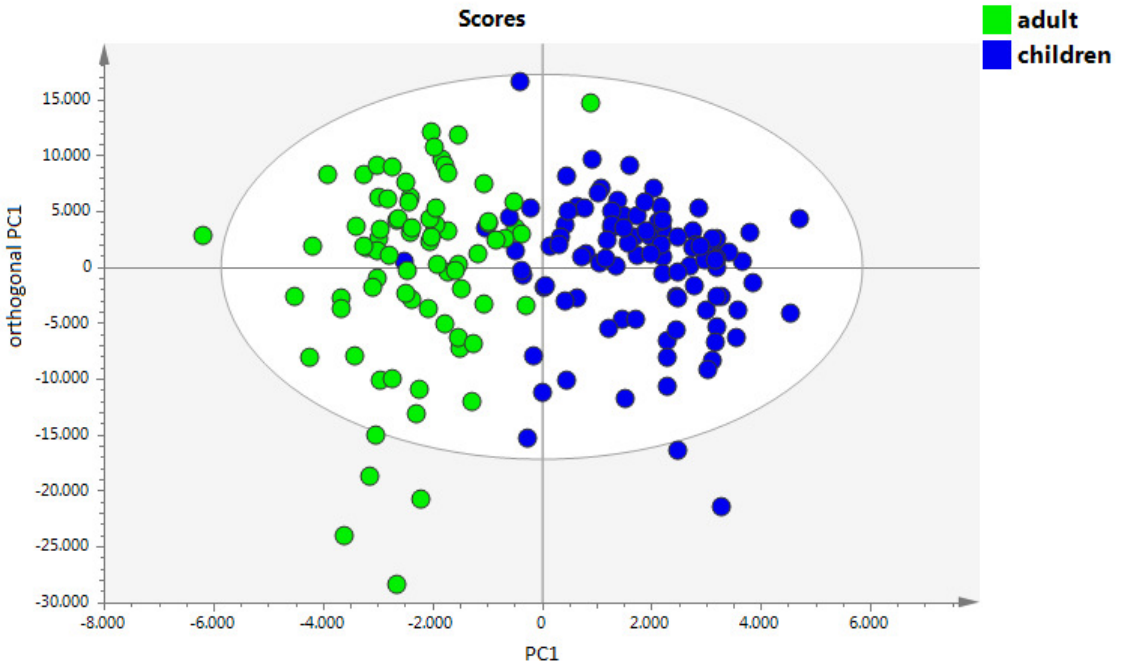

Figure 7 – OPLS-DA score plot of the first and the orthogonal components using ^{1}H-NMR data of control samples (n=176), colored according to the age of the patients (77 adults and 99 children). R2Y (cum) = 0.726 and Q^2 (cum) = 0.511.

The loadings for this model indicated the metabolites that contribute for this separation are: formate, histidine, tyrosine, glucose, ascorbate, *myo*-inositol, acetate, lactate, 3-hydroxybutyrate, valine, isoleucine and leucine are increased in the children and consequently decreased in the adults; while mannose, glycerol, citrate, alanine and 2-hydroxybutyrate are found decreased in the children and increased in the adults (Figure 8).

When comparing this results to the ones obtained in the loading plot of PCA (Figure 6), it is possible to see that most of the metabolites that are varying are the same in the two analyses, i.e. formate, tyrosine, ascorbate, *myo*-inositol, acetate, lactate, 3-hydroxybutyrate, isoleucine and leucine are increased in the children and glycine, citrate and alanine are increased in the adults. However, glucose is increased in children in PCA, but decreased in OLPS-DA.

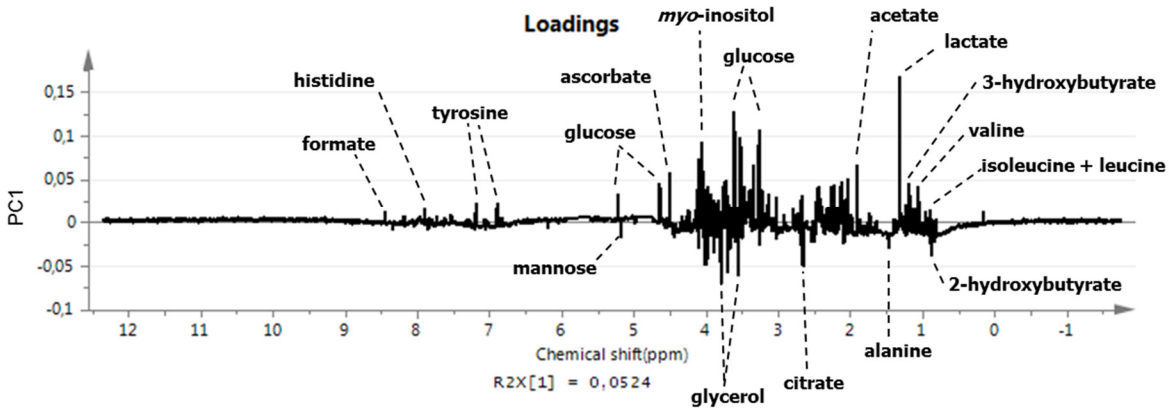

Figure 8 – OPLS-DA loading plot of PC1 using ^{1}H-NMR data of control samples (n=176), with the metabolites that are found increased (positive part of PC1) and decreased (negative part of PC1) in the children and that are increased (negative part of PC1) and decreased (positive part of PC1) in the adults.

These results coincide with the results previously obtained in other studies. Because ethical considerations prohibit subjecting young infants to a potentially painfully procedure (ie, lumbar puncture) before they are able to assent, the number of studies regarding children are limited.

It is known that a healthy neonate's CSF protein concentration is normally 2 to 3 times higher than an adult and declines between birth and early childhood. The most rapid rate of decline is thought to occur in the first 6 months of life as the infant's blood-CSF barrier matures (Statz & Felgenhauer, 1983). Immaturity of the blood-CSF barrier is thought to result in higher CSF protein concentrations for neonates and young infants when compared with older children and adults (Bonadio *et al.*, 1992; Wong *et al.*, 2000). But since lumbar punctions are only performed when required by physicians, there could be a limitation that could potentially lead to the inclusion of infants with conditions associated with higher CSF protein concentrations (Shah *et al.*, 2011)

For the adults, CSF total protein concentrations were found increased with age: elderly had higher concentrations than the young (May *et al.*, 1990).

Daners and co-workers (2012) also verified that in healthy humans, age significantly influences various components of cerebral arterial blood flow and CSF dynamics (Daners *et al.*, 2012).

Since there are differences between children's CSF and adults CSF, the further analysis was performed taking into account these differences. For each sub-group, two other clinical parameters (gender and type of primary tumor) were analyzed.

Figure 9 and Figure 10 show the PCA scores plot of the two first PCs based on the gender of children (n=99) and adults (n=77), respectively. In both situations, no differences are clear between the groups. This indicates that a large source of the variance in the data does not correspond to these two sub-groups. It is important to mention that further PCs also did not show clusters either. There is no clustering of male and female CSF samples in both children and adults group (Figure 8 and 9, respectively).

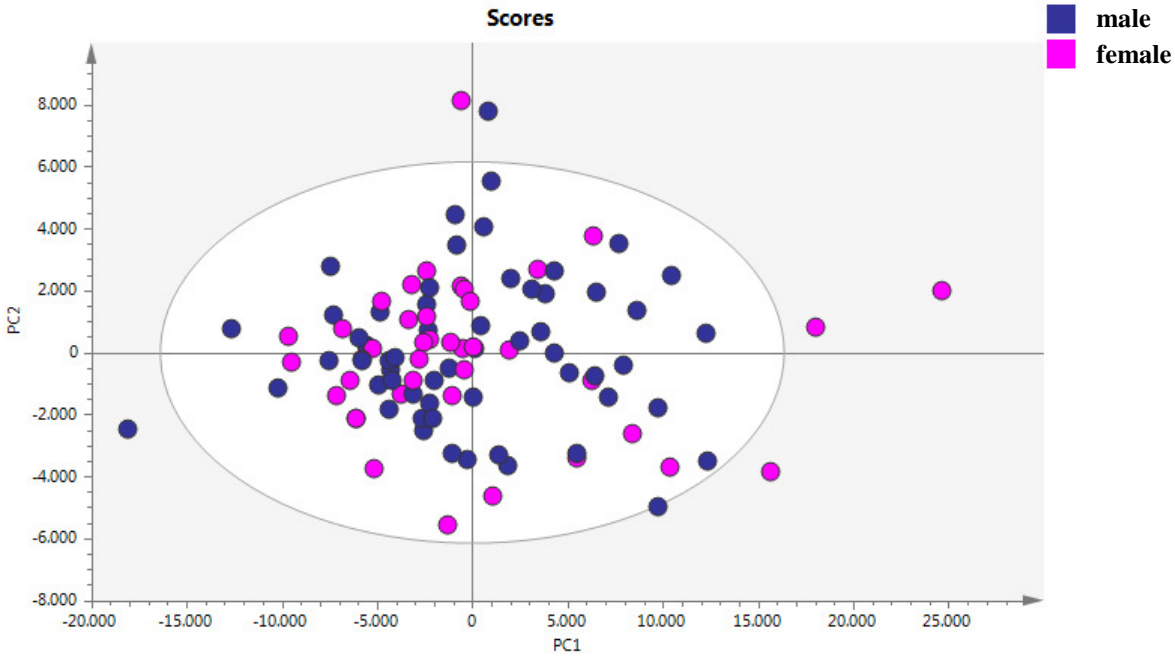

Figure 9 – PCA score plot of the two first PCs using ^{1}H-NMR data of children samples (n=99) and colored according to gender (58 males and 41 females). PC1 = 43.8 % and PC2 = 6.19 %.

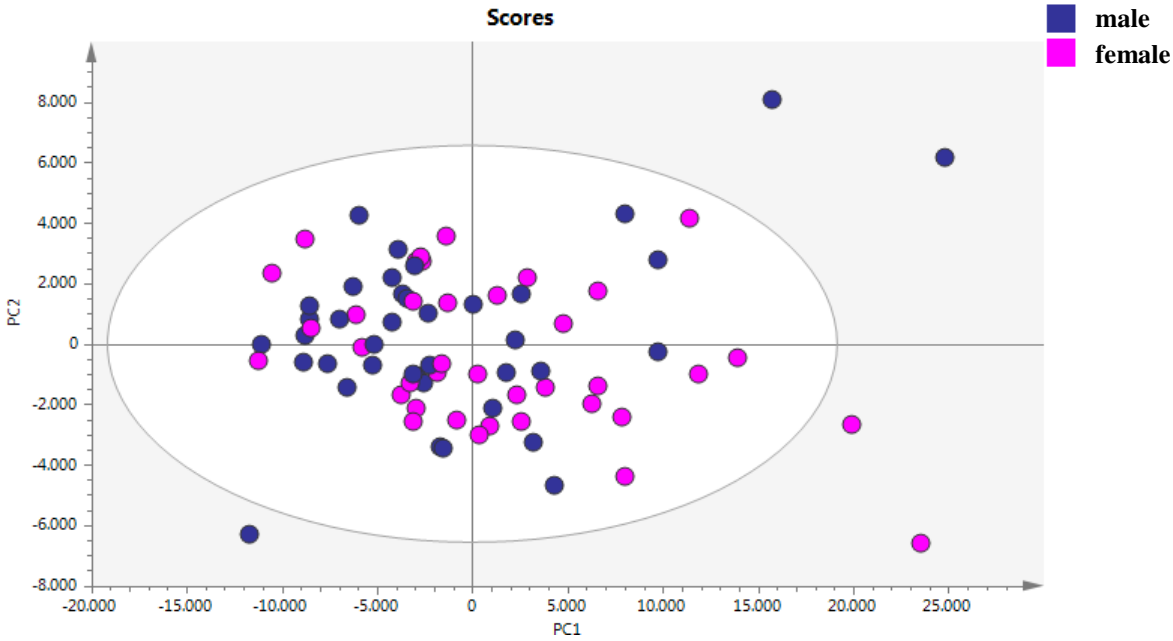

Figure 10 – PCA score plot of the two first PCs using ^{1}H-NMR data of adults samples (n=77) and colored according to gender (39 males and 38 females). PC1 = 52.7 % and PC2 = 6.19 %.

These results do not agree with some obtained previously, in other studies. Zubieta and co-workers (1999) in a study with healthy patients observed that gender is an important variable to consider in the interpretation of investigations related with the CNS since women's reproductive status (reproductive age versus postmenopausal) may influence the function of CNS opioid systems (Zubieta *et al.*, 1999). Yasuda and co-workers (1991) also verified differences in the CSF production rate between male and female. Hagenfeldt and co-workers (1984) also found sex differences in CSF amino acid levels (Hagenfeldt *et al.*, 1984). Stoop and co-workers (2010) in a metabolomics and proteomic analysis of normal CSF samples concluded that high inter-individual variance is influenced by gender only in a limited way (Stoop *et al.*, 2010). In contrast, Schiffer and co-workers (1999) found diferences in the CSF density of males and females (Schiffer *et al.*, 1999). Meissner and co-workers (2014) in a study about complex regional pain syndrome (CRPS)-related dystonia using NMR for the metabolic profiling of the CSF of patients with this disease verified that the PCA model did not reveal associations according to gender (Meissner *et al.*, 2014).

Other parameter analyzed was the origin of the primary tumor. In the case of children (n=99), this group is mainly composed by leukemia (83 out of 99) and by a small number of other types of primary tumor (13 lymphomas, 2 rhabomyosarcoma and 1 germ cell tumor) (Figure 11). Interestingly, the last types of primary cancer are on the negative part of PC2, but there are also lymphomas cases populating that axe. The small number of samples that are not from leukemia precluded to take more conclusions.

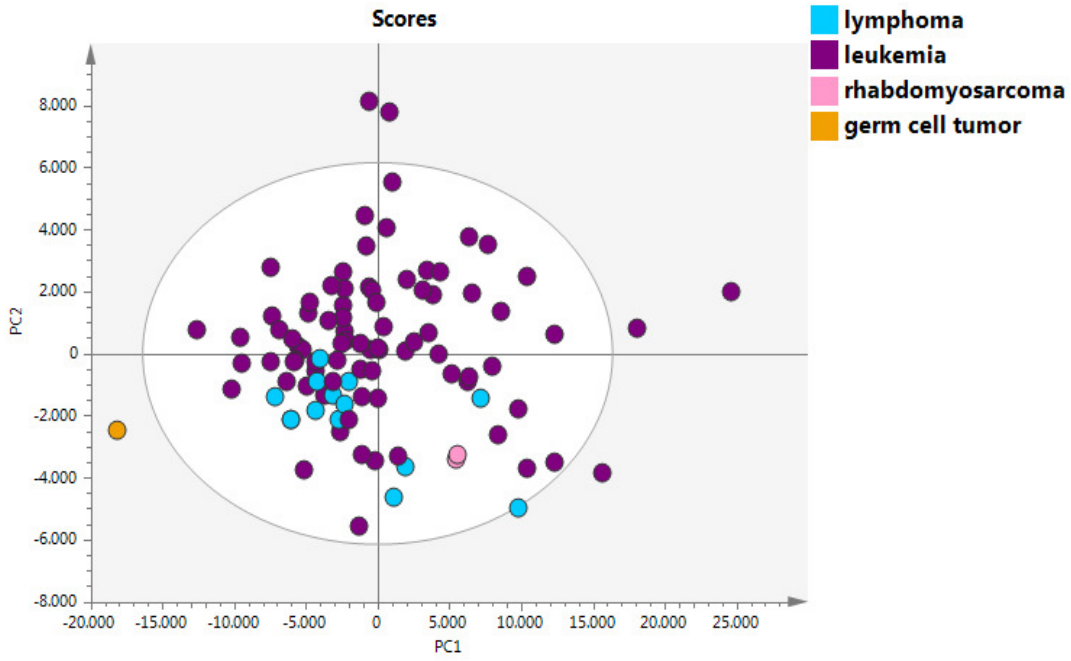

Figure 11 – PCA score plot of the two first PCs using ^{1}H-NMR data of children samples (n=99) and colored according to the type of primary tumor (13 lymphoma, 83 leukemia, 2 rhabdomyosarcoma, 1 germ cell tumor). PC1 = 43.8 % and PC2 = 6.19 %.

For the adults (n=77), the majority is also from lymphomas (46 out of 77) and leukemia (21 out of 77), but there are other types of primary tumor (5 breast carcinoma, 1 non-melanoma skin cancer, 1 multiple myeloma and 1 colorectal cancer). In this case, most of the variability is explained by PC1 (Figure 12). As observed for the children sub-group, there is no clustering based on the type of primary tumor and consequently there are no differences at metabolic level for this clinical parameter.

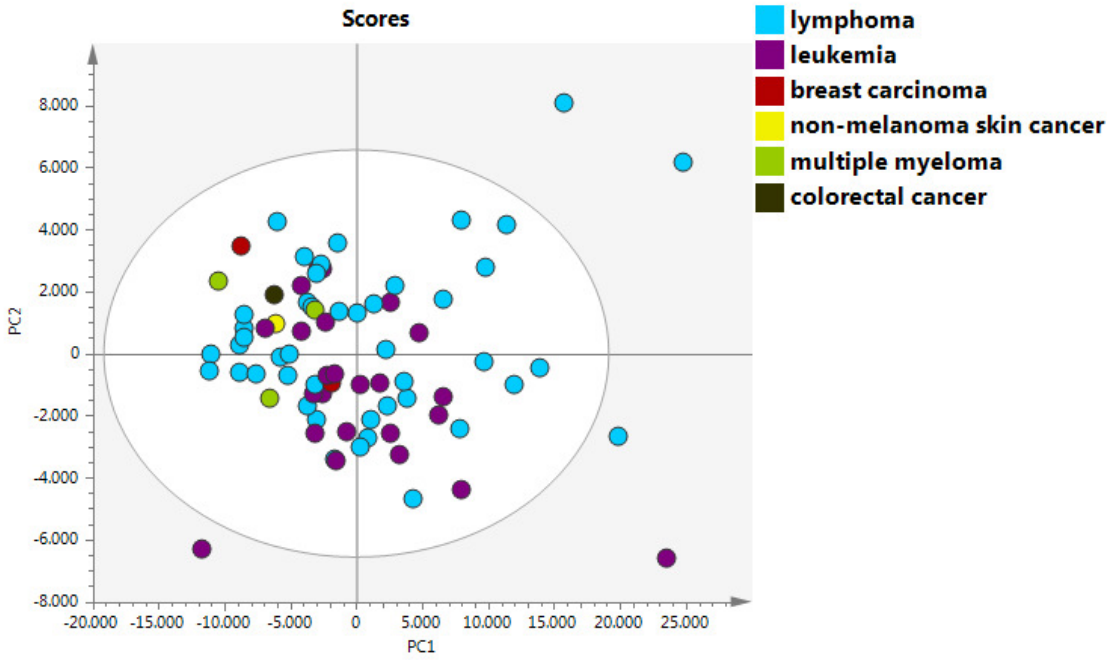

Figure 12 – PCA score plot of the two first PCs using ^{1}H-NMR data of adults samples (n=77) and colored according to the type of primary tumor (46 lymphoma, 21 leukemia, 5 breast carcinoma, 1 non-melanoma skin cancer, 1 multiple myeloma and 1 colorectal cancer). PC1 = 52.7 % and PC2 = 6.19 %.

4.1.3. Multivariate analysis of control and cell invasion samples

A first preliminary analysis using PCA model using all samples ^{1}H NMR dataset was performed. Figure 13 show the correspondent PCA score plot, with each point colored according to the presence or absence of cell invasion in the CNS. It is possible to observe a tendency for the samples originated from cell invasion patients separated from the controls. These results suggest that the metabolite profile of the control samples is somewhat different from the samples with cell invasion to the CNS.

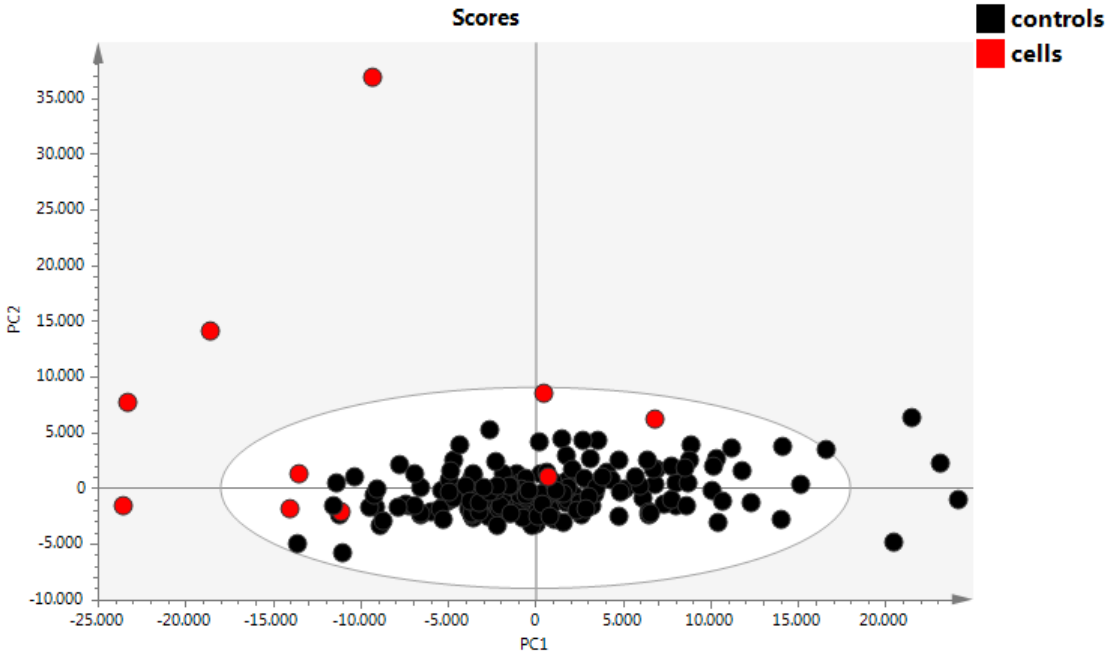

Figure 13 – PCA score plot of the two first PCs using ^{1}H-NMR data of all samples (n=99) and colored according to the presence or absence of cell invasion in the CNS. PC1 = 44.8 % and PC2 = 11.3 %.

To explore the discrimination between the two groups of samples, supervised methods (OPLS-DA) were applied.

Since previous analyses concluded that there are differences between the metabolic profile of children, this OPLS-DA model is only applied to the sub-group of adults samples (n=77), from which 9 are samples with cell invasion. For children this model in not applied since in this case there is only one case of cell invasion to the CNS.

The OPLS-DA score plot of the first and the orthogonal components using the class controls and cell invasion as response variable (Y) showed a cumulative explained variance (R2Y) of 0.626 and goodness of prediction (Q^2) of 0.327, which is not higher than the empirically inferred acceptable value of ≥ 0.4 for a biological model (Figure 14). In this plot there aren't two clear separated clusters, however the control samples are majorly distributed in the center of the plot and the cell invasion samples are majorly found in the positive part of PC1. These results suggest that there are some differences between the metabolic composition of CSF in the absence and presence of cells in the

CSF, but this parameter influence appears limited. There could be others factors that influence this result, including the small number of samples included in this study.

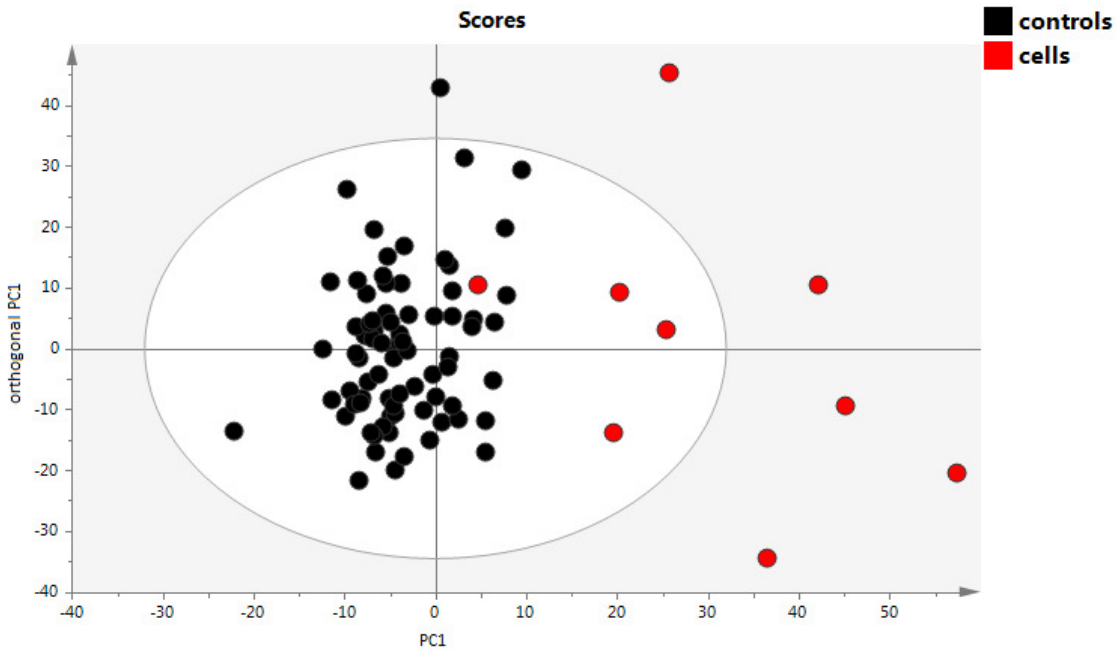

Figure 14 – OPLS-DA score plot of the first and the orthogonal components using ^{1}H-NMR data of controls and cell invasion samples from the sub-group of adults (n=77). R2Y (cum) = 0.626 and Q^2 (cum) = 0.327.

The PCA analysis based on the control and cell invasion samples shows that cells invasion group have a tendency to be separated from the controls along the PC1. The metabolites that contribute for this separation are: histidine, phenylalanine, tyrosine, glucose, glutamate, acetate, lactate, 3-hydroxybutyrate, isoleucine, leucine, valine and other unidentified metabolites are increased in the control samples; xanthine, glycine and citrate are increased in the cell invasion samples (Figure 15).

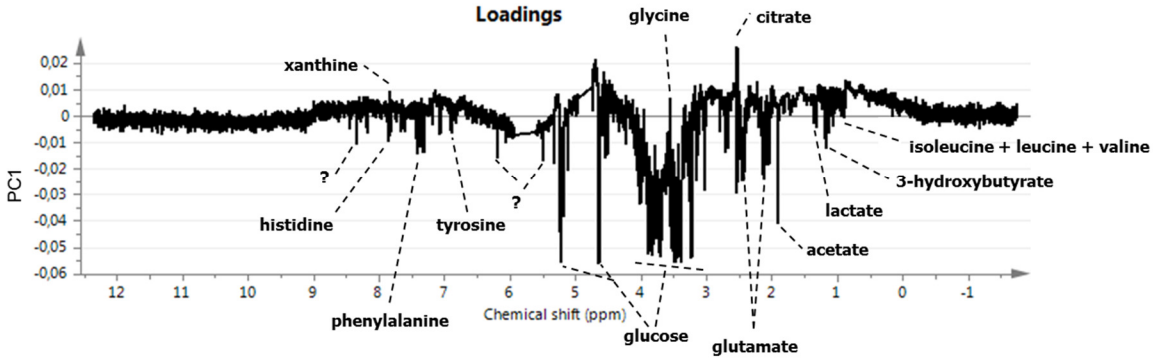

Figure 15 – OPLS-DA loading plot of PC1 using 1H-NMR data of control and cell invasion samples (n=77), with the metabolites that are increased (positive part of PC1) and decreased (negative part of PC1) in the cell invasion samples and that are increased (negative part of PC1) and decreased (positive part of PC1) in the control samples.

4.2. *In vitro* study of CNS metastasis in human acute lymphoblastic leukemia (697-GFP) cell line

The work presented on this chapter aims at studying the tumor progression and the importance of tumor's microenvironment in a leukemia murine model exposed to different diets (normal and fat diet) using different approaches including metabolomics, gene and protein expression and analysis of cell cycle and apoptosis.

4.2.1. Luminescence analysis

Luminescence analysis was performed by our collaborators in the *Instituto de Medicina Molecular*. This analysis allows monitor the disease burden. Mice exposed to a fat diet have more extensive disease spread and colonization of organs by leukemia cells than the mice exposed to a normal diet (Figure 16).

This evidence suggests that cholesterol plays an important role in cancer progression and development. Cholesterol is a highly insoluble molecule that is transported in the circulation via endogenous transporters, the lipoproteins. They are responsible for the mediation of the processing and delivery of dietary and endogenous cholesterol to systemic tissues and the uptake of cholesterol from the blood stream by the liver, allowing the homeostatic cholesterol balance. In cancer, it has been found that HDL (high density lipoprotein) are the most affected by malignant tumor development (Muntoni *et al.*, 2009) and that LDL (low density lipoprotein) may play a fundamental role in cancer progression via supplying malignant cells and tumors with cholesterol to most peripheral tissues via the LDL-receptor (Brown & Goldstein, 1986; Silvente-Poirot & Poirot, 2012). Other studies have revealed that lipoproteins can enhance the aggressiveness of malignant tumors in mouse models (Danilo & Frank, 2012).

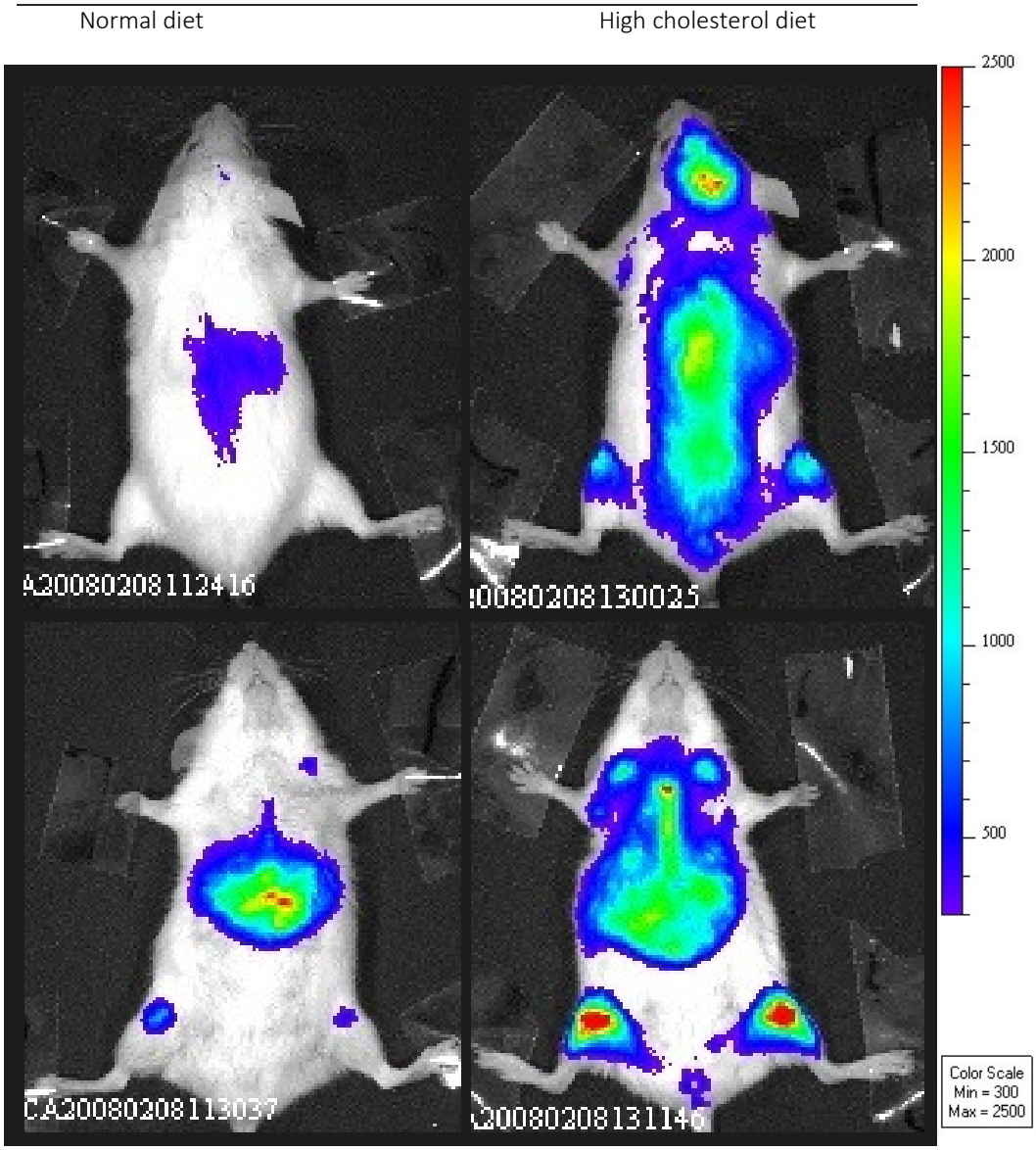

Figure 16 – Luminescence analysis of tumor cells from 697-GFP lineage in mice exposed to a normal diet (on the left) and in mice exposed to fat diet (on the right). The scale shows the grade of disease burden. This analysis was performed by our collaborators in the *Instituto de Medicina Molecular*.

4.2.2. Metabolic profiling by NMR spectroscopy

As mentioned in section **3.2.2**, ^{1}H NMR spectra were obtained from a total of 9: aqueous extracts, organic extracts and supernatants, in which 1 was from the parental lineage, 1 from mice with tumor on the skin and exposed to normal diet (named S), 1 from mice with tumor on the brain and exposed to normal diet (named B), 3 from mice with tumor on the skin and exposed to fat diet (named S1, S2 and S3) and 2 from mice with tumor on the brain and exposed to fat diet (named B1 and B2).

The representative NMR spectra for the aqueous extracts, organic extracts and supernatants are shown in Figure 17. Aqueous extracts and supernatants are majorly composed by amino acids, organic acids and sugars. Organic extracts are majorly composed by different lipids. There are some metabolites that couldn't be identified.

The spectra were analyzed by multivariate analysis (PCA) on the entire spectral dataset for the cells extracts (aqueous and organic) and supernatants, taking into account the localization of tumor metastasis and the type of mice diet.

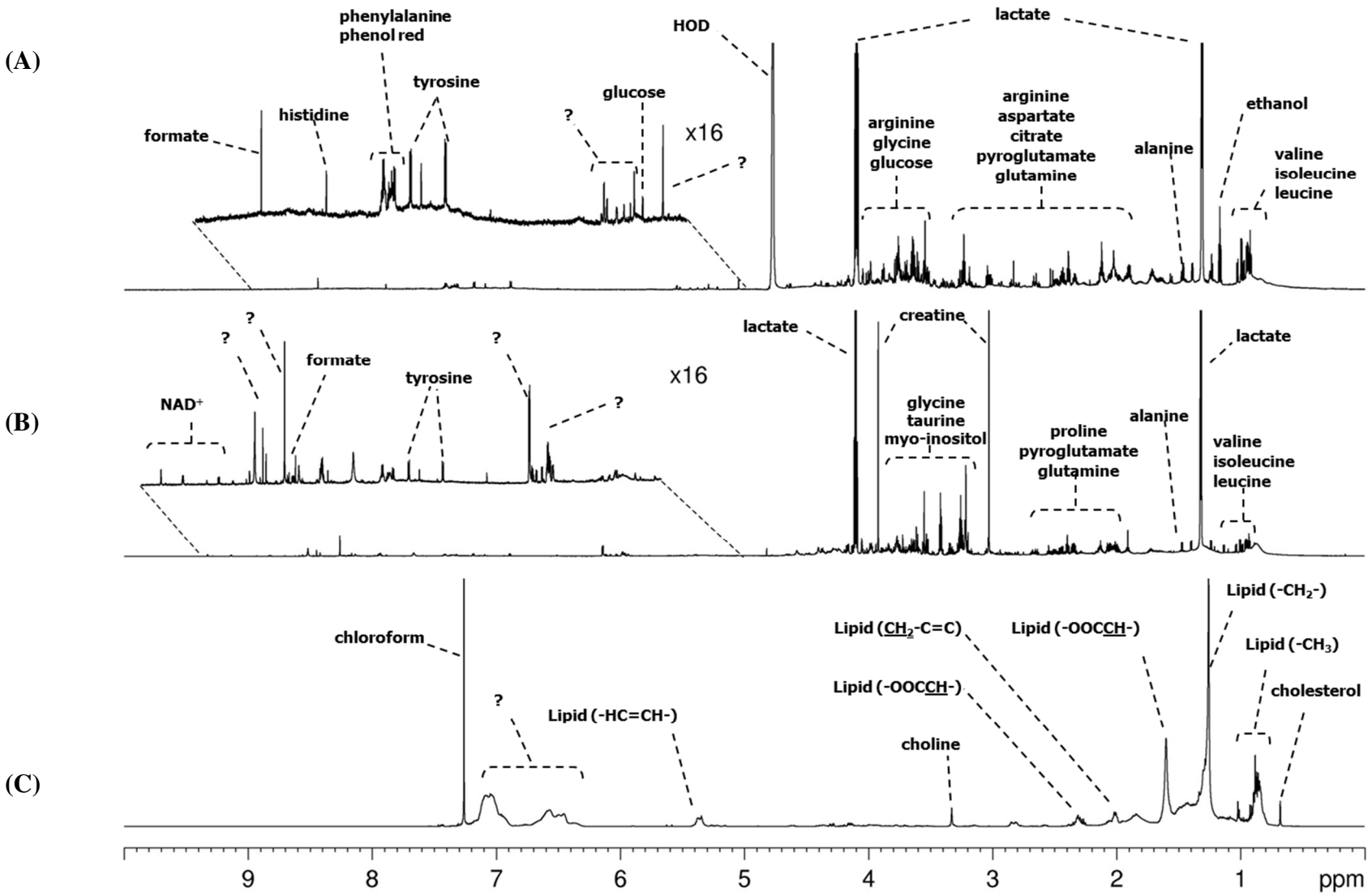

Figure 17 – Representative ^{1}H NMR spectra of (A) culture medium (B) aqueous extract and (C) organic extract, with some of the metabolites identified.

In the PCA score plots of the two first PCs (PC1 vs PC2) for the supernatants is not observable the formation of clusters considering the localization of tumor metastasis or the mice diet (Figure 18 and Figure 19, respectively). In addition, further PCs also did not show independent clusters when taking into account these information's.

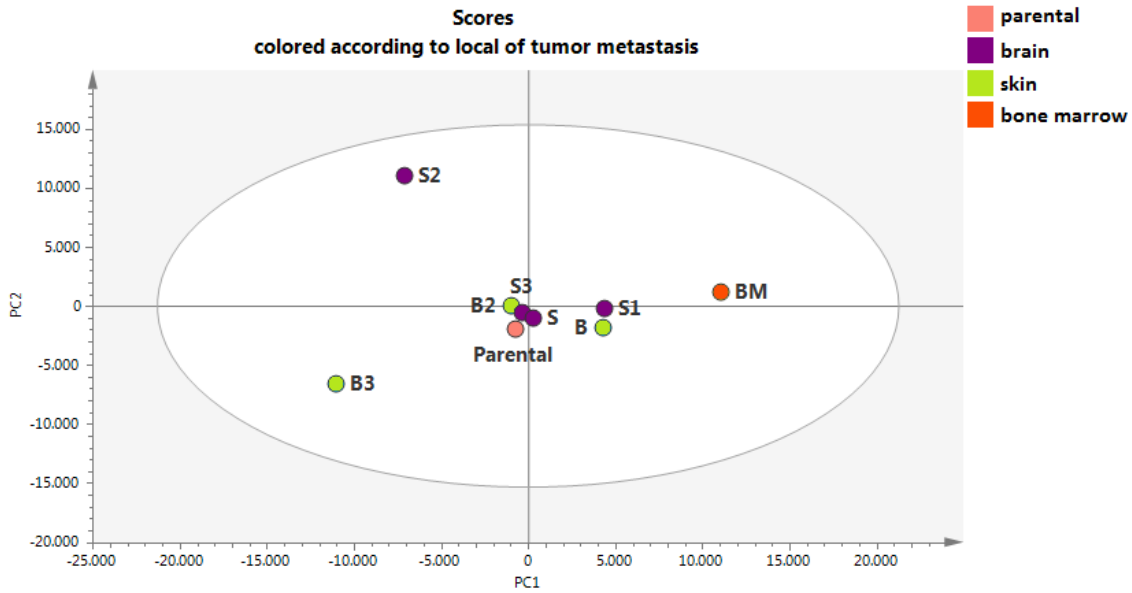

Figure 18 – PCA score plot of the two first PCs using ^{1}H-NMR data of supernatants (n=9) and colored according to the localization of tumor metastasis on the mice (1 parental lineage, 3 brain metastases, 4 skin metastasis and 1 bone marrow metastasis). PC1 = 43.5 % and PC2 = 22.6 %.

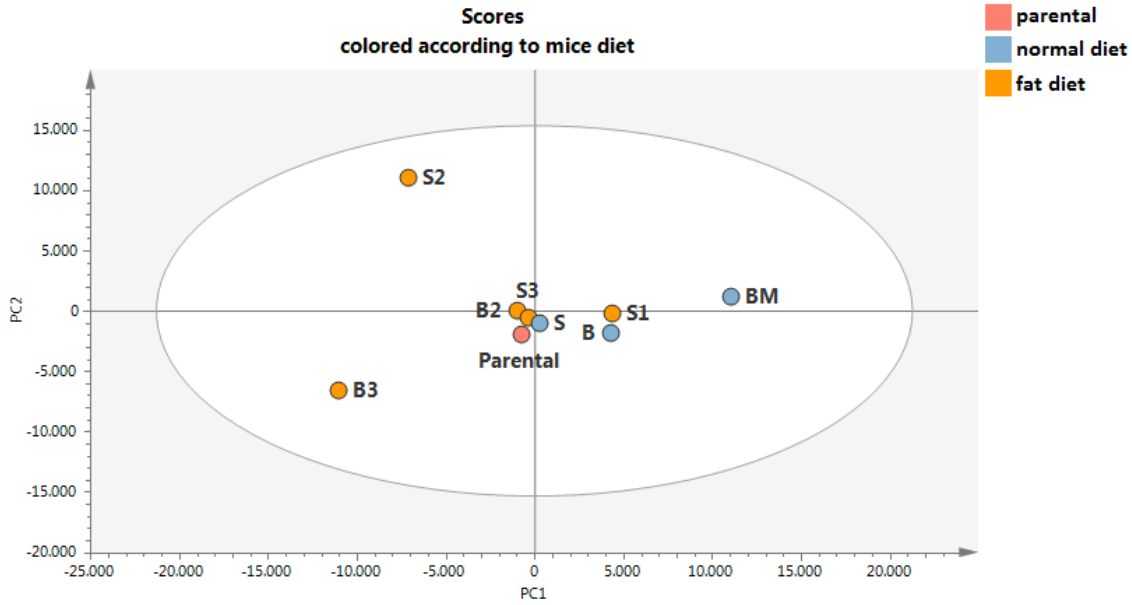

Figure 19– PCA score plot of the two first PCs using ^{1}H-NMR data of supernatants (n=9) and colored according to the type of mice diet (1 parental lineage, 3 normal diet and 5 fat diet). PC1 = 43.5 % and PC2 = 22.6 %.

Lipid metabolism is a complex metabolic network involved in many aspects of cancer cell biology. Lipids production is a prerequisite for cell growth and proliferation, but in cancerous cells they are also active players in the signaling processes that are involved in cell transformation and tumor development. They also appear to have a potential role in facilitating the spread of cancer cells to secondary sites, but this phenomenon is not yet fully understood (Baenke *et al.*, 2013).

Figure 20 and Figure 21 is observed that there is no clustering of samples based on the local of metastasis or mice diet in the PCA score plots (PC1 vs PC2) of organic extracts. These results show that there aren't significant differences at metabolic level between the organic extracts from brain, skin and bone marrow and from normal and fat diet. Interestingly, despite be result of only one sample of the parental 697-GFP cell line, appears that the lipid content of the cells lineages isolated from the mice are different from the parental cell line.

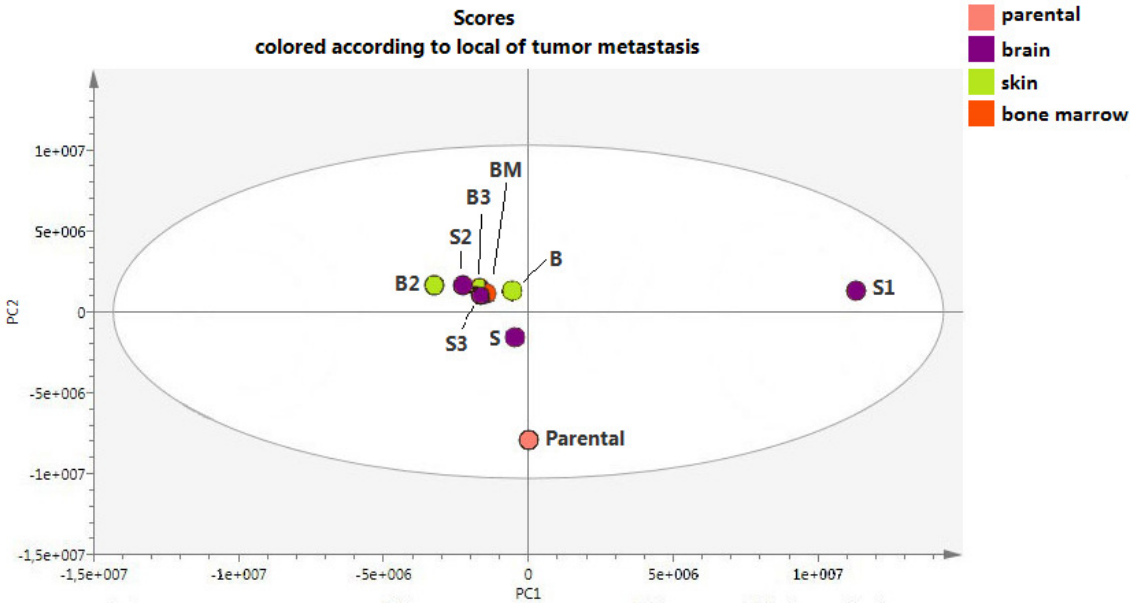

Figure 20 – PCA score plot of the two first PCs using ^{1}H-NMR data of organic extracts (n=9) and colored according to the localization of tumor metastasis on the mice (1 parental lineage, 3 brain metastases, 4 skin metastasis and 1 bone marrow metastasis). PC1 = 57.4 % and PC2 = 29.6 %.

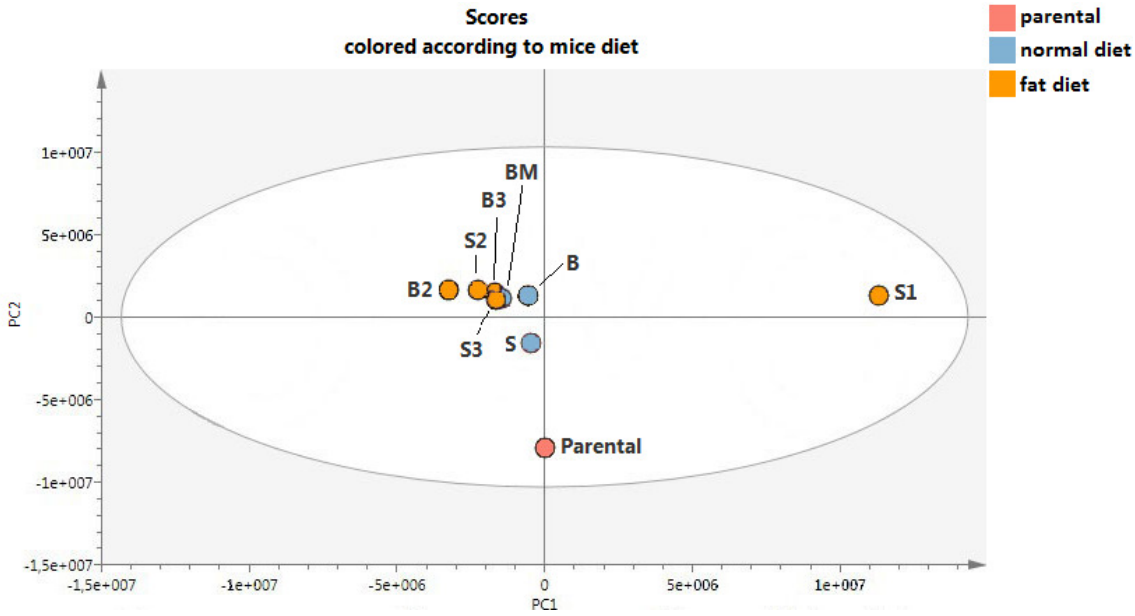

Figure 21– PCA score plot of the two first PCs using ^{1}H-NMR data of organic extracts (n=9) and colored according to the type of mice diet (1 parental lineage, 3 normal diet and 5 fat diet). PC1 = 57.4 % and PC2 = 29.6 %.

No clustering is observed, when the same analysis is performed to the aqueous extracts, considering the localization of tumor metastasis (Figure 22). This means that there are no significant differences at metabolite level between the aqueous extracts from brain, skin and bone marrow.

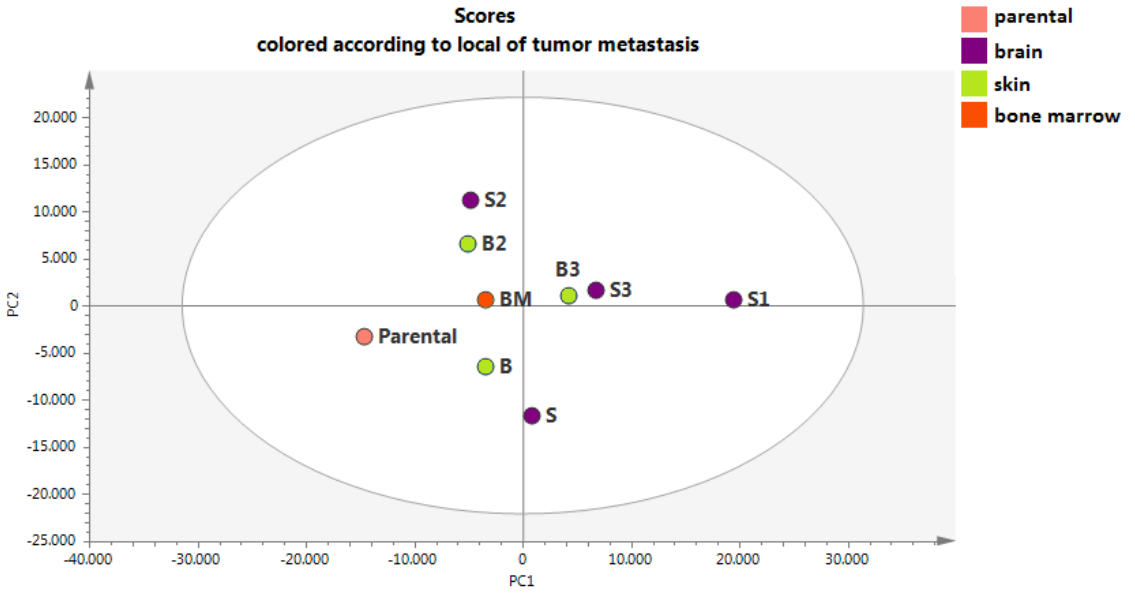

Figure 22 – PCA score plot of the two first PCs using ^{1}H-NMR data of aqueous extracts (n=9) and colored according to the localization of tumor metastasis on the mice (1 parental lineage, 3 brain metastases, 4 skin metastasis and 1 bone marrow metastasis). PC1 = 41.9 % and PC2 = 20.8 %.

However, considering the type of mice diet, the plot suggests that normal diet and fat diet form two different clusters (Figure 23). With the fat diet samples are placed tendentiously on the positive part of PC2, while the normal diet samples on the negative part of PC2. This plot suggests that the metabolic profile of the aqueous extracts from cells of mice exposed to normal diet is different from the cells of mice exposed to fat diet. These differences are explained by PC2, the second PC that represents most of the variance between samples.

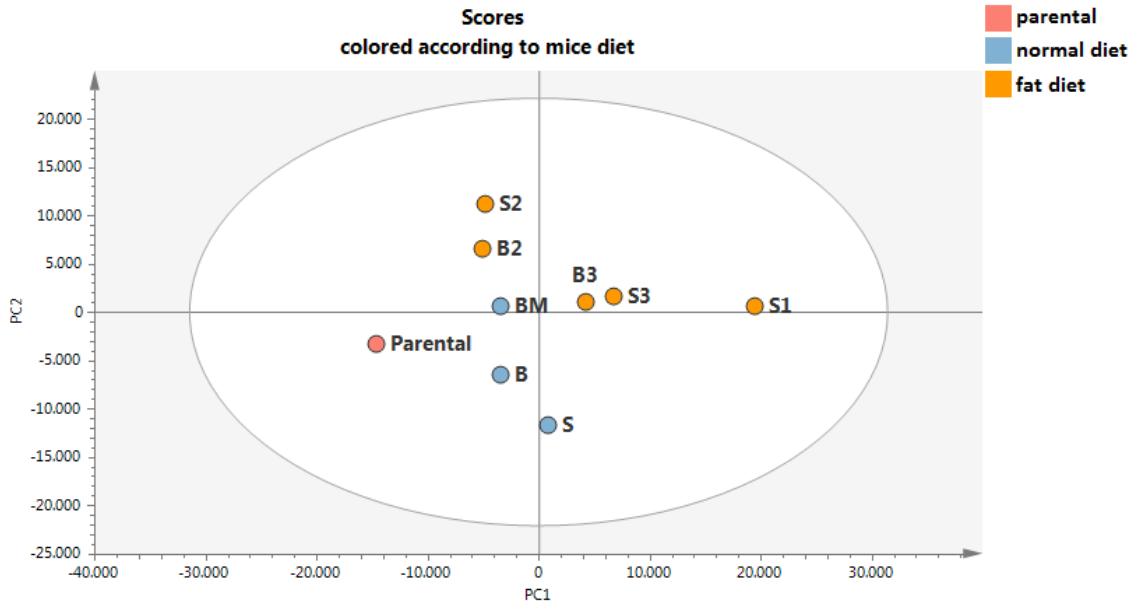

Figure 23 – PCA score plot of the two first PCs using ^{1}H-NMR data of aqueous extracts (n=9) and colored according to the type of mice diet (1 parental lineage, 3 normal diet and 5 fat diet). PC1 = 41.9 % and PC2 = 20.8 %.

In the loading plot correspondent to PC2, it is possible observe that formate, glucose, creatine, glutamine, lactate, isoleucine, leucine, valine and other unidentified metabolite are increased the mice exposed to fat diet while ADP, choline, creatinine, aspartate, glutamate are increased in the ones exposed to normal diet (Figure 24).

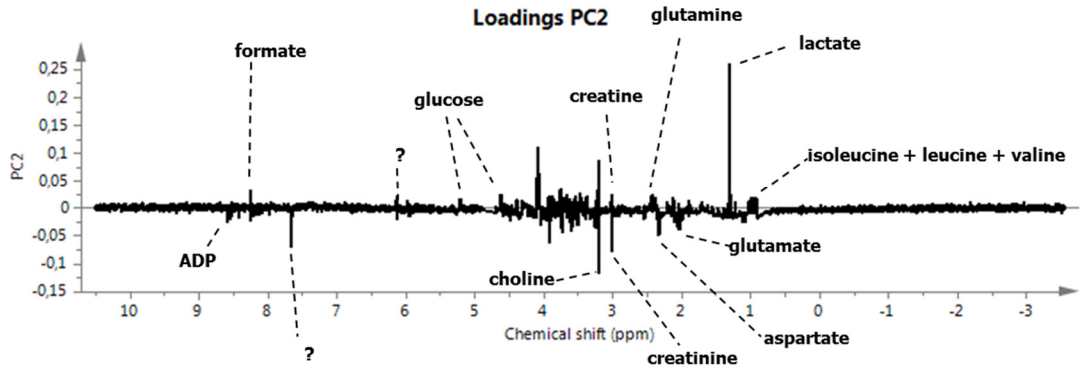

Figure 24 – PCA loading plot of PC2 using ^{1}H-NMR data of aqueous extracts with the identification of the metabolites that are increased (positive part of PC2) and decreased (negative part of PC2) in the cells from mice exposed to fat diet and that are increased (negative part of PC2) and decreased (positive part of PC2) in the cells from mice exposed to normal diet and from parental lineage.

One of the most significant differences between aqueous extracts from cells of mice with the two types of diets is the presence of glucose inside the cells of mice exposed to a fat diet. The relationship between dietary fat and glucose metabolism has been recognized for at least 80 years. The first studies about the possible effect of dietary fat on glucose metabolism in animals and humans were published by Himsworth (1935), where he concluded that "the glucose tolerance of a healthy individual is determined by the composition of the diet which he is receiving" (Himsworth, 1935). In experimental studies with animals it was seen that high fat diets result in impaired glucose tolerance (Lichtenstein & Schwab, 2000). Other studies have concluded that dyslipidemia (abnomal concentrations of lipids in the peripheral blood) is associated to tumor growth and metastasis (Alikhani *et al.*, 2013; Kimura & Sumiyoshi, 2007; Scholar, Violi *et al.*, 1989).

4.2.3. Gene and protein expression levels

The role of fat diet in leukemia growth and metastasis in mice models was evaluated in 697-GFP parental cell lines and in cells isolated from mice maintained in normal and fat diet grown in RPMI 1640 supplemented with glutamine and 10% FBS.

The expression levels of glucose transporters (SGLT1 and GLUT1) in parental lineage (control condition), in skin fat diet lineage (cells from mice exposed to fat diet

that metastasized to the skin) and in skin normal diet lineage (cells from mice exposed to normal diet that metastasized to the skin) was assessed by Real Time-PCR (Figure 25).

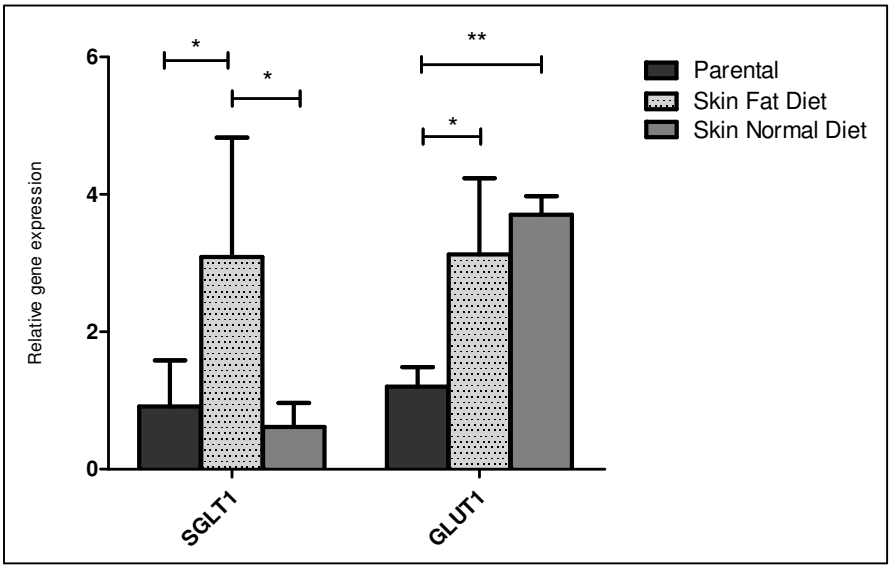

Figure 25 – Relative gene expression of SGLT1 and GLUT1. 18S gene was the endogenous control. Expression levels were normalized to parental lineage. Data are mean ± error bars of triplicates. * $p \leq 0.05$; ** $p \leq 0.01$.

Glucose is transported into cells by two families of transporters: a facilitative-type glucose transporter family (GLUT) and an active-type glucose transporter family (sodium/glucose cotransporter (SGLT)) (Wood & Tryhurn, 2003).

SGLT1 plays an important role in maintaining enough glucose for cell survival since it transports glucose into cells regardless of glucose concentration in the medium. Cells are dependent on this transporter to accumulate and maintain higher intracellular glucose levels (Wright *et al.*, 1994). The presence of SGLT1 allows cancer cells to uptake enough glucose for ATP generation via glycolysis (Nishimura *et al.*, 1998). In this study, SGLT1 were statistically increased in the cells from mice exposed to fat diet in relation to the other two cell lines. This may indicate that SGLT1 contributes significantly to the entry of glucose into these cells.

GLUT1 is responsible for serving many cell types for glucose uptake and is expressed ubiquitously in human tissues. Elevated expression of this transporter has been documented in most cancers (Airley & Mobasheri, 2007; Baer *et al.*, 1997; Macheda *et*

al., 2005; Smith, 1999; Zierler, 1999). In this study, GLUT1 was found statistically increased in cells of mice exposed to both diets, when comparing to the parental cell line. These results suggest that this gene does not play a role in cells from mice with fat diet though it may be relevant to select cancer cells *in vivo* (in mice). Previous studies demonstrated that higher levels of expression of this transporter is observed in cancers of higher grade and proliferative index, since the more aggressive tumors probably have a greater demand for metabolic energy and consequently, a greater demand of glucose (Cantuaria *et al.*, 2001; Higashi *et al.*, 1998; Ravazoula *et al.*, 2003; Younes *et al.*, 1995). Accordingly, cancer cells to systemically survive in an animal model must have enough plasticity to adapt to the new environment. Hence, GLUT1 can be a key element in cancer selection in vivo, allowing glucose uptake and survival of cells that are able to express it.

By Real Time-PCR it was also assessed the gene expression levels of IDH1 and IDH2, which corresponding enzymes belong to Kreb's cycle (Figure 26). These enzymes are homodimeric enzymes that act in the cytoplasm and mitochondria, respectively, to produce NADPH by the conversion of isocitrate to α-ketoglutarate (Cairns *et al.*, 2011).

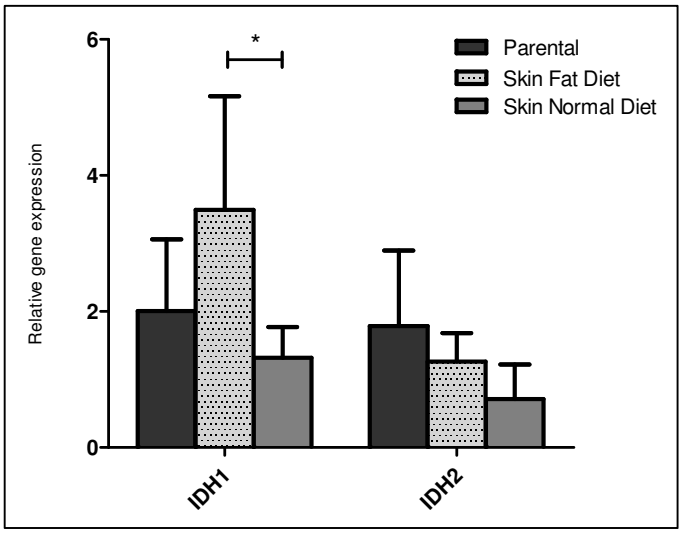

Figure 26 – Relative gene expression of IDH1 and IDH2. 18S gene was the endogenous control. Expression levels were normalized to parental lineage. Data are mean ± error bars of triplicates.* $p \leq 0.05$.

The gene expression levels of IDH1 was increased in parental cells and in cells from mice exposed to fat diet in relation to the ones from mice maintained in a normal diet. For IDH2 expression, no statistically significant differences were found between the

three cell lines. Recent studies demonstrate that specific mutations in IDH1 and IDH2 are linked to the regulation of cancer cell growth in glioblastoma (Parsons *et al.* 2008) and acute myeloid leukemia (AML) (Mardis, 2009). Such mutations are expected to limit the function of the TCA cycle and consequently increase the glycolytic dependence of these tumors, since it synthesizes preferentially the oncometabolite 2-hydroxyglutarate, reducing the rate of α-ketoglutarate synthesis to supply Kreb's cycle. It is likely that tumors with these types of mutations could be especially vulnerable to management through dietary energy restriction, since it could inhibit multiple signaling pathways required for progression of malignant tumors regardless of tissue origin (Seyfried & Shelton, 2010). However, in the studied cell lines the mutational profile of IDH1 and IDH2 was not assessed and it may further clarify our results.

It was also investigated the gene and protein expression levels of genes involved in lactate metabolism (LDHA, LDHB, LDHC) and transport (MCT1 and MCT4).

The reversible pyruvate reduction into lactate reaction is catalyzed by the LDH family of tetrameric enzymes. This reaction also allows glycolytic cells to maintain the levels of pyruvate low enough to avoid cell death (Thangaraju *et al.*, 2006, Thangaraju *et al.*, 2008), since it is converted into lactate and exported to extracellular media. The biochemical features of LDHA and LDHC favor the conversion of pyruvate into lactate whereas those of LDHB favor the conversion of lactate into pyruvate (Ganapathy *et al.*, 2009). While LDHA and LDHB are expressed in somatic mammalian tissues, LDHC is only found expressed in testis and sperm (Holmes & Goldberg, 2009). In addition, different combinations of LDHA and LDHB subunits constitute the 5 LDH tetrameric (homo and hetero tetramers) isoforms, whereas LDHC subunit only constitute a single homotetrameric enzyme. In some types of tumors, production of lactate also occurs in response to genetic features and to stimuli from the tumor microenvironment (Draoui & Feron, 2011; Xiong *et al.*, 2011). Lactate production is necessary for sustaining glycolysis at a high rate (Ganapathy *et al.*, 2009). Expression levels of LDHA, LDHB and LDHC have been found increased in several types of cancer (Kinoshita *et al.*, 2011; Koslowski *et al.*, 2002; Lewis *et al.*, 2000; Walenta & Mueller-Klieser, 2004). Lactate is also considered an alternative metabolic fuel for cancer cells, being oxidized into pyruvate, the last metabolite of glycolytic pathway and entering the Kreb's cycle as acetyl-CoA.

In this study, the relative mRNA levels of LDHA, LDHB and LDHC enzymes are shown in Figure 27. The protein expression levels obtained by western blot only for LDHB are shown in Figure 28.

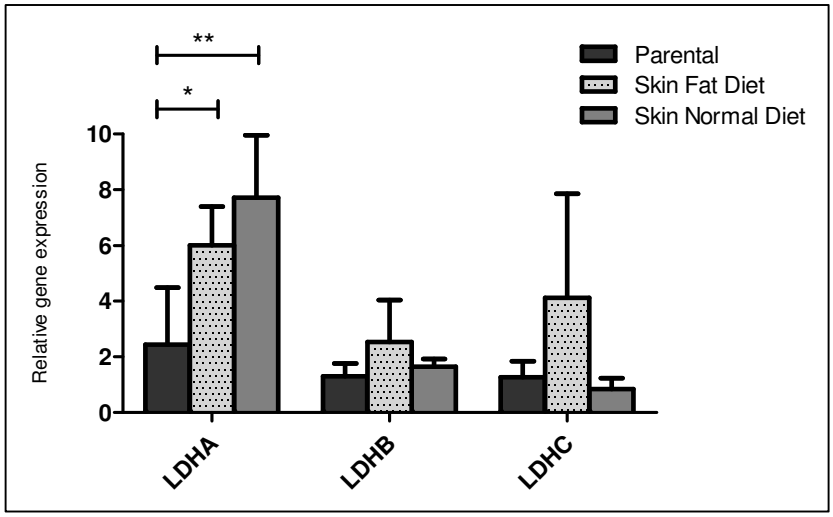

Figure 27 – Relative gene expression of enzymes involved in lactate metabolism LDHA, LDHB and LDHC. 18S gene was the endogenous control. Expression levels were normalized to parental lineage. Data are mean ± error bars of triplicates. * $p \leq 0.05$; ** $p \leq 0.01$.

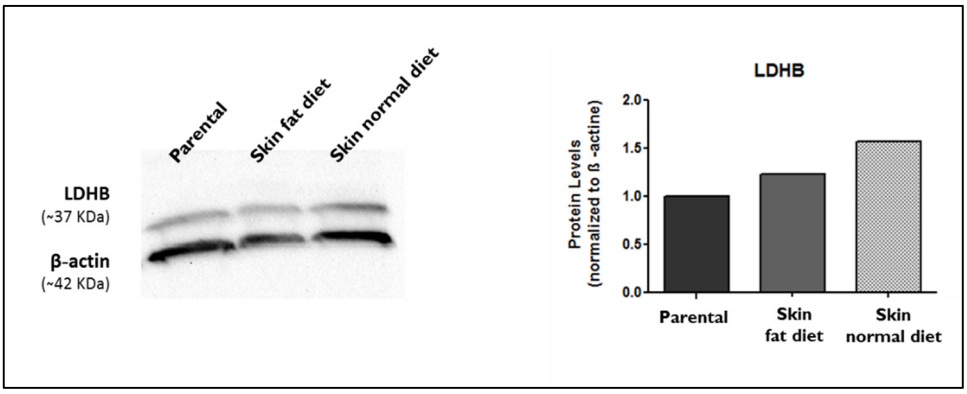

Figure 28– LDHB protein levels assessed by western blot. Protein levels were normalized to β-actin and are relative to those obtained in the parental lineage.

At mRNA level, for LDHA there is statistically significant differences between parental lineage and both cells from mice under fat and normal diets, which is in concordance with results obtained by other authors that found increased levels of LDHA in invasive melanoma cancer (Agarwala *et al.* , 2009; Bedikian *et al.*, 2008) in more advanced adenocarcinomas (Beer *et al.*, 2002). Interestingly, this result is in agreement with the increased expression levels of GLUT1 in both cells from mice under fat and

normal diets, since a high rate of glucose uptake allows an increased glycolysis rate and consequently lactate production catalysed by LDHA subunit.

Expression levels of LDHC are not statistically different between cell lineages. LDHC has been recently found expressed in a broad spectrum of human tumors, with high frequency in lung cancer, melanoma, breast cancer (Koslowski et al, 2002) and in some prostate cancers (Tang & Goldberg, 2009).

Expression levels of LDHB did not reveal statistically significant differences between parental lineage and both cells from mice exposed to normal and fat diet. Despite no differences were observed in gene expression, at protein level it was observed a slightly increase of LDHB in cells from mice exposed to normal diet, comparing to the other two cell lineages. However, protein measurement by densitometry was only performed in a single replicate, being necessary a further analysis in two more replicates in order to certify the results. Nevertheless, discrepancies between mRNA and protein levels can be observed often due to diverse post-transcriptional mechanisms that are involved in turning the mRNA into protein (mRNA degradation) or due to the different in vivo protein half-life resultant from protein synthesis and degradation (Greenbaum, Colangelo *et al.*, 2003). Moreover, recent data as shown that LDHA was overexpressed in neoplastic cells and the expression of LDHB was downregulated (Singer *et al.*, 2011). Anyway, the quantification of native tetrameric enzymes (LDH1 to 5) will give rise to more clear conclusions about the predominant LDH activity, since as mentioned before the functional enzymes are combinations from LDHA and/or LDHB subunits. This quantification will be further performed by ELISA (Enzyme-Linked Immunosorbent Assay).

Lactate is transported by monocarboxylate anion transporters, the MCTs (Halestrap & Price, 1999). MCT1 regulates preferentially the entry of lactate into tumor cells whereas MCT4 preferentially exports lactate out of the cell (Draoui and Feron, 2011). Studies have demonstrated that these two transporters are overexpressed in neuroblastoma, colorectal cancer, cervix cancer and lung tumor metastatic cells, indicating bad prognosis (Fang *et al.*, 2006; Izumi *et al.*, 2011; Pinheiro *et al.*, 2008, 2009; Sonveaux *et al.*, 2008).

The relative mRNA levels of MCT1 and MCT4 transporters are shown in Figure 29. The protein expression levels for MCT1 and MCT4 obtained by western blotting are shown in Figure 30 and by immunofluorescence is shown in Figure 31.

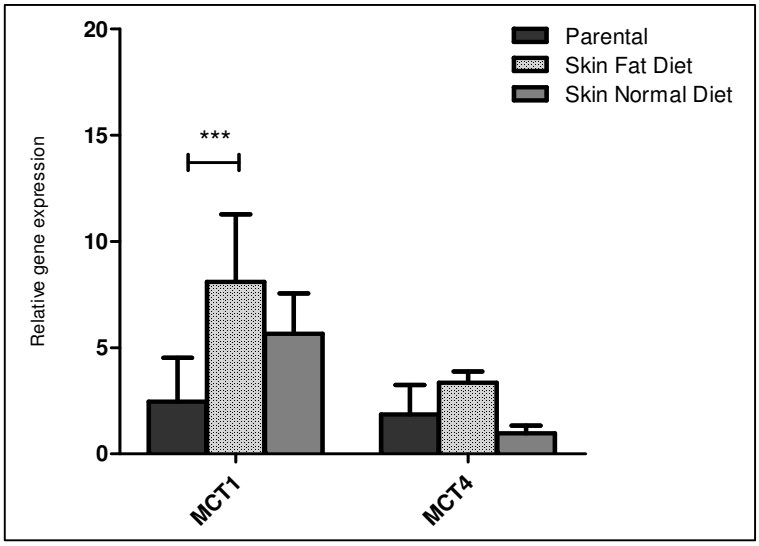

Figure 29 – Relative gene expression of lactate transporters MCT1 and MCT4. 18S rRNA gene was the endogenous control. Expression levels were normalized to parental lineage. Data are mean ± error bars of triplicates. *** $p \leq 0.001$.

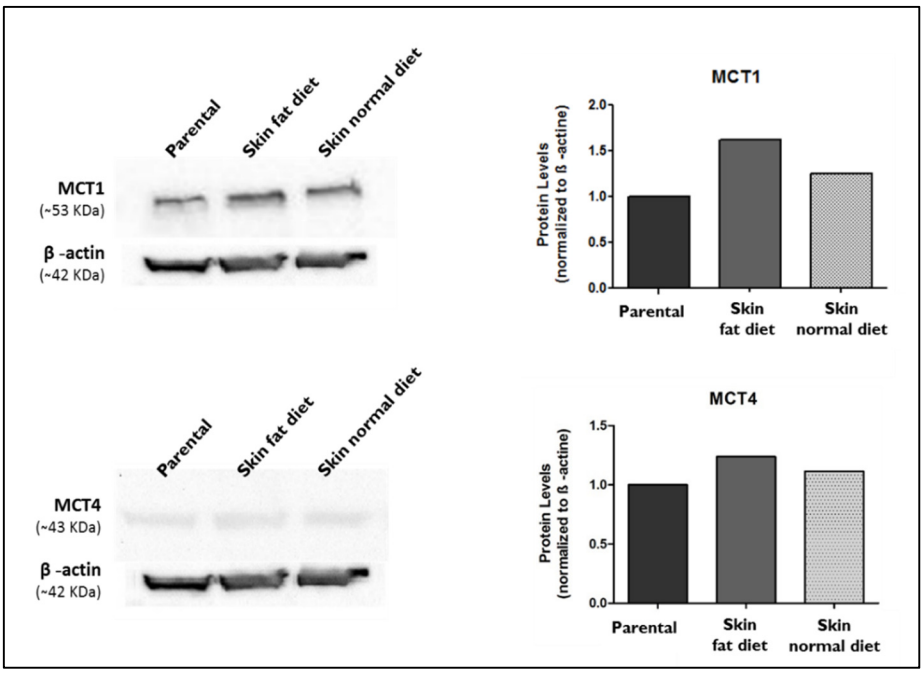

Figure 30 – MCT1 and MCT4 protein levels assessed by western blot. Protein levels were normalized to β-actin and are relative to those obtained in the parental lineage.

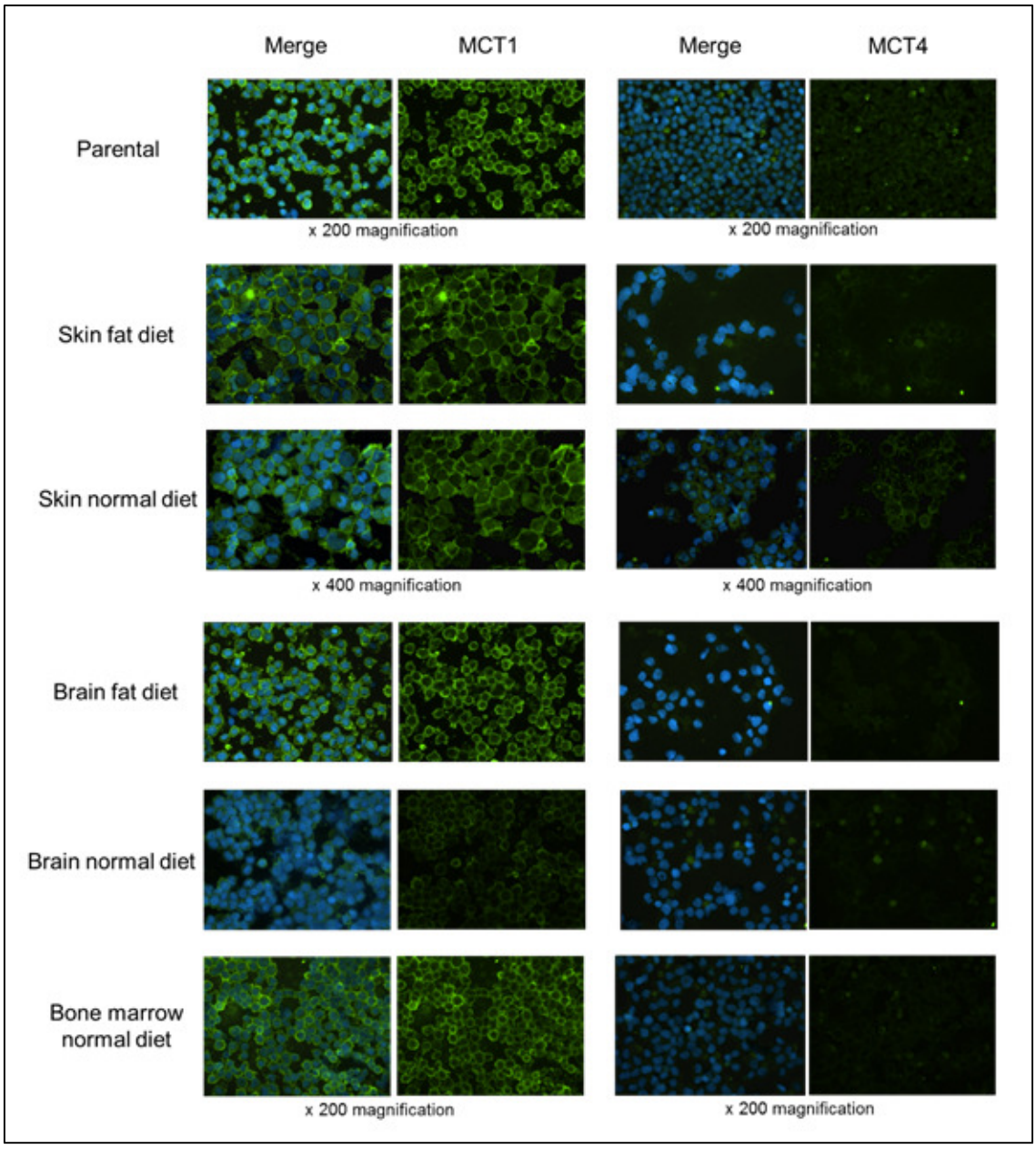

Figure 31 – Immunofluorescence for MCT1 and MCT4 (green) in parental lineage, skin fat diet lineage, skin normal diet lineage, brain fat diet lineage, brain normal diet lineage and bone marrow normal diet lineage. Nuclei were labelled with dapi (blue). Fluorescence microscopy (magnification: 200x and 400x).

A statistically significant increase of mRNA levels of MCT1 was observed in the tumor cells lineage from mice exposed to fat diet, when comparing to the parental lineage. Concerning protein levels of MCT1 assessed by western blotting, the dynamics was similar to the observed at the mRNA levels. In contrast, protein levels assessed by immunofluorescence only showed a decrease in MCT1 expression in cells from brain

normal diet, comparing to all the other lineages. However, despite being a more accurate method to quantify protein then immunofluorescence, western blotting must be performed in 3 replicates for all lineages, in order to ensure the results. This difference between mRNA and protein expression has been identified before (Kang, Im, Go, & Han, 2009). According to Greenbaum *et al.* (2003) this absence of correlation could be due to varied post-transcriptional mechanisms that participate in turning mRNA into protein or that proteins expression may vary in *in vivo* (Greenbaum *et al.*, 2003). Jackson *et al.* (1997) also reports little correlation between the mRNA and protein levels of MCT1 (Jackson *et al.*, 2007).

MCT1 is significantly increased in breast carcinomas when compared with normal breast tissue and has been associated with poor prognostic variables including high-grade tumors (Pinheiro *et al.*, 2010). MCT1 expression has also been associated with advanced gastric carcinoma and lymph node metastasis (Pinheiro *et al.*, 2009).

Concerning MCT4, no differences cell lineages were observed at both protein (assessed by western blot and immunofluorescence) and mRNA levels. However, recent studies have suggested an association between MCT4 expression and primary tumor size, further infiltration, growth and resistance to cell death, in colorectal cancer (Gotanda *et al.*, 2013) and in breast cancer (Whitaker-Menezes *et al.*, 2011).

Since in NMR analysis glucose was detected in certain cell extracts, the expression of key genes involved in gluconeogenesis was also analyzed in order to certify if some cells are synthesizing glucose.

The mRNA levels of ALT, PCK1, PCK2, FBP1 and PFKFB1 was assessed by Real Time-PCR (Figure 32).

By western blotting, only the protein expression levels of PCK1 and PFKFB1 were evaluated, due to technical problems related to antibodies for ALT, PCK2 and FBP1 (Figure 33).

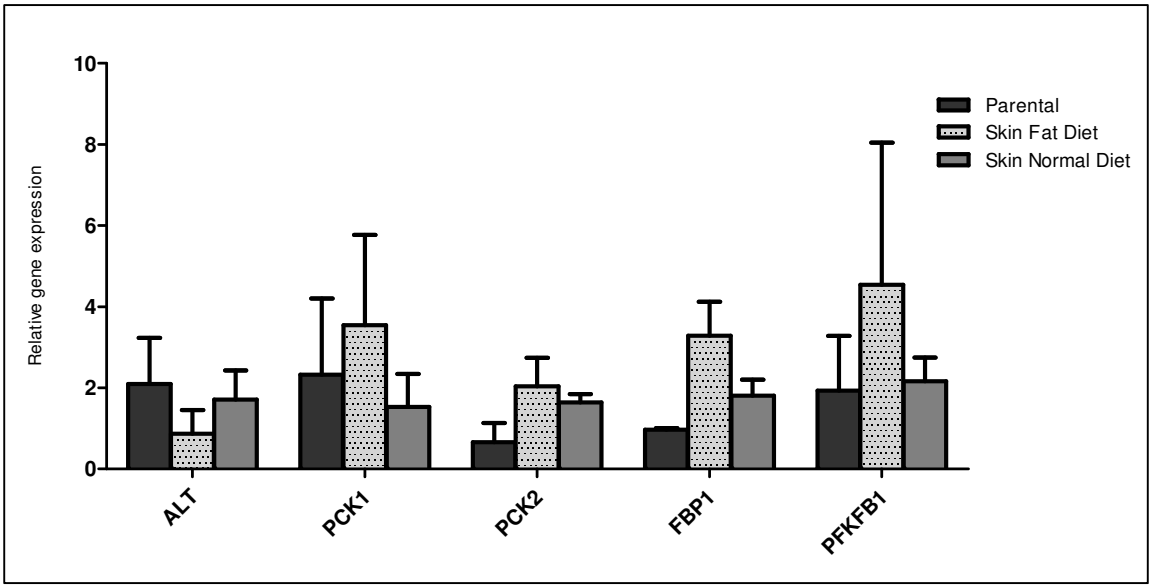

Figure 32– Relative gene expression of gluconeogenic enzymes ALT, PCK1, PCK2, FBP1 and PFKFB1. 18S rRNA gene was the endogenous control. Expression levels were normalized to parental lineage. Data are mean ± error bars of triplicates.

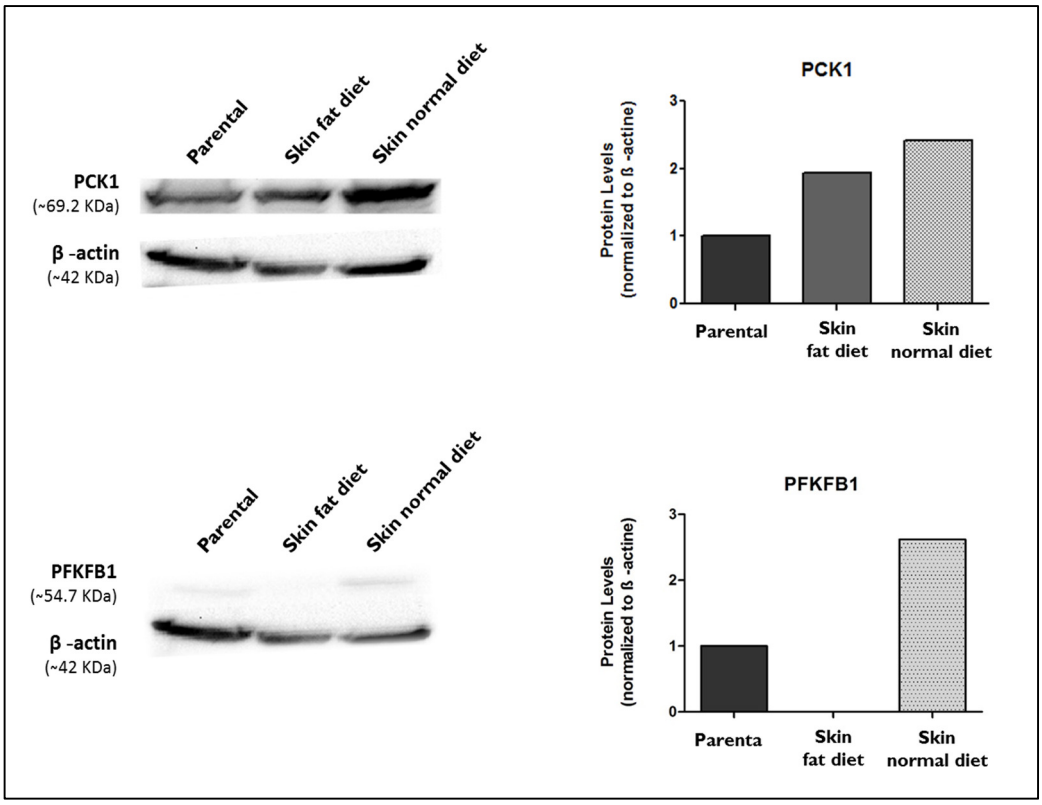

Figure 33 – PCK1 and PFKFB1 protein levels assessed by western blot. Protein levels were normalized to β-actin and are relative to those obtained in the parental lineage.

Alanine is one of the gluconeogenic substrates which through transamination is converted into pyruvate. This reaction is catalyzed by alanine aminotransaminase (ALT). In this study, no differences were detected at mRNA level between the different cell lineages. However, studies have demonstrated higher levels of ALT in colorectal cancer patients with liver metastasis (Wu *et al.*, 2012), which can be related to the fact that the liver is the main gluconeogenic organ as the ALT in those patients was measured in peripheral blood.

In the expression of phosphoenolpyruvate carboxykinase cytosolic (PCK1) that catalyzes the main reaction in cytoplasmic gluconeogenesis, the conversion of oxaloacetate into phosphoenolpyruvate (Granner & Pilkis, 1990), the results obtained at mRNA level are different from those obtained at protein level. The relative gene expression is similar between the cell lineages. However, cells from both skin fat diet and skin normal diet mice revealed an increased protein expression in relation to the parental lineage. The absence of correlation between mRNA and protein levels could be a result of varied post-transcriptional mechanisms involved in convertion of mRNA into protein or due to the different in vivo half-lives of proteins resultant from protein synthesis and degradation (Greenbaum *et al.*, 2003). Moreover, other studies have found that PCK1 mRNA levels were significantly higher in the liver metastatic lesions in comparison to the primary pancreatic tumors (Chaika *et al.*, 2012). Again the gluconeogenic expertise of the liver can be the key element in this observation.

Phosphoenolpyruvate carboxykinase mitochondrial (PCK2) catalyzes the main reaction of mitochondrial gluconeogenesis, the conversion of oxaloacetate into phosphoenolpyruvate (Granner and Pilkis, 1990). mRNA levels show no significant differences between cell lineages. Studies suggest PCK2 may be associated with cell proliferation in hepatocelular carcinoma (Y.-X. Liu *et al.*, 2012), that may be due to the fact that hepatocarcinoma cells retain the ability of normal hepatocytes of fulfilling gluconeogenesis.

Fructose-1,6-bisphosphatase (FBP1) is the gluconeogenic enzyme that catalyzes the conversion of fructose-1, 6-biphosphate (F1,6BP) in fructose-6-phosphate (F6P) (Quintas *et al.*, 2008). mRNA levels of this enzyme also show no differences between cell lineages. In the literature, this key enzyme is found silenced in gastric, liver and colon

cancer (Quintas *et al.*, 2008). Accordingly, in a study about breast cancer, *FBP1* expression inhibited tumorigenicity *in vitro* and suppressed tumor formation *in vivo* (Dong *et al.*, 2013).

The last evaluated enzyme was PFKFB1, an enzyme associated with the promotion of glycolysis and the inhibition of gluconeogenesis through the activation or inhibition, respectively, of their kinase activity, being mainly expressed in the liver (Noguchi *et al.*, 2013). In this study, no differences were verified at mRNA level between the different cell lineages. However, the results obtained by western blotting at protein level revealed that this enzyme was downregulated in cells skin fat diet and overexpressed in cells skin normal diet. The characterization of this enzyme expression profile, in cancer context, is not depicted in the literature (Ros & Schulze, 2013).

In resume, in the mRNA levels of these gluconeogenic enzymes (ALT, PCK1, PCK2, FBP1 and PFKFB1) there aren't statistically significant differences between the cell lineages in study. However, the protein analysis revealed that PFKFB1 was downregulated in cells from the skin of mice exposed to fat diet. Since this enzyme has its function associated with the promotion of glycolysis and the inhibition of gluconeogenesis through the modulation of their kinase activity (Noguchi *et al.*, 2013), its inhibition may indicate that gluconeogenesis is one of the pathways involved in the accumulation of glucose inside of the cells of mice exposed to a fat diet.

4.2.4. Cell cycle analysis by FACS

Increased proliferation is one of the hallmarks in cancer. Cell cycle analysis was performed to evaluate the effect of different diets on cell cycle proliferation in all cultures. This analysis revealed that the cell lineages in study do not present statically significant differences in cell cycle status for all the evaluated time points (Figure 34).

Previous studies have indicated that high fat diet (LDL enriched) may be associated with an increased cell proliferation and cancer progression in prostate cancer (Huang *et al.*, 2012) and in colon cancer (Liu *et al.*, 2001). However, in our *in vitro* study this was not observed. Controversially, other data as shown that the addition of HDL to cell cultures increased the proliferation of human breast cancer cells (Uda *et al.*, 2012).

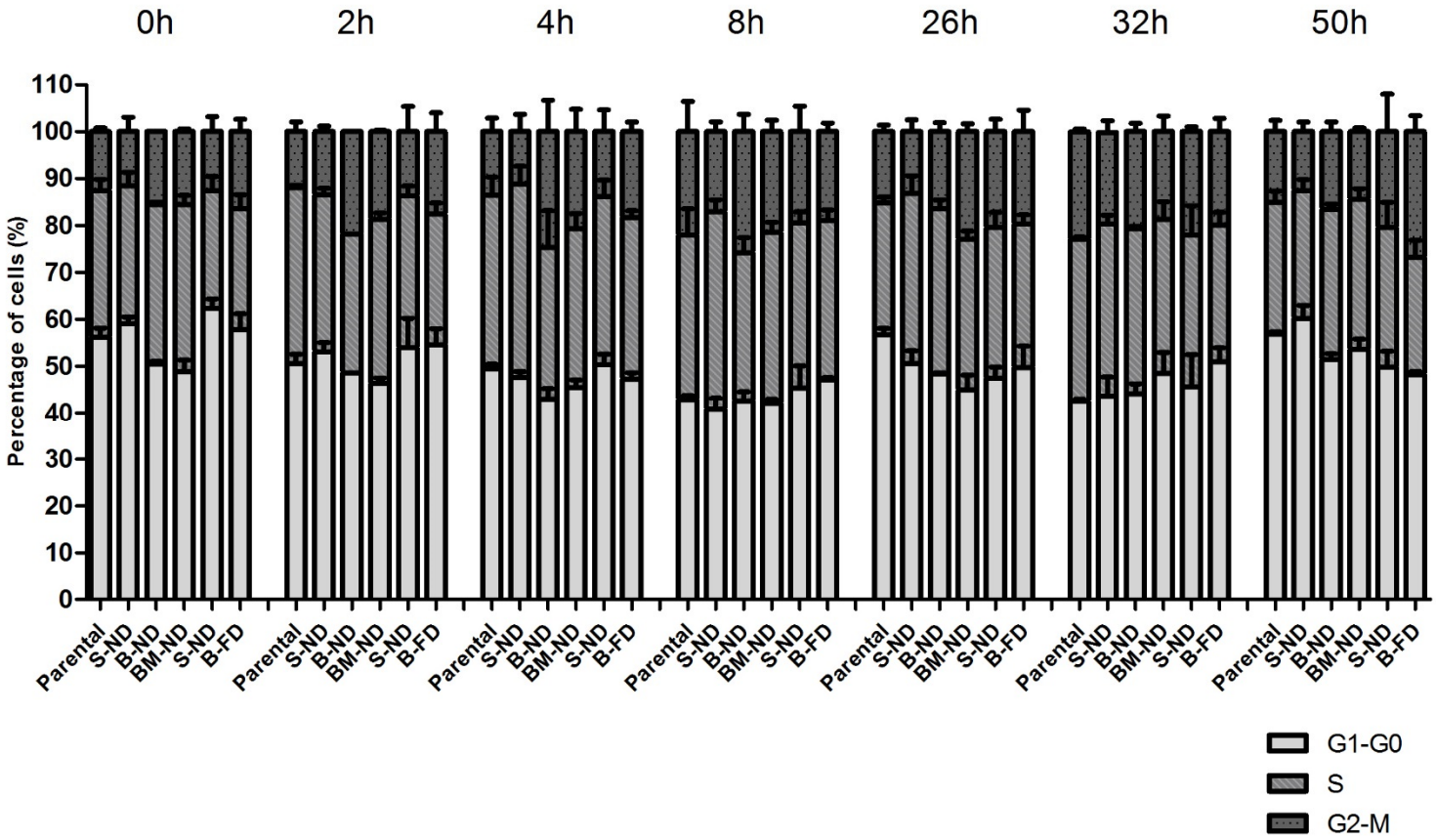

Figure 34 – Cell cycle analysis by FACS (PI staining) in all cell lineages, at time point 0, 2, 4, 8, 26, 32 and 50 h. Data are means of triplicates. In brain fat diet lineage it is included the results of the two cultures and in skin fat diet is included the results of the three cultures.

4.2.5. Cell death (apoptosis and necrosis) analysis by FACS

Another important area of interest is the study of active programmed cell death (apoptosis), compared with passive cell death (necrosis), due to the fact that resistance to apoptosis is one of the hallmarkers of cancer (Seyfried & Shelton, 2010).

In this study, apoptosis and necrosis analysis was performed to all cell lines, at 0 h and at 24 h (Figure 35).

The percentage of cells in apoptosis and necrosis is very low, showing no significant differences between cell lineages at any evaluated time point. These results suggest that in the *in vitro* conditions evaluated in our study, the *in vivo* selection of cells with a diet rich in cholesterol does not increase resistance to cell death. In a study of breast tumor cells calorie restriction appeared to promote apoptosis, whereas consumption of a high fat diet reduced apoptosis (Dogan *et al.*, 2007). Additionally, a study of prostate cancer cells in xenografts indicated that cholesterol elevation reduced apoptosis (Zhuang, *et al.*, 2005). Nevertheless, in our study cells were exposed to fat diet *in vivo* but *in vitro* this selective pressure was not maintained. Hence, in order to confirm that resistance to cell death is an adaptive process and not a selectively acquired cell feature that become constitutive, additional experiments will be performed by culturing cell lineages in cholesterol enriched culture medium.

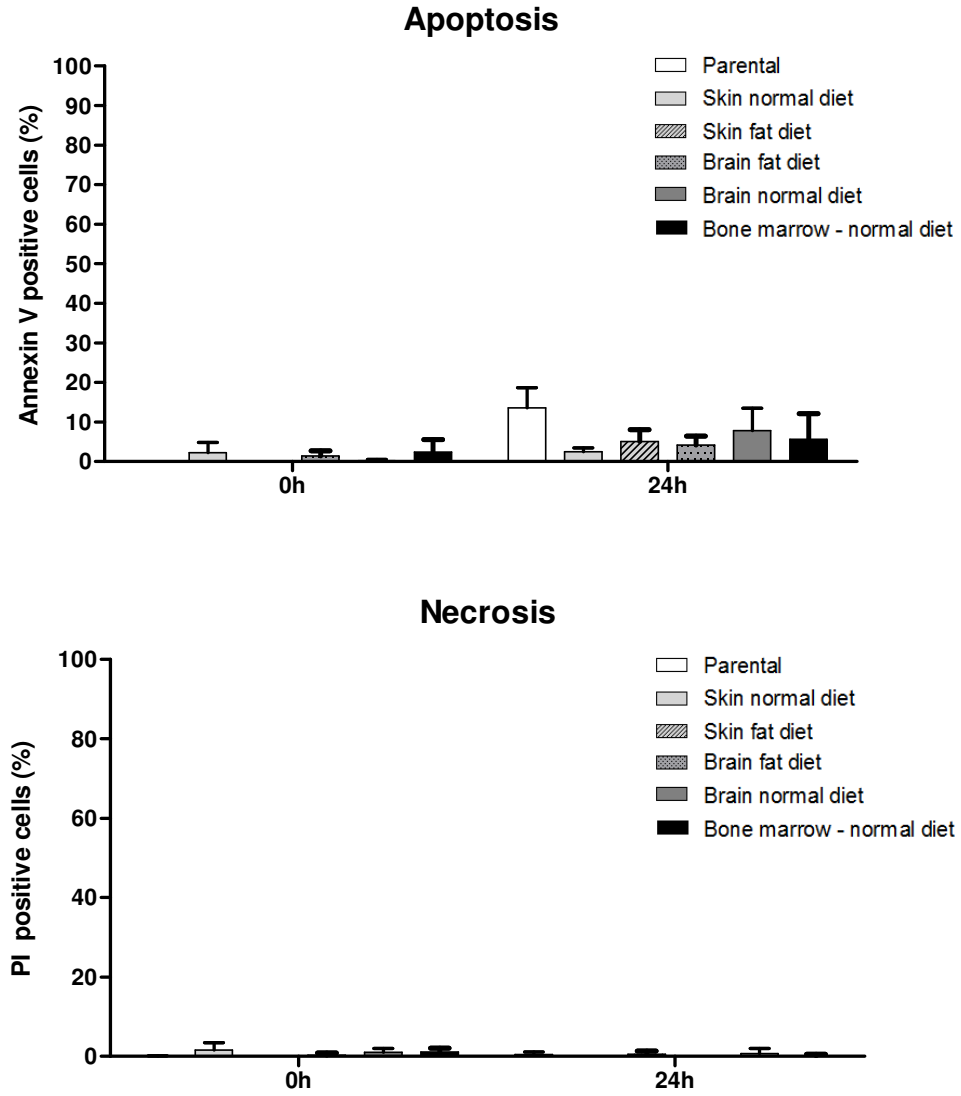

Figure 35 – Apoptosis (annexin V positive cells) and necrosis (PI positive cells) analysis by FACS, at time points 0 and 24 h. Data are means of triplicates ± error bars of triplicates. In brain fat diet lineage it is included the results of the two cultures and in skin fat diet is included the results of the three cultures.

5. Concluding Remarks

The spread of cancer into the central nervous system (CNS) is a serious problem leading to neurological symptoms and rapid mortality. The ability to detect and characterize malignant cells in the cerebrospinal fluid (CSF) can help in understanding the biology of metastatic spread In addition to detecting cancer cells in the CSF through direct methods, studies have focused in the indirect detection of CSF malignancy through changes in expression patterns of proteins and metabolites in CSF samples. Since the current diagnostic tools available lack of sensitivity, metabolomic approach could be promising in detecting the earliest meaningful sign of neoplastic presence in the CSF (Schold, Wasserstrom, Fleisher, Schwartz, & Posner, 1980; Weston *et al.*, 2011). Moreover, the determination of the CSF metabolome in cell invansion situation gives insights about the interaction of the tumoral cells and the CSF, and can help to explain the preference of some tumors for the CNS.

Nuclear magnetic ressonance (NMR) analysis of CSF samples from patients without cell invasion revealed that the metabolic profile of CSF from children is different from adults. However, CSF composition is not affected by gender and primary tumor origin.

The NMR analyses of CSF from patients with and without cell invasion indicates that there are differences between the two groups, but the number of CSF samples is still small to obtain a more concrete conclusion.

The preliminary study of a leukemia murine model (697-GFP cell line) exposed to different diets (normal and fat diet) revealed that the metabolic prolile of the cells from mice exposed to fat diet is different from the ones exposed to a normal diet. In contrast, there are not significant differences between the metabolic profiles of these cells with different localizations of tumor metastasis. Gene and protein expression analysis of these cells suggests that gluconeogenesis may be one of the pathways that could underlie the differences found between the cells from mice exposed to different diets.

Overall, these studies may help in understanding the pathophysiology of this disease, including the site-specific properties of tumor cells and the CNS microenvironment.

6. Future Perspectives

For the study of CSF from patients with and without metastasis in the CNS, it is necessary a bigger number of samples with cell invasion in other to clarify if there are differences between these two groups at metabolic level and which metabolites are responsible for that differences. In order, to extend our analysis, the utilization of other techniques, such LC-MS and GC-MS, would be useful. A proteomic analysis of the CSF is also planned to be performed in the near future.

In the in vitro study of cancer metastasis using leukemia murine model (697-GFP cell line) exposed to normal and fat diet, it is necessary to perform gene and protein expression analyses to the others cell lineages (brain fat diet, brain normal diet and bone marrow normal diet). In addition, metabolic analysis by NMR of these cultures with ^{13}C-labeled glucose could be performed in order to better understand the metabolism of tumor cells and identify the main carbon source of tumor cells.

7. References

Agarwala, S., Keilholz, U., & Gilles, E. (2009). LDH correlation with survival in advanced melanoma from two large, randomised trials (Oblimersen GM301 and EORTC 18951). *Eur J Cancer*, *45*, 1807–1814.

Airley, R., & Mobasheri, A. (2007). Hypoxic regulation of glucose transport, anaerobic metabolism and angiogenesis in cancer: novel pathways and targets for anticancer therapeutics. *Chemotherapy*, *53*(4), 233–256.

Alikhani, N., Ferguson, R., Ruslan, N., Gallagher, E., Scheinman, E., Yakar, S., & LeRoith, D. (2013). Mammary tumor growth and pulmonary metastasis are enhanced in a hyperlipidemic mouse model. *Oncogene*, *32*(8), 961–967.

Allen, R., Hunter, W. 3rd, & Agrawal, D. (1997). Morphological and biochemical characterization and analysis of apoptosis. *J Pharmacol Toxicol Methods*, *37*(4), 215–228.

An, Y. J., Cho, H. R., Kim, T. M., Keam, B., Kim, J. W., Wen, H., … Park, S. (2014). An NMR metabolomics approach for the diagnosis of leptomeningeal carcinomatosis in lung adenocarcinoma cancer patients. *International Journal of Cancer. Journal International Du Cancer*. doi:10.1002/ijc.28949

Aragon-Ching, J. B., & Zujewski, J. A. (2007). CNS metastasis: an old problem in a new guise. *Clinical Cancer Research : An Official Journal of the American Association for Cancer Research*, *13*(6), 1644–7. doi:10.1158/1078-0432.CCR-07-0096

Atkinson, A., Colburn, W., DeGruttola, V., DeMets, D., Downing, G., Hoth, D., … Grp, B. (2001). Biomarkers and surrogate endpoints: Preferred definitions and conceptual framework. *Clinical Pharmacology & Therapeutics*, *69*(3), 89–95.

Bacac, M., & Stamenkovic, I. (2008). Metastatic cancer cell. *Annu Rev Pathol*, *3*, 221–247.

Baenke, F., Peck, B., Miess, H., & Schulze, A. (2013). Hooked on fat: the role of lipid synthesis in cancer metabolism and tumour development. *Disease Models & Mechanisms*, *6*(6), 1353–63. doi:10.1242/dmm.011338

Baer, S., Casaubon, L., & Younes, M. (1997). Expression of the human erythrocyte glucose transporter Glut1 in cutaneous neoplasia. *J Am Acad Dermatol*, *37*(4), 575–577.

Barnholtz-Sloan, J., Sloan, A., Davis, F., Vigneau, F., Lai, P., & Sawaya, R. (2004). Incidence proportions of brainme- tastases in patients diagnosed (1973 to 2001) in the Metropolitan Detroit Cancer Surveillance System. *J Clin Oncology*, *22*(14), 2865–2872.

Beckonert, O., Keun, H., Ebbels, T., Bundy, J., Holmes, E., Lindon, J., & Nicholson, J. (2007). Metabolic profiling, metabolomic and metabonomic procedures for NMR spectroscopy of urine, plasma, serum and tissue extracts. *Nature Protocols*, *2*(11), 2692–2703.

Bedikian, A., Johnson, M., Warneke, C., Papadopoulos, N., Kim, K., Hwu, W., … Hwu, P. (2008). Prognostic factors that determine the long-term survival of patients with unresectable metastatic melanoma. *Cancer Invest*, *26*(6), 624–633.

Beer, D. G., Kardia, S. L., Huang, C.-C., Giordano, T. J., Levin, A. M., Misek, D. E., … Hanash, S. (2002). Gene-expression profiles predict survival of patients with lung adenocarcinoma. *Nature Medicine*, *8*(8), 816–824. doi:10.1038/nm

Beger, R., Schnackenberg, L., Holland, R., Li, D., & Dragan, Y. (2006). Metabonomic models of human pancreatic cancer using 1D proton NMR spectra of lipids in plasma. *Metabolomics*, *2*(3), 125–134.

Blasco, H., Corcia, P., Moreau, C., Veau, S., Fournier, C., Vourc'h, P., … Andres, C. (2010). 1H-NMR-based metabolomic profiling of CSF in early amyotrophic lateral sclerosis. *PLoS One*, *5*, 10.

Bogdanov, M., Matson, W., Wang, L., Matson, T., Saunders-Pullman, R., Bressman, S., & Beal, M. (2008). Metabolomic profiling to develop blood biomarkers for Parkinson's disease. *Brain*, *131*, 389– 396.

Bonadio, W., Stanco, L., Bruce, R., Barry, D., & Smith, D. (1992). Reference values of normal cerebrospinal fluid composition in infants ages 0 to 8 weeks . *Pediatr Infect Dis J.*, *11*(7), 589–591.

Brown, M., & Goldstein, J. (1986). A receptor-mediated pathway for cholesterol homeostasis. *Science*, *232*(4746), 34–47.

Buckner, J., Brown, P., O'Neill, B., Meyer, F., Wetmore, C., & Uhm, J. (2007). Central nervous system tumors. *Mayo Clin Proc*, *82*(10), 1271–1286.

Cairns, R. a, Harris, I. S., & Mak, T. W. (2011). Regulation of cancer cell metabolism. *Nature Reviews. Cancer*, *11*(2), 85–95. doi:10.1038/nrc2981

Cantuaria, G., Fagotti, A., Ferrandina, G., Magalhaes, A., Nadji, M., Angioli, R., … Scambia, G. (2001). GLUT-1 expression in ovarian carcinoma: association with survival and response to chemotherapy. *Cancer*, *92*(5), 1144–1150.

Cecchini, M., Amiri, M., & Dick, F. (2012). Analysis of cell cycle position in mammalian cells. *Journal of Visualized Experiments*, *7*, 1–7.

Chaika, N. V, Yu, F., Purohit, V., Mehla, K., Lazenby, A. J., DiMaio, D., … Singh, P. K. (2012). Differential expression of metabolic genes in tumor and stromal components of primary and metastatic loci in pancreatic adenocarcinoma. *PloS One*, *7*(3), e32996. doi:10.1371/journal.pone.0032996

Chambers, A., Groom, A., & MacDonald, I. (2002). Dissemination and growth of cancer cells in metastatic sites. *Nat Rev Cancer*, *2*(8), 563–572.

Clifford, S. (2012). Cancer genetics: Evolution after tumour spread. *Nature*, 482–481.

Coen, M., Holmes, E., Lindon, J., & Nicholson, J. (2008). NMR-based metabolic profiling and metabonomic approaches to problems in molecular toxicology . *Chemical Research in Toxicology*, *21*(1), 9–27.

Constantinou, M., Papakonstantinou, E., Spraul, M., Sevastiadou, S., Costalos, C., Koupparis, M., … Mikros, E. (2005). H-1 NMR-based metabonomics for the diagnosis of inborn errors of metabolism in urine . *Analytica Chimica Acta*, *542*(2), 169–177.

Danilo, C., & Frank, P. (2012). Cholesterol and breast cancer development. *Curr Opin Pharmacol*, *12*(6), 677–682.

Darzynkiewicz, Z., Bruno, S., Del Bino, G., Gorczyca, W., Hotz, M. a, Lassota, P., & Traganos, F. (1992). Features of apoptotic cells measured by flow cytometry. *Cytometry*, *13*(8), 795–808. doi:10.1002/cyto.990130802

Derveaux, S., Vandesompele, J., & Hellemans, J. (2010). How to do successful gene expression analysis using real-time PCR. *Methods*, *50*, 227–230.

DeVita, T., Hellman, T., & Rosenberg, S. (2008). *DeVita, Hellman, and Rosenberg's cancer : principles & practice of oncology.* Philadelphia: Wolters Kluwer/Lippincott Williams & Wilkins.

Dogan, S., Hu, X., Zhang, Y., Maihle, N., Grande, J., & Cleary, M. (2007). Effects of high-fat diet and/or body weight on mammary tumor leptin and apoptosis signaling pathways in MMTV-TGF-alpha mice. *Breast Cancer Research*, *9*(6), R91.

Dong, C., Yuan, T., Wu, Y., Wang, Y., Fan, T., Miriyala, S., … Zhou, B. P. (2013). Loss of FBP1 by Snail-mediated repression provides metabolic advantages in basal-like breast cancer. *Cancer Cell*, *23*(3), 316–331.

Draoui, N., & Feron, O. (2011). Lactate shuttles at a glance: from physiological paradigms to anti-cancer treatments. *Dis Model Mech*, *4*(6), 727–732.

Duarte, I. F., Lamego, I., Rocha, C., & Gil, A. M. (2009). NMR metabonomics for mammalian cell metabolism studies. *Bioanalysis*, *1*(9), 1597–614. doi:10.4155/bio.09.151

Duarte, I. F., Rocha, C. M., Barros, A. S., Gil, A. M., Goodfellow, B. J., Carreira, I. M., … Carvalho, L. (2010). Can nuclear magnetic resonance (NMR) spectroscopy reveal different metabolic signatures for lung tumours? *Virchows Archiv : An International Journal of Pathology*, *457*(6), 715–25. doi:10.1007/s00428-010-0993-6

Duffy, M., McGowan, P., & Gallagher, W. (2008). Cancer invasion and metastasis: changing views. *J Pathol*, *214*(3), 283–293.

Dumas, M., Maibaum, E., Teague, C., Ueshima, H., Zhou, B., Lindon, J., … Holmes, E. (2006). Assessment of analytical reproducibility of H-1 NMR spectroscopy based metabonomics for large-scale epidemiological research: the INTERMAP study. *Anal Chem*, *1*(78), 2199–2208.

Dunn, W., Goodacre, R., Neyses, L., & Mamas, M. (2011). Integration of metabolomics in heart disease and diabetes research: current achievements and future outlook. *Bioanalysis*, *3*(19), 2205–2222.

Duvall, E., & Wyllie, A. (1986). Death and the cell. *Immunol Today*, *7*, 115–119.

Eidukevicius, R., Characiejus, D., Janavicius, R., Kazlauskaite, N., Pasukoniene, V., Mauricas, M., & Den Otter, W. (2005). A method to estimate cell cycle time and growth fraction using bromodeoxyuridine-flow cytometry data from a single sample. *BMC Cancer*, *5*, 122. doi:10.1186/1471-2407-5-122

Ellis, D., Dunn, W., Griffin, J., Allwood, J., & Goodacre, R. (2007). Metabolic fingerprinting as a diagnostic tool. *Pharmacogenomics*, *8*(9), 1243–1266.

Eriksson, L., Kettaneh-Wold, E., & Wold, N. (2001). *Multi- and Megavariate Data Analysis—Principles and Applications*. Umeå: Umetrics Academy.

Fang, J., Quinones, Q., Holman, T., Morowitz, M., Wang, Q., Zhao, H., … Wahl, M. (2006). The H+ -Linked Monocarboxylate Transporter (MCT1 / SLC16A1): A Potential Therapeutic Target for High-Risk Neuroblastoma. *Mol Pharmacol*, *70*(6), 2108–2115.

Ferlay, J., Soerjomataram, I., Ervik, M., Dikshit, R., Eser, S., Mathers, C., … Bray, F. (2013). GLOBOCAN 2012 v1.0, Cancer Incidence and Mortality Worldwide: IARC CancerBase No. 11 [Internet]. Lyon, France. *International Agency for Research on Cancer*. Retrieved from http://globocan.iarc.fr

Fidler, I. (2003). The pathogenesis of cancer metastasis: the “seed and soil” hypothesis revisited. *Nat Rev Cancer*, *3*(6), 453–458.

Fiehn, O. (2002). Metabolomics--the link between genotypes and phenotypes. *Plant Mol Biol*, *48*(1-2), 155–171.

Freeman, W. M., Walker, J., & Vrana, K. E. (1999). Review Quantitative RT-PCR : Pitfalls and Potential. *BioTechniques*, *26*, 112–125.

Ganapathy, V., Thangaraju, M., & Prasad, P. D. (2009). Nutrient transporters in cancer: relevance to Warburg hypothesis and beyond. *Pharmacology & Therapeutics*, *121*(1), 29–40. doi:10.1016/j.pharmthera.2008.09.005

Gillies, R., Bhujwalla, Z., Evelhoch, J., Garwood, M., Neeman, M., Robinson, S., … Van Der Sanden, B. (2000). Applications of magnetic resonance in model systems: tumor biology and physiology. *Neoplasia*, *2*(1-2), 139–151.

Ginzinger, D. G. (2002). Gene quantification using real-time quantitative PCR: an emerging technology hits the mainstream. *Experimental Hematology*, *30*(6), 503–12. Retrieved from http://www.ncbi.nlm.nih.gov/pubmed/12063017

Gotanda, Y., Akagi, Y., Kawahara, A., Kinugasa, T., Yoshida, T., Ryu, Y., … Shirouzu, K. (2013). Expression of Monocarboxylate Transporter (MCT)-4 in Colorectal Cancer and its Role: MCT4 Contributes to the Growth of Colorectal Cancer with Vascular Endothelial Growth Factor. *Anticancer Research*, *33*, 72941–72947.

Gowda, G., Zhang, S., Gu, H., Asiago, V., Shanaiah, N., & Raftery, D. (2008). Metabolomics-based methods for early disease diagnostics. Expert Review of Molecular Diagnostics. *Expert Review of Molecular Diagnostics*, *8*(5), 617–633.

Granner, D., & Pilkis, S. (1990). The genes of hepatic glucose metabolism. *J. Biol. Chem*, *265*(18), 10173–10176.

Greenbaum, D., Colangelo, C., Williams, K., & Gerstein, M. (2003). Comparing protein abundance and mRNA expression levels on a genomic scale. *Genome Biol*, *4*(9), 117.

Hagenfeldt, L., Bjerkenstedt, L., Edman, G., Sedvall, G., & Wiesel, F. (1984). Amino acids in plasma and CSF and monoamine metabolites in CSF: interrelationship in healthy subjects. *Journal of Neurochemistry*, *42*(3), 833–837.

Halestrap, A., & Price, N. (1999). The proton-linked monocarboxylate transporter (MCT) family: structure, function and regulation. *Biochem J*, *343*(Pt 2), 281–299.

Hanahan, D., & Weinberg, R. a. (2011). Hallmarks of cancer: the next generation. *Cell*, *144*(5), 646–674. doi:10.1016/j.cell.2011.02.013

Hanahan, D., & Weinberg, R. A. (2000). The Hallmarks of Cancer. *Cell*, *100*, 57–70.

Higashi, T., Tamaki, N., Torizuka, T., Nakamoto, Y., Sakahara, H., Kimura, T., … Konishi, J. (1998). FDG uptake, GLUT-1 glucose transporter and cellularity in human pancreatic tumors. *J Nucl Med*, *39*(10), 1727–1735.

Himsworth, H. (1935). The dietetic factor determining the glucose tolerance and sensitivity to insulin of healthy men. *Clin Sci*, *2*, 67–94.

Holmes, E., Tsang, T., & Tabrizi, S. (2006). The application of NMR-based metabonomics in neurological disorders. *NeuroRx*, *3*(3), 358–372.

Holmes, R., & Goldberg, E. (2009). Computational analyses of mammalian lactate dehydrogenases: human, mouse, opossum and platypus LDHs. *Comput Biol Chem*, *33*(5), 379–385.

Hori, S., Nishiumi, S., Kobayashi, K., Shinohara, M., Hatakeyama, Y., Kotani, Y., … Yoshida, M. (2011). A metabolomic approach to lung cancer. *Lung Cancer*, *74*(2), 284–292.

Huang, M., Narita, S., Numakura, K., Tsuruta, H., Saito, M., Inoue, T., … Habuchi, T. (2012). A high-fat diet enhances proliferation of prostate cancer cells and activates MCP-1/CCR2 signaling. *Prostate*, *72*(16), 1779–1788.

Izumi, H., Takahashi, M., Uramoto, H., Nakayama, Y., Oyama, T., Wang, K., … Kohno, K. (2011). Monocarboxylate transporters 1 and 4 are involved in the invasion activity of human lung cancer cells. *Cancer Sci*, *102*(5), 1007–1013.

Jackson, V., Price, N., Carpenter, L., & Halestrap, A. (2007). Cloning of the monocarboxylate transporter isoform MCT2 from rat testis provides evidence that expression in tissues is species-specific and may involve post-transcriptional. *Biochem J*, *324*(Pt2), 447–453.

Jolliffe, I. (2002). *Principal Component Analysis* (2nd Editio., p. 488). New York: Springer Series in Statistics.

Kang, K., Im, Y., Go, W., & Han, H. (2009). c-Myc Amplification Altered the Gene Expression of ABC- and SLC-Transporters in Human Breast Epithelial Cells. *Mol Pharm*, *6*(2), 627–633.

Keun, H., Beckonert, O., Griffin, J., Richter, C., Moskau, D., Lindon, J., & Nicholson JK. (2002). Cryogenic probe 13C NMR spectroscopy of urine for metabonomic studies. *Anal Chem*, *74*(17), 4588–4593.

Kimura, Y., & Sumiyoshi, M. (2007). High-fat, high-sucrose, and high-cholesterol diets accelerate tumor growth and metastasis in tumor-bearing mice. *Nutr Cancer*, *59*(2), 207–216.

Kinoshita, T., Nohata, N., Yoshino, H., Hanazawa, T., Kikkawa, N., Fujimura, L., … Seki, N. (2011). Tumor suppressive microRNA-375 regulates lactate dehydrogenase B in maxillary sinus squamous cell carcinoma. *Int J Oncol*, *40*(1), 185–193.

Kork, F., Holthues, J., Hellweg, R., Jankowski, V., Tepel, M., Ohring, R., … Jankowski, J. (2009). A Possible New Diagnostic Biomarker in Early Diagnosis of Alzheimer's Disease . *Current Alzheimer Research*, *6*(6), 519–524.

Koslowski, M., Türeci, Ö., Bell, C., Krause, P., Lehr, H., Brunner, J., … Sahin, U. (2002). Multiple splice variants of lactate dehydrogenase C selectively expressed in human cancer. *Cancer Res*, *62*, 6750–6755.

Kroemer, G., Petit, P., Zamzami, N., Vayssière, J., & Mignotte, B. (1995). The biochemistry of programmed cell death. *FASEB J*, *9*(13), 1277–1287.

Kumar, A., Bala, L., Kalita, J., Misra, U. K., Singh, R. L., Khetrapal, C. L., & Babu, G. N. (2010). Metabolomic analysis of serum by (1) H NMR spectroscopy in amyotrophic lateral sclerosis. *Clinica Chimica Acta; International Journal of Clinical Chemistry*, *411*(7-8), 563–7. doi:10.1016/j.cca.2010.01.016

Kurien, B., & Scofield, R. (2006). Western blotting. *Methods*, *38*(4), 283–293.

Lewis, B., Prescott, J., Campbell, S., Shim, H., Orlowski, R., & Dang, C. (2000). Tumor Induction by the c-Myc Target Genes rcl and Lactate Dehydrogenase A. *Cancer Res*, *60*(21), 6178–6183.

Lichtenstein, A., & Schwab, U. (2000). Relationship of dietary fat to glucose metabolism. *Atherosclerosis*, *150*(2), 227–43. Retrieved from http://www.ncbi.nlm.nih.gov/pubmed/10856515

Lincz, L. (1998). Deciphering the apoptotic pathway: all roads lead to death. *Immunol Cell Biol*, *76*(1), 1–19.

Lindon, J., Holmes, E., Bollard, M., Stanley, E., & Nicholson, J. (2004). Metabonomics technologies and their applications in physiological monitoring, drug safety assessment and disease diagnosis. *Biomarkers*, *9*(1), 1–31.

Lindon, J., Holmes, E., & Nicholson, J. (2007). Metabonomics in pharmaceutical R&D. *FEBS J*, *274*(5), 1140–1151.

Liu, Y.-X., Zhang, S.-F., Ji, Y.-H., Guo, S.-J., Wang, G.-F., & Zhang, G.-W. (2012). Whole-exome sequencing identifies mutated PCK2 and HUWE1 associated with carcinoma cell proliferation in a hepatocellular carcinoma patient. *Oncol Lett*, *4*(4), 847–851.

Liu, Z., Uesaka, T., Watanabe, H., & Kato, N. (2001). High fat diet enhances colonic cell proliferation and carcinogenesis in rats by elevating serum leptin. *International Journal of Oncology*, *19*(5), 1009–1014.

Lutz, N., & Cozzone, P. (2011). Metabolic Profiling in Multiple Sclerosis and Other Disorders by Quantitative Analysis of Cerebrospinal Fluid Using Nuclear Magnetic Resonance Spectroscopy. *Current Pharmaceutical Biotechnology*, *12*(7), 1016–1025.

Lutz, N., Viola, A., Malikova, I., Confort-Gouny, S., Audoin, B., Ranjeva, J., & Pelletier, J. (2007). Inflammatory multiple-sclerosis plaques generate characteristic metabolic profiles in cerebrospinal fluid. *PLoS One*, *2*(7), 595.

Macey, M. (2007). *Flow Cytometry: Principles and Applications* (Humana Pre., p. 290). London.

Macheda, M., Rogers, S., & Best, J. (2005). Molecular and cellular regulation of glucose transporter (GLUT) proteins in cancer. *J Cell Physiol*, *202*(3), 654–662.

Madsen, R., Lundstedt, T., & Trygg, J. (2010). Chemometrics in metabolomics--a review in human disease diagnosis. *Analytica Chimica Acta*, *659*(1-2), 23–33. doi:10.1016/j.aca.2009.11.042

Mardis, E. (2009). Recurring mutations found by sequencing an acute myeloid leukemia genome. *N Engl J Med*, *361*(11), 1058–1066.

May, C., Kaye, J., Atack, J., Schapiro, M., Friedland, R., & Rapoport, S. (1990). Cerebrospinal fluid production is reduced in healthy aging. *Neurology*, *40*(3), 500–503.

Meissner, A., van der Plas, A. a, van Dasselaar, N. T., Deelder, A. M., van Hilten, J. J., & Mayboroda, O. a. (2014). 1H-NMR metabolic profiling of cerebrospinal fluid in patients with complex regional pain syndrome-related dystonia. *Pain*, *155*(1), 190–6. doi:10.1016/j.pain.2013.10.005

Muntoni, S., Atzori, L., Mereu, R., Satta, G., Macis, M., Congia, M., … Muntoni, S. (2009). Serum lipoproteins and cancer. *Nutr Metab Cardiovasc Dis*, *19*(3), 218–225.

Nicholson, J., & Lindon, J. (2008). Systems biology: Metabonomics. *Nature*, *455*(7216), 1054–1056.

Nicholson, J., Lindon, J., & Holmes, E. (1999). "Metabonomics": understanding the metabolic responses of living systems to pathophysiological stimuli via multivariate statistical analysis of biological NMR spectroscopic data. *Xenobiotica*, *29*(11), 1181–1189.

Nishimura, Y., Romer, L. H., & Lemasters, J. J. (1998). Mitochondrial dysfunction and cytoskeletal disruption during chemical hypoxia to cultured rat hepatic sinusoidal endothelial cells: The pH paradox and cytoprotection by glucose, acidotic pH, and glycine. *Hepatology*, *27*, 1039–1049.

Noguchi, R., Kubota, H., Yugi, K., Toyoshima, Y., Komori, Y., Soga, T., & Kuroda, S. (2013). The selective control of glycolysis, gluconeogenesis and glycogenesis by temporal insulin patterns. *Molecular Systems Biology*, *9*, 664.

Nussbaum, E., Djalilian, H., Cho, K., & Hall, W. (1996). Brain metastases. Histology, multiplicity, surgery, and survival. *Cancer*, *78*(8), 1781–1788.

Odell, I., & Cook, D. (2013). Immunofluorescence techniques. *J Invest Dermatol*, *133*(1), e4.

Oliver, S., Winson, M., Kell, D., & Baganz, F. (1998). Systematic functional analysis of the yeast genome. *Trends in Biotechnology*, *16*(9), 373–378.

Palmieri, D., Chambers, A., Felding-Habermann, B., Huang, S., & Steeg, P. (2007). Biology of metastasis to a sanctuary site. *Clin Cancer Res*, *13*(6), 1656–1662.

Patchell, R. (2003). The management of brain metastases. *Cancer Treat Rev*, *29*, 533–540.

Pawelek, J. (2008). Cancer-cell fusion with migratory bone-marrow-derived cells as an explanation for metastasis: new therapeutic paradigms. *Future Oncol*, *4*(4), 449–452.

Pekmezci, M., & Perry, A. (2013). Neuropathology of brain metastases. *Surgical Neurology International*, *4*(Suppl 4), S245–55. doi:10.4103/2152-7806.111302

Pinheiro, C., Albergaria, A., Paredes, J., Sousa, B., Dufloth, R., Vieira, D., … Baltazar, F. (2010). Monocarboxylate transporter 1 is up-regulated in basal-like breast carcinoma. *Histopathology*, *56*, 860–867.

Pinheiro, C., Longatto-filho, A., Scapulatempo, C., Ferreira, L., Martins, S., Pellerin, L., … Baltazar, F. (2008). Increased expression of monocarboxylate transporters 1 , 2 , and 4 in colorectal carcinomas. *Virchows Arch*, *452*(2), 139–146.

Pinheiro, C., Longatto-Filho, A., Simões. K, Jacob, C., Bresciani, C., Zilberstein, B., … Baltazar, F. (2009). The prognostic value of CD147/EMMPRIN is associated with monocarboxylate transporter 1 co-expression in gastric cancer. *Eur J Cancer*, *45*, 2418–2424.

Pui, C. (2006). Central nervous system disease in acute lymphoblastic leukemia: prophylaxis and treatment. *HematologyAm Soc Hematol Educ Program*, 142–146.

Pui, C., & Evans, W. (2006). Treatment of acute lymphoblastic leukemia. *N Engl J Med*, *354*, 166–178.

Quinones, M., & Kaddurah-Daouk, R. (2009). Metabolomics tools for identifying biomarkers for neuropsychiatric diseases. *Neurobiology of Disease*, *35*(2), 165–176.

Quintas, A., Freire, A., & Halpern, M. (2008). Quintas, A., Freire, A., and Halpern, M. (2008a). In *Organização Molecular Da Vida* (Lidel., pp. 431–446). Lisboa.

Ravazoula, P., Batistatou, A., Aletra, C., Ladopoulos, J., Kourounis, G., & Tzigounis, B. (2003). Immunohistochemical expression of glucose transporter Glut1 and cyclin D1 in breast carcinomas with negative lymph nodes. *Eur J Gynaecol Oncol*, *24*(6), 544–546.

Ros, S., & Schulze, A. (2013). Balancing glycolytic flux: the role of 6-phosphofructo-2-kinase/fructose 2,6-bisphosphatases in cancer metabolism. *Cancer & Metabolism*, *1*(8).

Savorani, F., Tomasi, G., & Engelsen, S. (2010). icoshift: A versatile tool for the rapid alignment of 1D NMR spectra. *Journal of Magnetic Resonance*, *202*(2), 190–202.

Schiffer, E., Van Gessel, E., & Gamulin, Z. (1999). Influence of sex on cerebrospinal fluid density in adults. *British Journal of Anaesthesia*, *83*(6), 943–4. Retrieved from http://www.ncbi.nlm.nih.gov/pubmed/10700797

Schmid Daners, M., Knobloch, V., Soellinger, M., Boesiger, P., Seifert, B., Guzzella, L., & Kurtcuoglu, V. (2012). Age-specific characteristics and coupling of cerebral arterial inflow and cerebrospinal fluid dynamics. *PloS One*, *7*(5), e37502. doi:10.1371/journal.pone.0037502

Scholar, E., Violi, L., Newland, J., Bresnick, E., & Birt, D. (1989). The effect of dietary fat on metastasis of the lewis lung carcinoma and the BALB/c mammary carcinoma. *Nutrition and Cancer*, *12*(2), 109–119.

Schold, S., Wasserstrom, W., Fleisher, M., Schwartz, M., & Posner, J. (1980). Cerebrospinal fluid biochemical markers of central nervous system metastases. *Ann Neurol*, *8*, 597–604.

Seeley, R. R., Stephens, T. D., & Tate, P. (2003). *Anatomia e Fisiologia*. (McGraw-Hill, Ed.) (6th ed.). New York.

Seyfried, T. N., & Shelton, L. M. (2010). Cancer as a metabolic disease. *Nutrition & Metabolism*, *7*, 7. doi:10.1186/1743-7075-7-7

Shah, S. S., Ebberson, J., Kestenbaum, L. a, Hodinka, R. L., & Zorc, J. J. (2011). Age-specific reference values for cerebrospinal fluid protein concentration in neonates and young infants. *Journal of Hospital Medicine : An Official Publication of the Society of Hospital Medicine*, *6*(1), 22–7. doi:10.1002/jhm.711

Siegel, R., Desantis, C., Virgo, K., Stein, K., Mariotto, A., Smith, T., … Fedewa, S. (2012). Cancer Treatment and Survivorship Statistics , 2012. *CA: A Cancer Journal for Clinicians*, *62*(4), 220–241. doi:10.3322/caac.21149.

Silvente-Poirot, S., & Poirot, M. (2012). Cholesterol metabolism and cancer: the good, the bad and the ugly. *Curr Opin Pharmacol*, *12*(6), 673–676.

Sinclair, A. J., Viant, M. R., Ball, A. K., Burdon, M. a, Walker, E. a, Stewart, P. M., … Young, S. P. (2010). NMR-based metabolomic analysis of cerebrospinal fluid and serum in neurological diseases--a diagnostic tool? *NMR in Biomedicine*, *23*(2), 123–32. doi:10.1002/nbm.1428

Singer, K., Kastenberger, M., Gottfried, E., Hammerschmied, C., Büttner, M., Aigner, M., … Kreutz, M. (2011). Warburg phenotype in renal cell carcinoma: high expression of glucose-transporter 1 (GLUT-1) correlates with low CD8(+) T-cell infiltration in the tumor. *Int J Cancer*, *128*(9), 2085–2095.

Smith, T. (1999). Facilitative glucose transporter expression in human cancer tissue. *Br J Biomed Sci*, *56*(4), 285–292.

Smolinska, A., Posma, J. M., Blanchet, L., Ampt, K. a M., Attali, A., Tuinstra, T., … Wijmenga, S. S. (2012). Simultaneous analysis of plasma and CSF by NMR and hierarchical models fusion. *Analytical and Bioanalytical Chemistry*. doi:10.1007/s00216-012-5871-4

Sonveaux, P., Végran, F., Schroeder, T., Wergin, M. C., Verrax, J., Rabbani, Z. N., … Dewhirst, M. W. (2008). Targeting lactate-fueled respiration selectively kills hypoxic tumor cells in mice. *The Journal of Clinical Investigation*, *118*(12), 3930–3942. doi:10.1172/JCI36843.however

Spencer, M., Neto, A., Fuller, G., & Luna, M. (2005). Intracranial extension of acinic cell carcinoma of the parotid gland. *Arch Pathol Lab Med*, *129*(6), 780–782.

Statz, A., & Felgenhauer, K. (1983). Development of the blood-CSF barrier. *Dev Med Child Neurol*, *25*(2), 152–161.

Steeg, P. (2006). Tumor metastasis: mechanistic insights and clinical challenges. *Nat Med* , *12*(8), 895–904.

Steeg, P. (2008). Heterogeneity of Drug Target Expression Among Metastatic Lesions: Lessons from a Breast Cancer Autopsy Program. *Clin Cancer Res*, *14*, 3643–3645.

Stoop, M. P., Coulier, L., Rosenling, T., Shi, S., Smolinska, a. M., Buydens, L., … Luider, T. M. (2010). Quantitative Proteomics and Metabolomics Analysis of Normal Human Cerebrospinal Fluid Samples. *Molecular & Cellular Proteomics*, *9*(9), 2063–2075. doi:10.1074/mcp.M110.000877

Takei H, & Powell, S. (2009). Tumor-to-tumor metastasis to the central nervous system. *Neuropathology*, *29*, 303–308.

Tang, H., & Goldberg, E. (2009). Homo sapiens lactate dehydrogenase c (Ldhc) gene expression in cancer cells is regulated by transcription factor Sp1, CREB, and CpG island methylation. *Journal of Andrology*, *30*(2), 157–67. doi:10.2164/jandrol.108.005785

Thangaraju, M., Cresci, G., Itagaki, S., Mellinger, J., Browning, D., Berger, F., … Ganapathy, V. (2008). Sodium-coupled transport of the short chain fatty acid butyrate by SLC5A8 and its relevance to colon cancer. *J Gastrointest Surg*, *12*(10), 1773–1781.

Thangaraju, M., Gopal, E., Martin, P., Ananth, S., Smith, S., Prasad, P., … Ganapathy, V. (2006). SLC5A8 triggers tumor cell apoptosis through pyruvate-dependent inhibition of histone deacetylases. *Cancer Res*, *15*(66), 11560–11564.

Uda, S., Accossu, S., Spolitu, S., Collu, M., Angius, F., Sanna, F., … Batetta, B. (2012). A lipoprotein source of cholesteryl esters is essential for proliferation of CEM-CCRF lymphoblastic cell line. *Tumour Biol*, *33*(2), 443–453.

Ulrich, E., Akutsu, H., Doreleijers, J., Harano, Y., Ioannidis, Y., Lin, J., … Markley, J. (2008). BioMagResBank. *Nucleic Acids Research*, *36*, D402–D408.

Van Engeland, M., Nieland, L., Ramaekers, F., Schutte, B., & Reutelingsperger, C. (1998). Annexin V-affinity assay: a review on an apoptosis detection system based on phosphatidylserine exposure. *Cytometry*, *1*(31), 1–9.

Vermes, I., Haanen, C., Steffens-Nakken, H., & Reutelingsperger, C. (1995). A novel assay for apoptosis. Flow cytometric detection of phosphatidylserine expression on early apoptotic cells using fluorescein labelled Annexin V. *J Immunol Methods*, *184*(1), 39–51. Retrieved from http://www.sciencedirect.com/science/article/pii/0022175995000072I

Vu, T., Valkenborg, D., Smets, K., Verwaest, K., Dommisse, R., Lemiere, F., … Laukens, K. (2011). An integrated workflow for robust alignment and simplified quantitative analysis of NMR spectrometry data. *BMC Bioinformatics*, *12*(405).

Walenta, S., & Mueller-Klieser, W. (2004). Lactate: mirror and motor of tumor malignancy. *Semin Radiat Oncol*, *14*(3), 267–274.

Weston, C. L., Glantz, M. J., & Connor, J. R. (2011). Detection of cancer cells in the cerebrospinal fluid: current methods and future directions. *Fluids and Barriers of the CNS*, *8*(1), 14. doi:10.1186/2045-8118-8-14

Whitaker-Menezes, D., Martinez-Outschoorn, U., Lin, Z., Ertel, A., Flomenberg, N., Witkiewicz, A., … Lisanti, M. (2011). Evidence for a stromal-epithelial “lactate shuttle” in human tumors: MCT4 is a marker of oxidative stress in cancer-associated fibroblasts. *Cell Cycle*, *1*(10), 1772–1783.

Wishart, D. S., Lewis, M. J., Morrissey, J. a, Flegel, M. D., Jeroncic, K., Xiong, Y., … Li, L. (2008). The human cerebrospinal fluid metabolome. *Journal of Chromatography. B, Analytical Technologies in the Biomedical and Life Sciences*, *871*(2), 164–73. doi:10.1016/j.jchromb.2008.05.001

Wishart, D. S., Tzur, D., Knox, C., Eisner, R., Guo, A. C., Young, N., … Querengesser, L. (2007). HMDB: the Human Metabolome Database. *Nucleic Acids Research*, *35*, D521–6. doi:10.1093/nar/gkl923

Wong, M., Schlaggar, B., Buller, R., Storch, G., & Landt, M. (2000). Cerebrospinal fluid protein concentration in pediatric patients: defining clinically relevant reference values. *Arch Pediatr Adolesc Med*, *154*(8), 827–831.

Wood, I., & Tryhurn, P. (2003). Glucose transporters (GLUT and SGLT): Expanded families of sugar transport proteins. *Br. J. Nutr.*, *89*, 3–9.

Wright, E., Loo, D., Panayotova-Heiermann, M., Lostao, M., Hirayama, B., Mackenzie, B., … Zampighi, G. (1994). “Active” sugar transport in eukaryotes. *Experimental Biology*, *196*, 197–212.

Wu, X., Northcott, P., Dubuc, A., Dupuy, A., Shih, D., Witt, H., … Taylor, M. (2012). Clonal selection drives genetic divergence of metastatic medulloblastoma. *Nature*, *482*(7386), 529–533.

Xiong, Y., Lei, Q., Zhao, S., & Guan, K. (2011). Regulation of glycolysis and gluconeogenesis by acetylation of PKM and PEPCK. *Cold Spring Harbor Symposia on Quantitative Biology*, *76*, 285–289.

Younes, M., Brown, R., Mody, D., Fernandez, L., & Laucirica, R. (1995). GLUT1expression in human breast carcinoma: correlation with known prognostic markers. *Anticancer Res*, *15*(6B), 2895–2898.

Zhuang, L., Kim, J., Adam, R., Solomon, K., & Freeman, M. (2005). Cholesterol targeting alters lipid raft composition and cell survival in prostate cancer cells and xenografts. *J Clin Invest*, *115*(4), 959–968.

Zierler, K. (1999). Whole body glucose metabolism. *Am J Physiol*, *276*(3), 409–426.

Zubieta, J. K., Dannals, R. F., & Frost, J. J. (1999). Gender and age influences on human brain mu-opioid receptor binding measured by PET. *The American Journal of Psychiatry*, *156*(6), 842–8. Retrieved from http://www.ncbi.nlm.nih.gov/pubmed/10360121

Appendix A

Solutions prepared for the experimental work:

10X PBS (pH 7.4-7.6) (Sambrook & Russel, 2001)
For 1L: 80 g NaCl (1.37 M) (106404, Merck) 2 g KH_2PO_4 (14.7 mM) (104873, Merck) 11.1 g Na_2HPO_4 (78.1 mM) (S-0876, Sigma) 2 g KCl (26.8 mM) (104936, Merck) ddH_2O to 1 L

5X SDS gel loading buffer (Sambrook & Russel, 2001)
250 mM Tris HCl (pH 6.8) (0.5M 161-0799, Bio-rad) 10% SDS (V6551, *Promega*) 0.5 % bromophenol blue 50 % glycerol (1.04094.1000, *Merck*)

15 % resolving gel and 5 % stacking gel for Tris-glycine SDS-Polyacrylamide Gel Electrophoresis prepared accordingly to Sambrook & Russel, 2001

Transfer buffer
For 5 L: 75 g glycine (US16407, *USB*) 15 g Trizma-base (T-8524, *Sigma*) ddH2O to 4 L 1 L Methanol (107018, *Merck*) 5 mL 10% SDS (V6551, *Promega*)

PBS with 0.1% (v/v) Tween 20
For 1 L: 1 mL Tween 20 (20605, *USB*) PBS to 1 L

PBS with 0.2% (w/v) BSA
0.4 g BSA (A9647, *Sigma*) 200 mL PBS

5% (w/v) skimmed milk in PBS 0.1% (v/v) Tween 20
5 g skimmed milk (Molico, *Nestlé*) 100 mL PBS 0.1% (v/v) Tween 20

50 µg/mL Propidium Iodide (PI) solution – Cell cycle assay
For 50 mL: 1 mL of 2.5 mg/mL PI solution (P4170, Sigma) (prepared in PBS) 49 mL PBS 0.1 mg/mL RNase A (Easy spin kit, *Citomed*) 0.05% Triton X-100 (T8787, *Sigma*)

RIPA buffer
For 10 mL: 20 mM Tris-HCl pH 7.5 150 mM NaCl (106404, *Merck*) 5 mM KCl (104936, *Merck*) 5 mM $MgCl_2$ (M-8266, *Sigma*) 1% Triton X-100 (T8787, *Sigma*) ddH2O to 10 mL 1 Complete, Mini, EDTA-free Protease Inhibitor Cocktail Tablet (11836170001, *Roche*) 1 mM Orthovanadate (Na_3VO_4) 1 mM Sodium fluoride (NaF) (201154, *Sigma*)

Annexin binding buffer
0.01 M Hepes (pH 7.4) (391333, *Millipore*) 0.14 M NaCl (106404, *Merck*) 2.5 mM $CaCl_2$ (449709, *Sigma*)